The Dissertation Committee for Jong Suk Kim certifies that this is the approved version of the following dissertation:

Modeling, Control, and Optimization of Combined Heat and Power Plants

Committee:

Thomas Edgar, Supervisor

Michael Baldea

Roger Bonnecaze

Gary Rochelle

Glenn Masada

Modeling, Control, and Optimization of Combined Heat and Power Plants

by

Jong Suk Kim, B.S.; M.S.E.

Dissertation

Presented to the Faculty of the Graduate School of

The University of Texas at Austin

in Partial Fulfillment

of the Requirements

for the Degree of

Doctor of Philosophy

The University of Texas at Austin

May 2014

Dedication

To my parents and sisters, who deserves this degree as much as I do.

Acknowledgements

First and foremost, I would like to thank my supervisor Dr. Thomas Edgar for his tremendous help in guiding me through this work at the University of Texas at Austin (UT Austin). It was a great opportunity and a pleasure to be able to work with him. His patient efforts and encouragement on my behalf are sincerely appreciated.

The faculty and staff of the McKetta Department of Chemical Engineering at UT Austin were helpful and supportive during my time here. Special thanks to T stockman, Kay Costales-Swift, Sarah D. Berry-Caperton, Carrie Brown, Kristine Poland, and Randy Rife for their efforts.

The Utilities and Energy Management at UT Austin have been greatly acknowledged for providing the plant data needed to perform this work. Apart from the data, the staff, especially Ryan Thompson and Juan Ontiveros, and the operators were also helpful and supportive in providing insight into the power plant operation.

I would like to thank the sponsor of my research, CHEMSTATIONS. Without the generous support of this donor, none of this would be possible.

I am grateful for the association with the members of Dr. Edgar's research group (both past and present) here at UT Austin including: Dr. Kody Powell, Dr. Kriti Kapoor, Dr. Wesley Cole, Akshay Sriprasad, Bo Lu, Shu Xu, Matt Walters, Victor Duribe, Jungup Park, Ankur Kumar, Krystian Perez, and Abigail Ondeck. Their help and support are greatly appreciated. The members of the Baldea research group have become my friends as well, and I have learned so much from all of them.

Finally, I am most grateful for the love, encouragement, understanding and support of my parents and sisters. This work is a tribute to their sacrifice.

Jong Suk Kim

May 2014

Modeling, Control, and Optimization of Combined Heat and Power Plants

Jong Suk Kim, Ph.D.

The University of Texas at Austin, 2014

Supervisor: Thomas Edgar

Combined heat and power (CHP) is a technology that decreases total fuel consumption and related greenhouse gas emissions by producing both electricity and useful thermal energy from a single energy source. In the industrial and commercial sectors, a typical CHP site relies upon the electricity distribution network for significant periods, i.e., for purchasing power from the grid during periods of high demand or when off-peak electricity tariffs are available. On the other hand, in some cases, a CHP plant is allowed to sell surplus power to the grid during on-peak hours when electricity prices are highest while all operating constraints and local demands are satisfied. Therefore, if the plant is connected with the external grid and allowed to participate in open energy markets in the future, it could yield significant economic benefits by selling/buying power depending on market conditions. This is achieved by solving the power system generation scheduling problem using mathematical programming.

In this work, we present the application of mixed-integer nonlinear programming (MINLP) approach for scheduling of a CHP plant in the day-ahead wholesale energy markets. This work employs first principles models to describe the nonlinear dynamics of a CHP plant and its individual components (gas and steam turbines, heat recovery steam generators, and auxiliary boilers). The MINLP framework includes practical constraints

such as minimum/maximum power output and steam flow restrictions, minimum up/down times, start-up and shut-down procedures, and fuel limits. We provide case studies involving the Hal C. Weaver power plant complex at the University of Texas at Austin to demonstrate this methodology. The results show that the optimized operating strategies can yield substantial net incomes from electricity sales and purchases.

This work also highlights the application of a nonlinear model predictive control scheme to a heavy-duty gas turbine power plant for frequency and temperature control. This scheme is compared to a classical PID/logic based control scheme and is found to provide superior output responses with smaller settling times and less oscillatory behavior in response to disturbances in electric loads.

Table of Contents

List of Tables

List of Figures

Chapter 1: Introduction

The choice of energy sources plays an important role in determining environmental impact, costs, and plant reliability. Renewable energy resources such as solar, photovoltaic, geothermal, and wind are abundant and can be utilized as free energy sources in many industries (power generation, chemical, pulp and paper, refineries, etc.). They are indefinite and can substitute a finite resource, fossil fuels, to reduce the carbon footprint in these industries. However, the intermittency and unpredictability of renewable generation sources puts them at a disadvantage compared to fossil fuels. The oil and gas industry continues spend billions of dollars each year developing and deploying new technologies to allow more resources to be recovered, ensuring that fossil fuels remain competitive and readily available for customers. Therefore, fossil fuels will continue to supply the majority of our energy needs until renewable energies become more cost-competitive.

Efficient energy use in power generation industry also has a significant impact on operating costs due to volatile cost of energy today. As the use of fossil fuels for power generation and cogeneration is expected to grow during the next 20 years [1], it is necessary to analyze how to best operate existing plants that utilize fossil fuels as their primary energy sources. The efficient and clean energy solution is a combined heat and power technology.

Combined heat and power (CHP) plants produce electricity and thermal energy simultaneously from a single energy source such as natural gas, coal, oil, diesel, biomass, or a fuel cell. CHP plants mainly consist of a gas turbine, a heat recovery steam generator (HRSG), a boiler, and a steam turbine [2]. In a conventional energy supply system, electricity is generated at a power plant while thermal energy is generated separately via a

boiler. The waste heat from the system is vented via cooling towers or ponds without being utilized. The great majority of U.S. electric generation does not make use of waste heat. As a result, the average efficiency of utility generation has remained at about 34 percent since the 1960s. Also, the energy lost in the United States from wasted heat in the power generation sector is greater than the total energy use of Japan [3]. On the other hand, in CHP plants, the waste heat from the gas turbine is recovered by a HRSG and produces a high-pressure steam. This steam can be used directly for process heating in the manufacturing industries or for district heating to meet the thermal demands. The steam generated from a HRSG can drive a steam turbine to extract an additional power. If a CHP system is strategically located at or near the point of energy use (commercial or residential buildings), the effluent heat from a gas turbine can be readily recovered and used to heat the neighboring buildings [4, 5]. As a result, typical CHP systems exhibit high efficiencies up to 75 %, whereas conventional energy supply systems yield around 51 % efficiency [6, 7]. Figure 1.1 compares a conventional energy supply system with a CHP system and shows the energy inputs that each system requires to ultimately produce the same amount of energy.

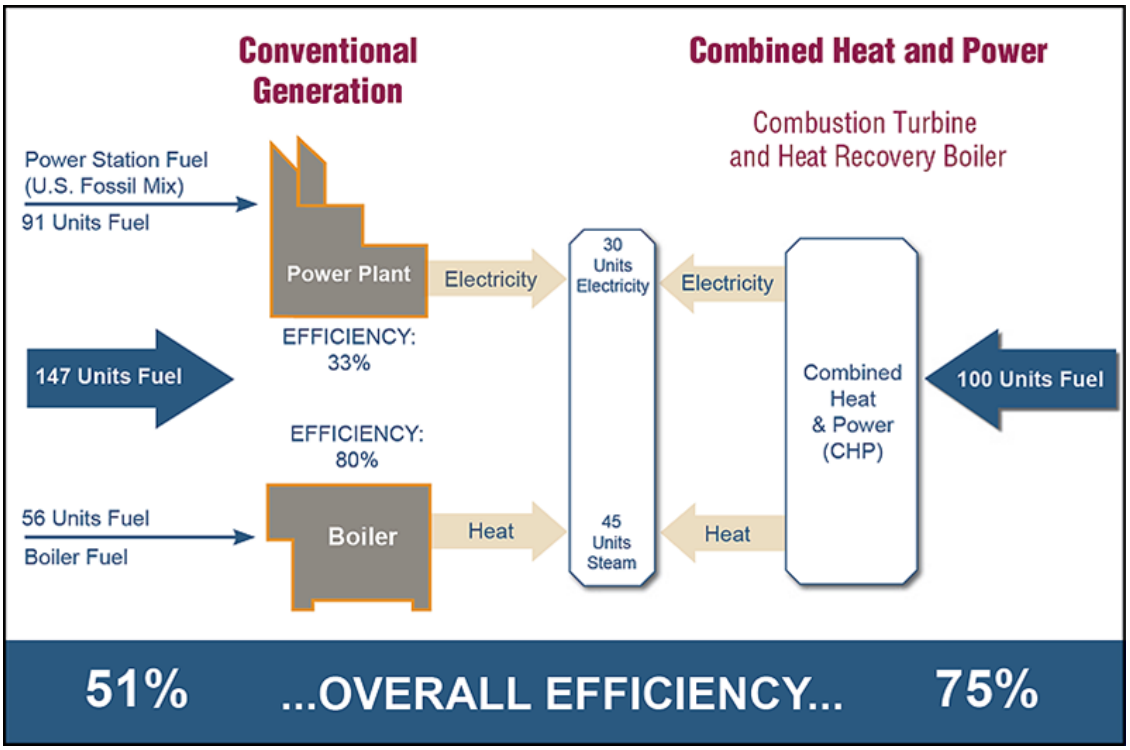

Figure 1.1: Conventional energy supply system (left) vs. combined heat and power (right). Image is from [7].

Distributed electricity generation systems, such as CHP, can also substantially reduce transmission costs and efficiency losses as the power does not have to be transported using high-voltage power lines over long distances as compared to larger, centralized power plants [8]. The vast majority of existing and planned CHP installations use natural gas as the primary fuel.

In the industrial and commercial sectors, a typical CHP site relies upon the electricity distribution network for significant periods, i.e., for purchasing power from the grid during periods of high demand or when off-peak electricity tariffs are available [9]. On the other hand, in some cases, a CHP plant is allowed to sell surplus power to the grid during on-peak hours when electricity prices are highest while all operating constraints and local demands are satisfied. This is achieved by the economic dispatch (ED), which

assigns the system load demand to the committed generating units for minimizing the power generation cost [10]. The net income of a CHP plant obtained by participating in wholesale energy markets can be significant, especially during the late afternoon or early evening hours when peak demand occurs. Due to such a compelling potential profit opportunity, the ED of a CHP plant is attracting a great deal of attention and is one of the two important tasks considered in power system generation scheduling problem. The other is the unit commitment (UC) that determines the unit start-up and shut-down schedules in order to minimize the system fuel expenditure when more than one generating unit exists. In other words, an important criterion in power system operation is to meet the power demand at minimum fuel cost using an optimal mix of different generating units [11].

Application of ED to district heating and cooling networks that incorporate CHP (i.e., university, airport, and hospital) have been popular as the system loads (heat and electrical) fluctuate considerably with time of day/year. CHP applications in district heating and cooling networks can be found in several references [12-15]. For example, the optimal size of a CHP system under British spot market conditions [12] and under German spot market conditions [15] is analyzed. Ristic et al. [13] used three different cost functions, each of which was formulated as a linear programming (LP) problem for each time step. By comparing the solutions from the three functions, the lowest cost during a time step defines the optimal operation of the CHP system. However, this model is empirical in that heat production was assumed to be proportional to electricity production. Rolfsman [14] showed that the optimal operating strategy allowed the CHP units that include thermal energy storage (TES) to operate at full-load condition when electricity prices are high, storing the excess heat produced in the TES units. The TES would then be discharged during off-peak hours when it was not economic to produce

electricity. Ito et al. [16] combined the dynamic programming method with mixed-integer programming to determine the optimal operation of a diesel engine cogeneration plant. Their study only covers 12 representative days for the whole year with a fixed-rate electricity price for summer and that for winter. So, the model does not reflect the diurnal variation in electricity prices. The work shown in [17] has similarities to [16], but it included a space-cooling demand. The optimization problem was formulated as a large-scale mixed-integer linear programming (MILP) problem and was solved by means of the decomposition method. Lawrence Berkeley National Laboratory developed one of the most advanced CHP optimization strategies [18]. This sophisticated model optimizes a distributed microgrid of several CHP systems, electricity generators, heat boilers, and heat storage tanks. The objective function takes into account fuel costs, operation and maintenance costs, carbon emission taxation, and investment costs. However, the model does not consider the possibility of interconnection to the external grid. Stoppato et al. [19] proposed a model that accounts for additional costs associated with the cyclic type of operation (i.e., unit start-ups and shut-downs) and with unplanned maintenance and unavailability of the plant if a failure occurs, due to creep and thermo-mechanical fatigue loadings. Nevertheless, this model is limited to a steam power plant.

Happ [20] presented a comprehensive survey on ED, which covers several aspects: developments in ED since early 1920's, valve point loading, multi-area concepts in economic dispatch, and optimal load flow. Chowdhury et al. [21] presented a survey addressing various aspects of ED during the period 1977-88, namely: optimal power flow, ED in relation to automatic generation control (AGC), dynamic dispatch, and ED with non-conventional generation sources. The fuel cost of the generator described in [20, 21] is approximately represented by polynomial functions (mostly a single quadratic function as this is convex in nature) for ED computation. It is also standard industrial

practice that polynomial functions are predominantly used to estimate the fuel cost of generator as the resulting ED problem can be solved as convex optimization problem. In actual practice, however, this assumption (quadratic or piecewise quadratic, monotonically increasing cost functions) is not valid because the cost functions exhibit higher order nonlinearities and discontinuities due to prohibited operating zones, multiple fuels, and valve point loading effects [22, 23]. Dynamic programming (DP) [24] has been used to overcome these difficulties, but due to the curse of dimensionality and excessive evaluation at each stage it has limitations. Genetic algorithm (GA) is a potential solution methodology for nonconvex ED problem due to the independence of the objective function from the auxiliary information such as differentiability and continuity [22, 23, 25-30]. However, the disadvantages of the GA are its slow convergence speed near the global optimum and long computational time. Particle swarm optimization (PSO) [31, 32] is another way to deal with a nonconvex ED problem but is prone to the same problems associated with GA (slow convergence and stagnation phenomenon in the proximity of the optimal solution). Dotzauer et al. [33] solved the operational optimization problem of a CHP plant that includes TES by using a Lagrangean relaxation (LR) approach. Rong et al. [34] extended the work shown in [33] and included restrictions on minimum up/down times. In a number of studies [35-37], a dynamic process was performed in conjunction with ED in order to satisfy the ramping constraints.

Operating constraints such as minimum up/down times and ramping limits that are modeled in some of the previously mentioned references result in a complex optimization problem and originate from the so-called unit commitment problem. Besides the methods mentioned previously, i.e., DP, GA, PSO, and LR, other approaches have been proposed to address the UC problem such as exhaustive enumeration [38], priority listing [39, 40], branch and bound [41, 42], interior point optimization [43], tabu search

[44, 45], simulated annealing [46], fuzzy logic [47], artificial neural networks [48, 49], evolutional programming [50, 51],and hybrid models [52-54] as well as mathematical programming, i.e., MILP and mixed-integer nonlinear programming (MINLP). For a detailed review on various methods of generation scheduling in electric power systems, see [55, 56]. Nowadays, among all methods, mixed-integer programming (MIP) is the method of choice due to advances in solution algorithms and computing power [57]. In practice, many US independent system operators (ISOs) use MIP for generation UC within the electric industry.

Arroyo and Conejo [58] proposed an MILP formulation for the UC and Carrion and Arroyo [59] improved the model shown in [58] by reducing the number of binary variables. Liu et al. [60] introduced an MINP model, which considers "units" of individual components within the plant, and showed that their model is superior to an aggregated mode model for the scheduling of combined cycle combustion turbine (CCCT) plants due to the more accurate description of the physical range of operation. Aghaei and Alizadeh [61] considered a scheduling problem of a CHP-based microgrid as an MIP-based multi-objective (i.e., minimizing total operational cost of the plant and minimizing carbon emissions) optimization problem. Mitra et al. [62] developed a deterministic MILP model that allows optimal production planning for continuous power-intensive processes. They emphasized the systematic modeling of operational transitions that result from switching the operating modes of the plant equipment, with logic constraints. Mitra et al. [63] extended their previous work and modeled transitional behavior (i.e., warm and cold start-ups and shut-downs) with different operating modes. However, all the works shown in [61-63] used empirical models to relate the power production rate to the fuel consumption, thus the operating cost of generator.

The solution of the scheduling problem strongly depends on the accuracy of the plant models used for simulations. Therefore, it is critical to develop the plant models that establish physically correct quantitative relationships between real systems and models of those real systems. For processes that operate over a wide range of operating conditions or often close to the boundaries of admissible regions due to tight economic and environmental conditions, linear or/and empirical models are unsuitable to adequately describe the process dynamics. Therefore, complex nonlinear models must be used.

The Electric Reliability Council of Texas (ERCOT) is one of 10 regional reliability councils in the North America Electric Reliability Council (NERC), as shown in Figure 1.2.

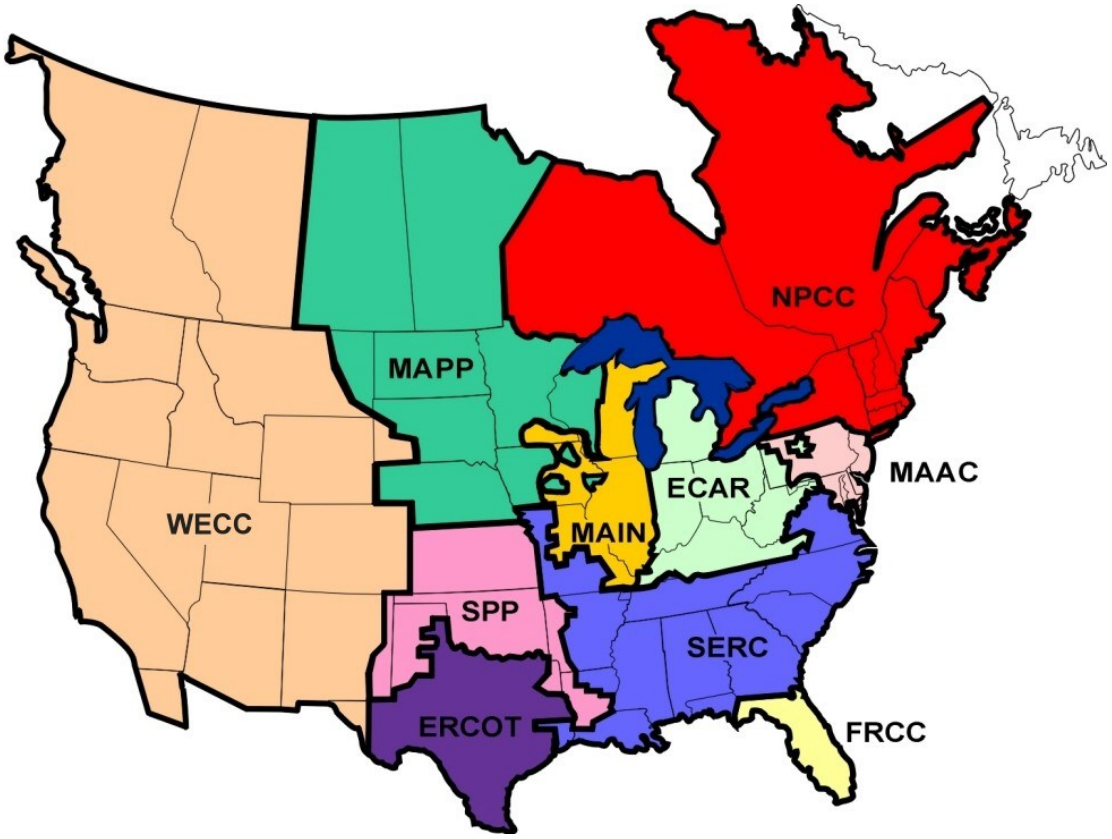

Figure 1.2: North American Reliability Council (NERC) Members Organizations. Image is from [64].

The ERCOT ISO is responsible for reliable power grid operations in the ERCOT region together with the electrical energy industry organizations that operate within that region. Also, ERCOT ensures open access to transmission and distribution systems in areas that permit competition, the timely conveyance of market information to market participants, and accurate accounting of power produced and delivered [64, 65]. About 85% of the electrical load in Texas (the largest electricity-consuming state in the U.S.) is satisfied through the ERCOT market. ERCOT has an overall generating capacity of approximately 90 Gigawatts (GW) from more than 550 generators [64]. ERCOT's members include retail consumers, investor-owned utilities, municipally-owned utilities, rural electric cooperatives, river authorities, independent generators, power marketers and retail electric providers. ERCOT market represents about 10% of the total electricity sales in the United States. Natural gas is used for over 44% of the electricity generation involved in market transactions and constitutes over 70% of the generating capacity [66]. Detailed descriptions of the ERCOT market can be found in [65].

ERCOT relies on the availability of generation capacity to provide energy to maintain the electric system within allowable reliability limits. Capacity and energy procurement, which are needed by ERCOT to perform reliability role, are competitively procured from qualified scheduling entities (QSEs) on a resource specific basis. Generation units, which can be on standby and available to be called upon to provide loads or energy that are available to be interrupted to relieve the need for additional energy, may provide these services upon meeting ERCOT qualification requirements. To ensure the reliable operation of the transmission system and increase grid stability, "ancillary services" are sourced from generation or load resources and provided to ERCOT. Types of ancillary services that ERCOT procures include regulation reserve,

responsive reserve, non-spinning reserve, black start, reliability must-run, voltage support service, and emergency response service (ERS) [64, 67].

ERCOT procures emergency response service (ERS) by selecting qualified loads generators (including aggregations of loads and generators) to make themselves available for deployment in an electric grid emergency. ERS is a valuable emergency service designed to decrease the likelihood of the need for firm load shedding such as rolling blackouts. Because ERCOT only accepts day-ahead or real-time wholesale transactions in accordance with ERCOT protocol from QSEs, customers meeting ERS criteria must provide the service through their QSEs [64]. In other words, all day-ahead or real-time financial settlement for the ERCOT wholesale market is between ERCOT and QSEs only.

This work also highlights the application of a nonlinear model predictive control scheme to a heavy-duty gas turbine power plant for frequency and temperature control. So, the reviews of plant models and their control strategies are presented next.

Recently, natural gas-fired turbines have found widespread use because of their higher efficiencies, lower capital costs, shorter installation times, abundance of natural gas supplies, lower greenhouse gas emissions compared to other energy sources, and fast start-up capability, which enables them to be used as peaking units that respond to peak demands [68]. Due to their special characteristics, natural gas-fired turbines are installed in numerous places in the world and have become an important source for power generation.

Because of their complexity, there is a need for simplified mathematical models of gas turbine generators that can be used to investigate power system stability, determine the best operating strategies, and develop contingency plans for system upsets. One of the most commonly used simplified models (Rowen-I) was presented by Rowen [69], taking

into account the load-frequency, temperature, and acceleration control of a heavy-duty gas turbine (HDGT). Rowen modified the model (Rowen-II) to be applicable for a combined heat and power plant by adding the influence of compressor inlet guide vanes (IGVs) on the gas turbine dynamics, especially the exhaust gas temperature [70]. Rowen's models (Rowen-I and Rowen-II) have provided a starting point for development of several models [71-75] that provided deeper insight into internal processes.

Although the classical feedback control system, i.e. proportional-derivative-integral (PID control), has been developed for the HDGT, it is important to develop more advanced process control (APC) strategies in order to minimize the operating cost while satisfying constraints. Model predictive control (MPC) is the most widely used APC technique that uses a model of the process to predict the values of outputs over a future interval called the prediction horizon. MPC is more powerful than classical feedback control, even for single loops without constraints, without being much more difficult to tune, even on difficult loops such as those containing long time delays [76]. The application of MPC to control a gas turbine was introduced by Vroemen and Essen [77]. Mu and Rees presented an approximate MPC used to control shaft speed of a gas turbine engine [78]. These models [77, 78] are either empirical or linear models. In practice; however, the process gains and dynamics of the gas turbine change with operating points, so more accurate nonlinear modeling and control of the gas turbine is needed.

The real-time implementation has been particularly challenging since the MPC requires solving an optimization problem with a large number of variables at each control step. D'Amato [79] developed and implemented the MPC solution for combined-cycle plant startups at Baglan Bay, South Wales. His study showed that the MPC startup controller resulted in reduced operating costs due to lower fuel consumption and lower emissions. However, once the generator is synchronized and connected to the power grid,

a nonlinear optimization problem needs to be solved and deployed at each control step faster than the sampling rate, which is on the order of a few seconds. Therefore, efficient algorithms compatible with real-time implementation are necessary.

1.1 RESEARCH OBJECTIVES

The objective of this work is to develop an optimal operating strategy for the CHP plant in the competitive Texas electricity market. As a result of competition among utility providers and fluctuations in prices of energy resources, CHP systems experience frequent start-up/shut-down operations. Depending on their profitability, the CHP units shut down for short periods of time or for longer periods. Therefore, they are subject to a large number of transients. Especially, the start-up process represents a major interest because the start-up costs of generating units are subject to the unit start-up types (i.e., hot, warm, and cold start-ups), which depend on the unit's prior reservation time.

Case studies involving the Hal C. Weaver power plant complex at the University of Texas at Austin (see Figure 1.3) are provided to demonstrate the effectiveness of the proposed methodology.

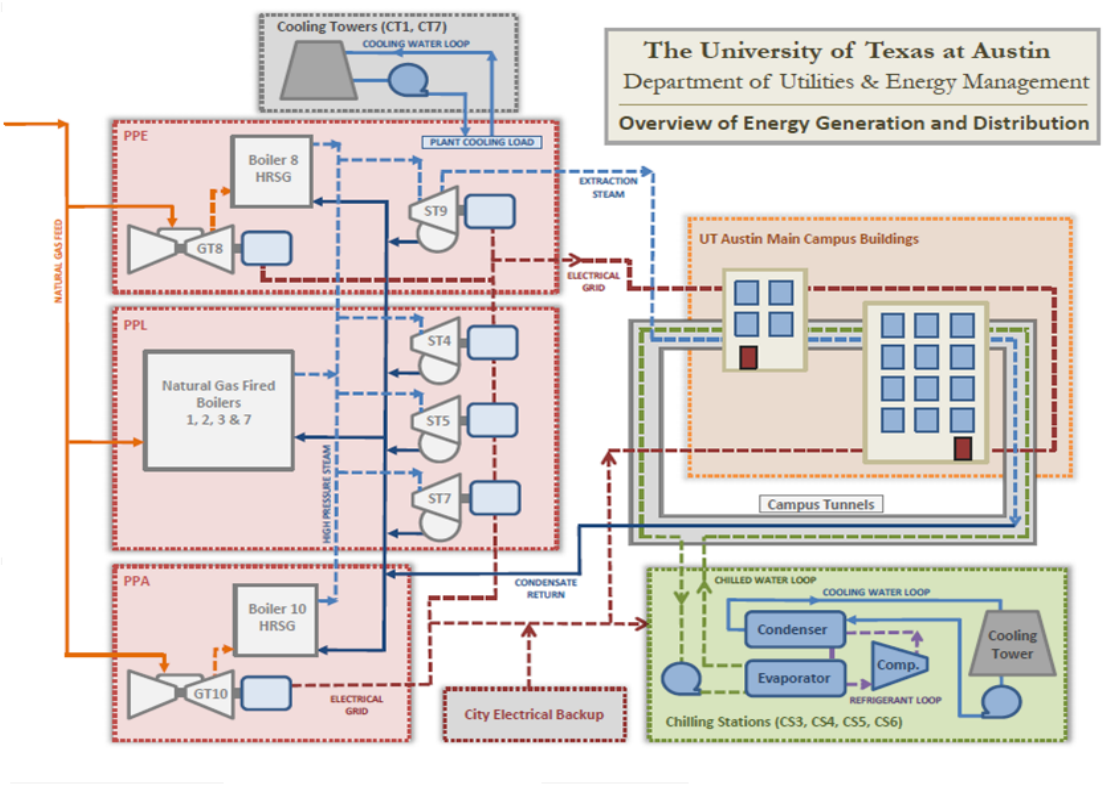

Figure 1.3: Overview of energy generation and distribution at the University of Texas at Austin campus

The power plant at the University of Texas at Austin (UT Austin) campus does not rely on the external grid, thus the campus is effectively an independent micro-grid [80, 81]. Although the plant is one of the most reliable CHP systems in the country, it does not participate in wholesale energy markets. If the plant is connected with external grid and allowed to participate in open energy markets in the future, it could yield economic benefits by selling/buying power to/from the grid depending on market conditions.

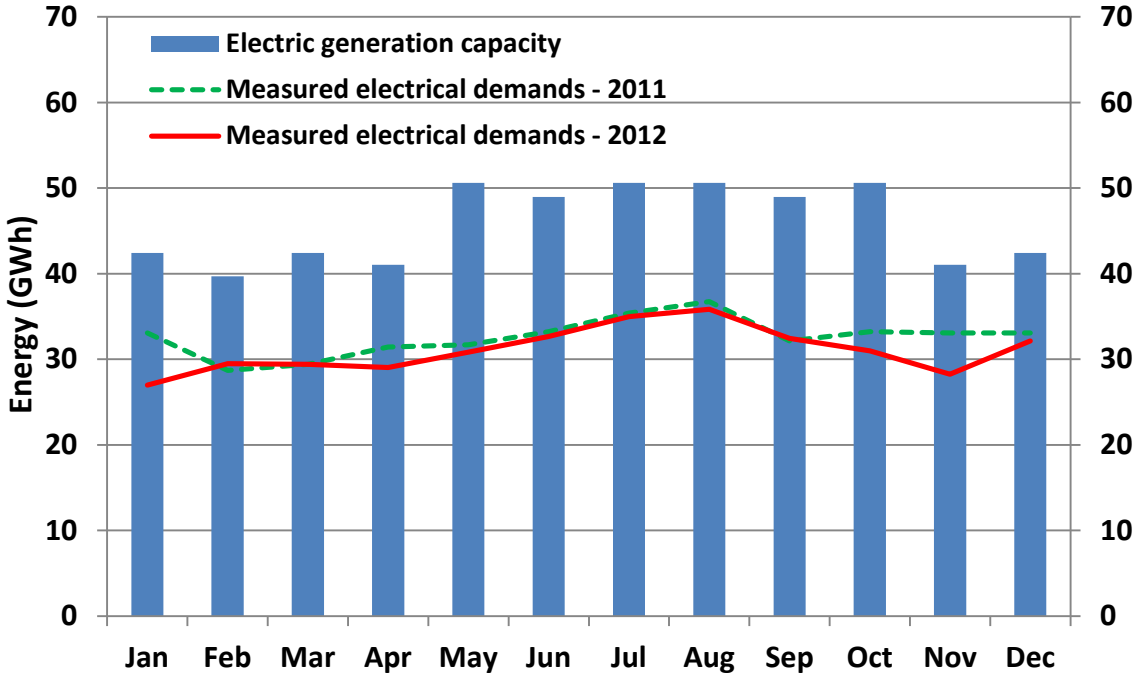

Figure 1.4: Electric generation capacity and actual electrical demands at UT Austin for 2011 (green dashed line) and 2012 (red solid line).

Figure 1.4 compares on-campus electric generation capacity with the actual electrical demands. It can be seen that UT Austin could have sold surplus electrical energy of 157 GWh to the grid in 2011 (or 176 GWh in 2012), yielding annual revenue of $ 3.14 million (or $ 3.53 million in 2012) at an average price of 2 ¢/kWh. However, the electricity prices vary on an hourly basis (in day-ahead electricity markets). Also, it is not economical to sell extra power to the grid at off-peak electricity tariffs or to self-generate the power during the off-peak hours when the electricity prices are cheap. The goal is to develop optimal scheduling of the CHP plant at UT Austin in the day-ahead wholesale energy market (electricity is purchased the day before it is used) of the ERCOT. The maximum profit of the plant from electricity sales and purchases should be recognized by committing more efficient and less expensive units in the plant while satisfying the

demands that fluctuate considerably with time of day/year and the system operating constraints on an hourly basis. Note that the unit commitment literature usually considers "unit" at a plant level [63]. In this work, "unit" at an individual component within the CHP plant (gas turbines with heat recovery steam generators, steam turbines, and boilers) is considered and the interactions of components are modeled using first principles models.

In order to assess the net incomes of a CHP plant in the future, one day ahead forecasts for loads (electrical, cooling, and heating) must be made as they are used to determine day-ahead prices for the electricity market and which units should be committed for economic dispatch [82-84]. However, the focus of this work is on the development of an optimal operating strategy of a CHP system based on historic plant and market data other than the development of accurate forecasting models. In this work, the solution of the scheduling problem is based on a totally deterministic case, i.e., 2011 or 2012 historical data are used for the economic analysis. Development of accurate forecasting models is beyond the scope of this work.

In this work, first principles dynamic modeling and multivariable control of natural-gas fired turbine power plants are also explored. The goal is to develop an advanced process control strategy that provides superior output responses with smaller settling times to the variations in the main disturbance (electric load) than those observed in the PID control system. The proposed control scheme should also prevent the tripping of the plant when a sudden large increase in the electric load is introduced into a power generation unit. Efficient algorithms compatible with real-time implementation must be proposed.

1.2 OVERVIEW OF DISSERTATION

Literature reviews surveying the power system generation scheduling problem and multivariable control of the GTPP are given in the previous sections. Section 1.1 presented the research objectives.

In Chapter 2, the first principle models that describe the nonlinear dynamics of a CHP plant and its individual components are developed and validated. The unit-specific model parameters are estimated via least mean squares (LMS) algorithm using the actual plant data. An overview of the CHP plant at UT Austin is also presented.

Chapter 3 proposes a methodology for optimizing operating of a CHP plant participating in the competitive wholesale electricity markets. The constrained nonlinear optimization problem is formulated to minimize the cost function (or maximizing the net income) while considering economic savings. The optimized operating schedules are compared to the historical operating schedules over a certain period of time. Also, the sensitivity of the net incomes to changes in the fuel costs is examined in Chapter 3.

Chapter 4 uses the model developed in Chapter 3 and goes a step further. An additional profit of the CHP plant by providing the emergency response service (ERS) through a QSE is evaluated. In this work, the ERS is assumed to be procured for a four-month contract period (June to September of 2012) for deployment in an electric grid emergency. Case studies demonstrate how the net incomes of the CHP plant change as a function of MWs sold to the ERCOT for the ERS while participating in the wholesale energy markets.

In Chapter 5, the optimization problem introduced in Chapter 3 is greatly expanded. An MINLP framework for optimal scheduling of a CHP plant in the day-ahead energy market is proposed. A 24-hour scheduling problem is solved to maximize the profit of the CHP plant from electricity sales over a four-month period (June to

September of 2012) while satisfying the demands. The model accounts for the different phases (synchronization, soak, dispatch, and desynchronization) during start-up and shut-down of each component. Three different start-up types (hot, warm, and cold) are explicitly modeled, each with distinct start-up cost, depending on the component's prior reservation time.

In Chapter 6, a nonlinear model predictive control (NMPC) scheme is applied to a HDGT power plant for frequency and temperature control. This scheme is compared to a classical PID/logic based control scheme to demonstrate the effectiveness of the proposed NMPC strategy. As the sampling rate observed in a HDGT power plant is fast (on the order of seconds), an efficient algorithm compatible with real-time implementation is suggested in order to reduce the computation time when solving a set of differential algebraic equations.

Finally, Chapter 7 summarizes the key contributions of this research and presents recommendations for future work.

All tests (case studies) are performed on a PC with Intel® Core™2 Duo processor 2.54 GHz and 4.00 GB of RAM, running 32-bit Windows. The nonlinear programming (NLP) problems are solved in MATLAB environment using the sequential quadratic programming (SQP) algorithm [85] in Chapters 2, 3, 4, and 5, whereas the NLP problems in Chapter 6 are solved using an interior-point (IP) algorithm [86].

Chapter 2: Mathematical Modeling of Combined Heat and Power Plants

In this section, the mathematical models of major pieces of equipment present in a CHP plant are developed using first principles models. System overview of the CHP plant (Hal C. Weaver power plant complex at UT Austin), to which the proposed models are applied and validated, is presented in the following sub-section in greater details.

2.1 System Overview of the Hal C. Weaver Power Plant Complex

The Hal C. Weaver power plant complex at UT Austin meets 100% of the university's utility needs (power, heat, and cooling demands) throughout the year, serving more than 160 buildings and about 17 million ft^2 of space via over 6 miles of underground distribution tunnels and electrical duct banks [80, 81, 87]. Ties to the city grid exist, but they are for emergency purposes only. The power plant includes 136 MW of onsite electrical power generation, 1.28 million lb/hr (161 kg/s) of steam generation, and 140 million ton-hours of chilled water capacity. The plant also provides the campus compressed air and demineralized water for buildings and laboratory use.

The simplified diagram of the CHP plant is presented in Figure 2.1. The plant mainly consists of a heavy-duty gas turbine (HDGT), a heat recovery steam generator (HRSG), an auxiliary boiler, and a steam turbine. A natural gas-fired gas turbine generates electrical power for distribution throughout the campus. Turbine inlet air cooling (TIAC) is used to increase the density of the combustion air by cooling the gas turbine air intake, thereby increasing both the throughput and the efficiency of the gas turbine compressor. As a result, the power output of the gas turbine increases with the use of TIAC [88]. For example, as shown in Figure 2.2, the air temperature coming out from

the TIAC system (or air temperature at compressor inlet) has been reduced to around 52 °F (11 °C) via the TIAC during the on-peak hours in hot summer days.

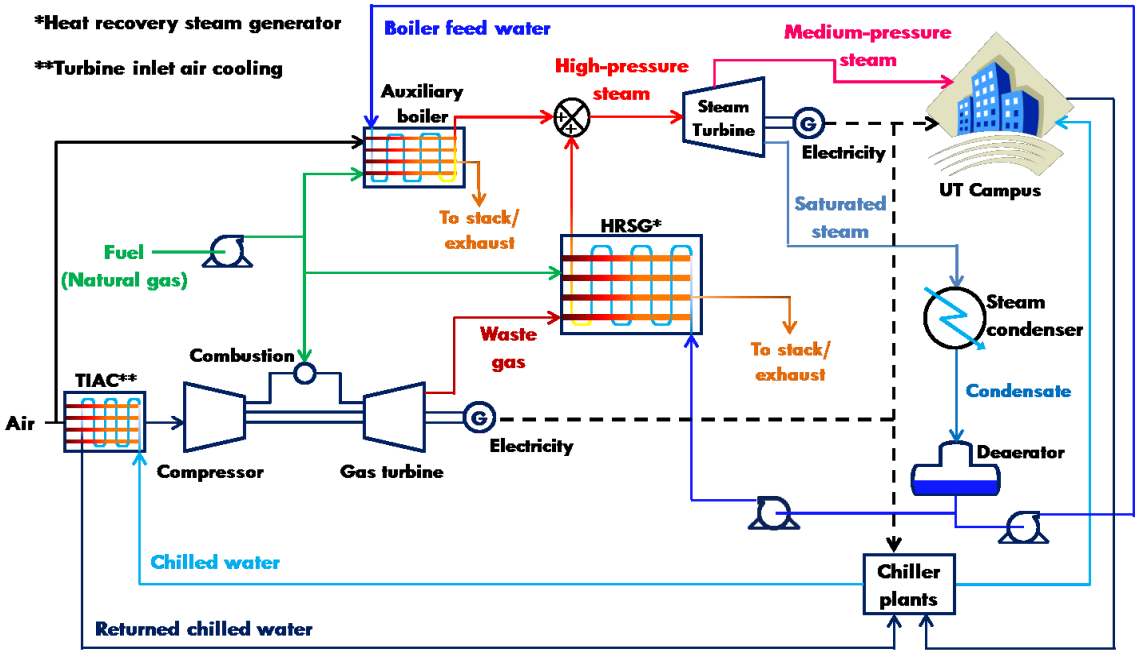

Figure 2.1: A simplified schematic of Hal C. Weaver Power Complex at UT Austin.

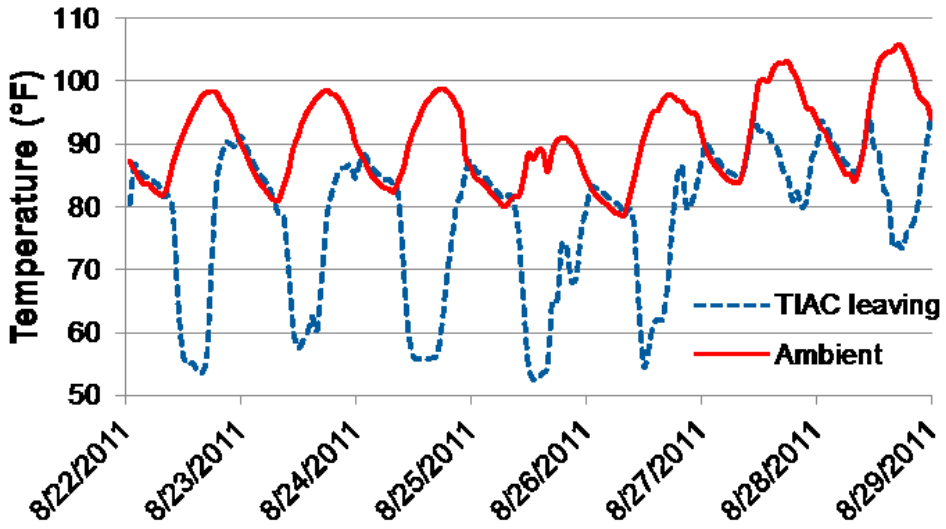

Figure 2.2: Air temperature at compressor inlet (blue dashed line) vs. ambient temperature (red solid line).

The waste heat from the gas turbine is recovered by a HRSG and produces high-pressure (HP) steam at 425 psi (30 bar) and 750 °F (399 °F) for use in campus. The boiler feed pump is connected to the discharge of the deaerator. The boiler feed pump raises the feedwater pressure to that of the boiler (43 bar) and pumps the feedwater through the high-pressure feedwater heaters. The HRSG is a natural-circulation boiler with natural gas-fired supplementary firing. Supplementary firing is carried out using an in-duct burner to raise the exhaust gas temperature, resulting in an increase in steam flow. There is an auxiliary boiler that burns natural gas and generates an additional HP steam when steam demand is high, especially during the winter. An extraction steam turbine is fed partially by the auxiliary boiler and partially by the HRSG. This combined steam flow drives the steam turbine to generate additional electricity during steam expansion. A portion of a medium-pressure (MP) steam at 160 psi (11 bar) is extracted from at an intermediate point in the turbine casting for distribution throughout the campus to meet the heating loads. After steam expansion, the rest is dropped to near atmospheric pressure at saturation conditions.

About 70% of the electricity produced from gas and steam turbines is consumed by the campus while the other 30% is used by the cooling system to make chilled water for air conditioning on campus, primarily by the centrifugal chillers, cooling towers and pumps [89]. This combination of the two power generation cycles (gas turbine in Brayton and steam turbine in Rankin cycles) enhances the efficiency of the plant. The plant is therefore a combined cycle and a tri-generation system, providing electricity, heating, and cooling. The rated capacity of major pieces of power plant equipment is summarized in Table 2.1.

Table 2.1: A rated capacity of designated run units.

Generator	Unit name	Electrical power (MW_e)[a]	Boiler	Unit name	Steam generation (kg/s)
Gas turbine 8	GT8	42	Boiler 8	HRSG8	36.4 (289[b])
Gas turbine 10	GT10	32	Boiler 10	HRSG10	24.3 (193[b])
Steam turbine 9	ST9	25	Boiler 3	BR3	18.9 (150[b])
Steam turbine 7	ST7	25	Boiler 7	BR7	63.0 (500[b])

[a] electrical MW
[b] steam generation defined in thousand lb/hr

There are back-up units (steam turbines 4 and 5 and boilers 1 and 2) that can be brought on-line in case of emergency, but they are excluded from this work as they are rarely used in practice. GT8 is always coupled with HRSG8, and GT10 is always coupled with HRSG10. ST9 is used throughout the year as it is more efficient than ST7, but ST7 replaces ST9 when ST9 is under maintenance. There are two gas turbines (GT8 and GT10), each of which is equipped with the TIAC system, two HRSGs (HRSG8 and HRSG10), and two auxiliary boilers (BR7 and BR3) in the plant, but in general only one unit operates at a time. For example, GT8, HRSG8, and BR3 are operated from May to October, whereas GT10, HRSG10, and BR7 are used during the rest of the year.

Overall the plant exhibits "utility efficiency" of greater than 80 % [80]. "Utility efficiency" is the sum of energy products (electric power, steam, and chilled water) defined in the same unit (i.e., MW_e) divided by the total fuel input. This is a useful metric in comparing the operation of the UT Austin power plant from year to year but is not really useful in comparison to other CHP systems, because CHP systems lack a cooling system. When calculating the utility efficiency of the plant, the amount of heat to be removed from the circulating water within the cooling tower is not taken into account,

resulting in the underestimation of the *COP* (the coefficient of performance of a chiller). As a result, cooling load defined in the electrical power is overestimated, yielding the overestimated plant efficiency. The actual "thermal efficiency" of the UT Austin power plant, which is a combined cycle system, is lower than what the typical CHP systems exhibit (i.e., less than 60 % vs. 75 %) as the form of the energy has to change from the thermal to electrical via the steam turbine.

2.2 MODEL DEVELOPMENT

In this work, the sampling rate Δt of one hour is used for parameter estimation, but the units present in a CHP system show relatively much faster dynamic responses. For this reason, a steady state assumption is made in modeling the system. The mathematical models are divided into units in an object-oriented fashion that correspond to the modular nature of the facility.

2.2.1 Turbine Inlet Air Cooling System

The TIAC system is used to pre-cool the ambient air before it is fed to the gas turbine's compressor in order to improve gas turbine efficiency. The effectiveness of a heat exchanger ε is the ratio of the actual heat transfer rate for a heat exchanger to the maximum possible heat transfer rate. For the TIAC system ε is defined by

$$\varepsilon = \frac{T_{w,\,TIAC,\,out} - T_{w,\,TIAC,\,in}}{T^{\min}_{air,\,TIAC,\,out} - T_{w,\,TIAC,\,in}} \tag{2.1}$$

where $T_{w,\,TIAC,\,out}$ and $T_{w,\,TIAC,\,in}$ are the temperatures of chilled water exiting and entering the TIAC system, respectively, and $T^{\min}_{air,\,TIAC,\,out}$ is the minimum possible air temperature at the outlet of the TIAC system [90]. A typical value for ε is 0.85-0.9 [91], so ε is

assumed to be 0.9 in this study. If condensation does not occur when the air is cooled, the energy balance equation across the TIAC system is expressed by

$$WC_{pc}\left(T_{amb}-T_{air,\,TIAC,\,out}\right) = \rho_w V_{w,\,TIAC} C_{pc}\left(T_{w,\,TIAC,\,out}-T_{w,\,TIAC,\,in}\right) \tag{2.2}$$

subject to

$$W=\left(\frac{MW_{air}}{R_g}\right)\left(\frac{P_c V_c}{T_c}\right) \tag{2.3}$$

where W is the actual dry-air mass flow, $T_{air,\,TIAC,\,out}$ (also referred to as T_c) is the air temperature coming out from the TIAC system, ρ_w is the water density, $V_{w,\,TIAC}$ is the volumetric flow rate of chilled water entering the TIAC system, C_{pc} is the specific heat of air flow, T_{amb} is ambient temperature, and P_{amb} is ambient pressure. In (2.3), MW_{air} is the molecular weight of the air, R_g is the ideal gas constant, and P_c and V_c are the pressure and volumetric air flow at the compressor inlet, respectively. The volumetric air flow V_c is adjusted by the compressor inlet guide vanes (*IGVs*) by the following relation:

$$V_c = V_{cn}\frac{\sin\left(\theta_{IGV}-\theta_{min}\right)}{\sin\left(\theta_{max}-\theta_{min}\right)} \tag{2.4}$$

where θ_{IGV} is the angular position of the *IGVs,* V_{cn} is the volumetric air flow at nominal operating condition, and θ_{max} and θ_{min} are the maximum and minimum guide van angles, respectively. By combining (2.2)-(2.4) and assuming ε is 1, $T^{min}_{air,\,TIAC,\,out}$ can be calculated. Then, $T_{w,\,TIAC,\,out}$ is obtained from (2.1) with a known $T_{w,\,TIAC,\,in}$ and is substituted back into (2.2) to solve for $T_{air,\,TIAC,\,out}$ (or T_c). Finally, W is determined by θ_{IGV} as shown in (2.4). The average pressure drop across the TIAC (ΔP_{TIAC}) can be

obtained from the data to estimate P_c. If condensation of air occurs in the TIAC system, W becomes a function of the relative humidity.

2.2.2 Gas Turbine

In deriving the gas turbine model parameters, the efficiencies of the units (compressor, combustor, and turbine), the specific heat of the working fluids (air and exhaust gas), and the lower heating value (LHV) of the fuel (natural gas) are assumed to be constant [92]. A schematic of a single-shaft heavy-duty gas turbine is shown in Figure 2.3. In the Brayton cycle shown in Figure 2.3, air with atmospheric conditions at point 1 is compressed adiabatically by the compressor to point 2. Segment 2-3 pertains to isobaric heating of compressed air in the combustor, which increases the temperature to point 3. The combustion product and compressor discharge air at point 3 will enter the turbine and expand adiabatically to point 4. The pressure loss in the air filters and the combustion chamber is neglected [93].

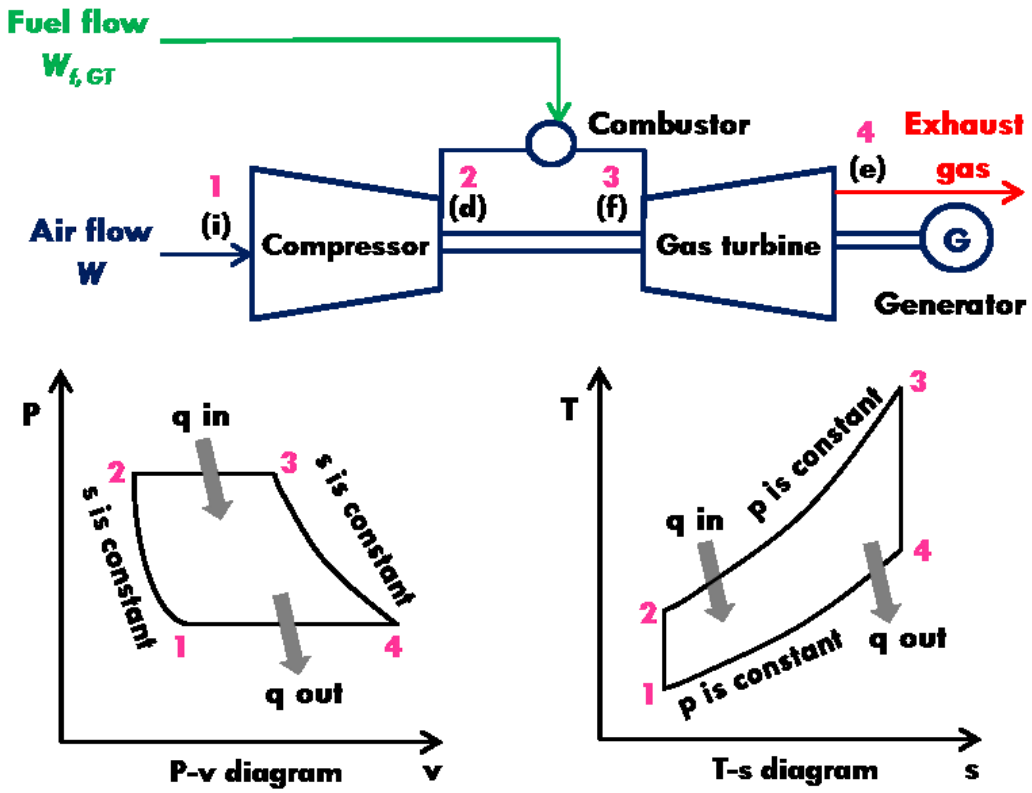

Figure 2.3: Schematic of a single-shaft heavy-duty gas turbine (upper) and P-v (lower left) and T-s (lower right) diagrams of an ideal Brayton cycle (q: heat, P: pressure, v: volume, T: temperature, s: entropy).

Adiabatic compression described in the process 1-2 in Figure 2.3 gives the following relationship:

$$T_d = T_c \cdot \left(1 + \frac{x_c - 1}{\eta_c} \right) \tag{2.5}$$

where

$$x_c = \left(PR \cdot \frac{W}{W_n} \right)^{\frac{\gamma_c - 1}{\gamma_c}} \tag{2.6}$$

In (2.5), T_d and T_c are the temperatures at compressor outlet and inlet, respectively, and η_c is the compressor efficiency. In (2.6), PR is the compression ratio, W_n is the air flow at nominal operating condition (full-load condition), and γ_c is the cold end ratio of specific heats. From the energy balance equation in the combustion chamber, gas turbine firing temperature T_f is defined by (2.7):

$$T_f = T_d + \left(\frac{\eta_{comb,\,GT} \cdot LHV}{C_{ph}} \right) \cdot \left(\frac{W_{f,\,GT}}{W_{f,\,GT} + W} \right) \tag{2.7}$$

where LHV is the lower heating value of the fuel, $\eta_{comb,\,GT}$ is the combustor efficiency, and C_{ph} is the specific heat of exhaust gas flow. The gas turbine fuel flow $W_{f,\,GT}$ is defined by (2.8):

$$W_{f,\,GT} = \left(F_{d,\,GT} \cdot \left(1 - K_{NL} \right) + K_{NL} \right) \cdot W_{fn,\,GT} \tag{2.8}$$

where $F_{d,\,GT}$ is the gas turbine's fuel demand, K_{NL} is the fuel valve lower limit, and $W_{fn,\,GT}$ is the gas turbine fuel flow at nominal operating condition. For the adiabatic expansion described in the process 3-4 in Figure 3, (2.9) relates T_f to the exhaust gas temperature T_e:

$$T_e = T_f \left(1 - \left(1 - \frac{1}{x_h} \right) \eta_t \right) \tag{2.9}$$

where η_t is the turbine efficiency. Equation (2.10) defines x_h in (2.9):

$$x_h = \left(PR \cdot \frac{W_{f,\,GT} + W}{W_{fn,\,GT} + W_n} \right)^{\frac{\gamma_h - 1}{\gamma_h}} \tag{2.10}$$

where γ_h is the hot end ratio of specific heats. The net energy supplied to HDGT P_{GT} is given by (2.11):

$$P_{GT} = \left(W + W_{f,GT}\right) \cdot C_{ph} \cdot \left(T_f - T_e\right) - W \cdot C_{pc} \cdot \left(T_d - T_c\right) \qquad (2.11)$$

The first term on the right-hand side (RHS) in (2.11) is the mechanical power generated by the turbine, and the second term is the power consumed by the compressor. Note that a greater difference between the turbine inlet and outlet temperatures allows more work to be extracted from the expanding gases. The parameters shown in (2.4)-(2.11) and process variables at nominal operating condition are summarized in Table 2.2.

Table 2.2: Gas turbines.

Symbol	Description	Unit	Value	
			GT8	GT10
$P_{n,GT}$	Gas turbine power output	MW_e	42.0	32.2
W_n	Air flow rate	kg/s	139	56.6
$W_{fn,GT}$	Gas turbine fuel flow rate	kg/s	2.44	1.81
T_f^{ref}	Turbine firing temperature	°C	1,115	1,744
T_e^{ref}	Exhaust gas temperature	°C	523	861
PR	Gas turbine compression ratio	-	13.1	24.4
θ_{min}	Minimum *IGV* angle	degrees	11.6	11.6
θ_{max}	Maximum *IGV* angle	degrees	85.0	85.0
C_{pc}	Specific heat of air flow	kJ/kg·K	1.005	1.005
C_{ph}	Specific heat of exhaust gas flow	kJ/kg·K	1.157	1.157
γ_c	Cold end ratio of specific heats	-	1.4	1.4
γ_h	Hot end ratio of specific heats	-	1.33	1.33
$\eta_{comb,GT}$	Gas turbine combustion efficiency	%	99	99
LHV	*LHV* of the fuel (natural gas)	kJ/kg	47,249	47,249
K_{NL}	Fuel valve lower limit	pu[a]	0.1094	0.1014
ΔP_{TIAC}	Pressure drop across the TIAC system	PSI	0.2639	0.3075

[a] per unit value

2.2.3 Heat Recovery Steam Generator

The main assumptions made about the HRSG in this study are as follows [94]. The HRSG is treated as a bulk heat exchanger to which governing equations are applied. Heat is transferred from the exhaust gas to water or steam by convection only. The temperature and pressure of process streams at the superheater outlet, economizer inlet, and stack do not vary significantly, so they are assumed to be constant.

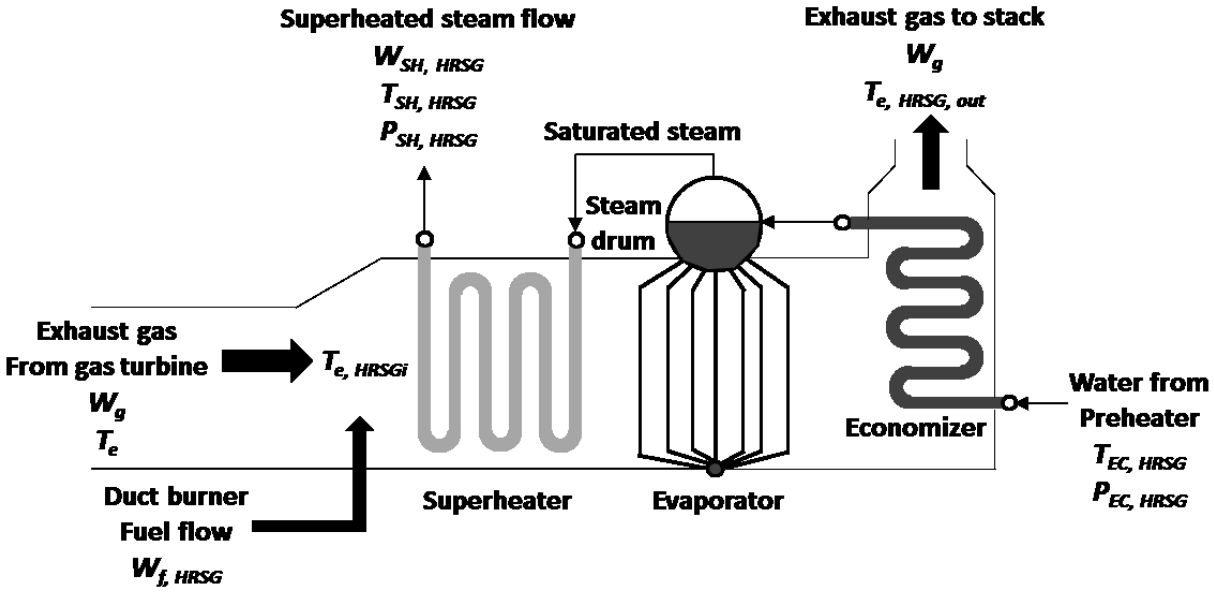

Figure 2.4: Schematic of the HRSG.

Figure 2.4 is a schematic diagram of an HRSG whose function is to convert the useful thermal energy in the gas turbine exhaust into steam. After heating in the economizer, the feedwater enters the drum at slightly subcooled conditions. From the drum, it is circulated to the evaporator and returns to the drum as a water/steam mixture where water and steam are separated. Saturated steam exits the drum and is fed to the superheater where it is heated to meet the desired superheated steam temperature. When additional superheated steam is desired from the HRSG or when the gas turbine exhaust

gas is not hot enough to produce the desired temperature of superheated steam, the exhaust gas temperature can be raised via supplementary firing using in-duct burner in the HRSG as the following:

$$T_{e,\,HRSG,\,in} = T_e + \frac{\beta_{HRSG}}{\alpha_{HRSG}} \cdot \left(\frac{W_{f,\,HRSG}}{W_{f,\,HRSG} + W_g} \right) \tag{2.12}$$

where α_{HRSG} and β_{HRSG} are lumped parameters (see Table 2.7 for the definitions), W_g is the gas turbine exhaust flow, $T_{e,\,HRSG,\,in}$ is the raised T_e after supplementary firing, and $W_{f,\,HRSG}$ is the duct burner fuel flow. The HRSG steam flow $W_{SH,\,HRSG}$ is calculated by an overall energy balance on the HRSG, shown in (2.13), where ΔH_{FWHTR} is the feedwater heat duty, $\hat{H}_{SH,\,HRSG}$ is the specific enthalpy of the superheated steam exiting the HRSG, and $\hat{H}_{EC,\,HRSG}$ is the specific enthalpy of the feedwater entering the economizer.

$$W_{SH,\,HRSG} = \frac{\alpha_{HRSG} \cdot \left(W_g + W_{f,\,HRSG}\right)\left(T_{e,\,HRSG,\,in} - T_{e,\,HRSG,\,out}\right) - \Delta H_{FWHTR}}{\hat{H}_{SH,\,HRSG} - \hat{H}_{EC,\,HRSG}} \tag{2.13}$$

As described in (2.13), the amount of heat which can be recovered from exhaust gas in the HRSG depends on: the flow rate and temperature of exhaust gas and the flow rate and temperature of circulating water [95]. The definitions of the variables shown in Figure 2.4 as well as their values are given in Table 2.3.

Table 2.3: HRSGs.

Symbol	Description	Unit	Value	
			HRSG8	HRSG10
$W_{SH,\ HRSG}$	HRSG steam flow rate	thousand lb/hr	289	193
$T_{SH,\ HRSG}$	Temperature at the outlet of the superheater	°C	400	399
$P_{SH,\ HRSG}$	Pressure at the outlet of the superheater	bar	30	31
$\hat{H}_{SH,\ HRSG}$	Enthalpy at the outlet of the superheater	kJ/kg	3,232	3,228
$T_{EC,\ HRSG}$	Temperature at the inlet of the economizer	°C	120	122
$P_{EC,\ HRSG}$	Pressure at the inlet of the economizer	bar	34	39
$\hat{H}_{EC,\ HRSG}$	Enthalpy at the inlet of the economizer	kJ/kg	506	515
$T_{e,\ HRSG,\ out}$	Exhaust gas temperature at the outlet of the HRSG	°C	191	188
ΔH_{FWHTR}	Heat duty for the feedwater preheater	kW	2,352	0

2.2.4 Auxiliary Boiler

The auxiliary boiler produces additional superheated steam when it is needed. The steam output of the auxiliary boiler $W_{SH,\ BR}$ depends on the fuel mass flow entering the boiler $W_{f,\ BR}$ as shown in (2.14):

$$W_{SH,\ BR} = \frac{\alpha_{BR} \cdot W_{f,\ BR}}{\hat{H}_{SH,\ BR} - \hat{H}_{EC,\ BR}} \tag{2.14}$$

where α_{BR} is the lumped parameter (see Table 2.8 for its definition and estimated value from the regression), $\hat{H}_{SH,\ BR}$ is the specific enthalpy of the superheated steam exiting the boiler, and $\hat{H}_{EC,\ BR}$ is the specific enthalpy of the feedwater entering the boiler. Table 2.4 summarizes the nominal values of the model parameters shown in (2.14).

Table 2.4: Boilers.

Symbol	Description	Unit	Value	
			BR3	BR7
$W_{SH,\,BR}$	Boiler steam flow rate	thousand lb/hr	150	500
$T_{SH,\,BR}$	Temperature at the outlet of the superheater	°C	339	375
$P_{SH,\,BR}$	Pressure at the outlet of the superheater	bar	30	30
$\hat{H}_{SH,\,BR}$	Enthalpy at the outlet of the superheater	kJ/kg	3,090	3,175
$T_{EC,\,BR}$	Temperature at the inlet of the economizer	°C	221	190
$P_{EC,\,BR}$	Pressure at the inlet of the economizer	bar	43	43
$\hat{H}_{EC,\,BR}$	Enthalpy at the inlet of the economizer	kJ/kg	945	810

2.2.5 Steam Turbine

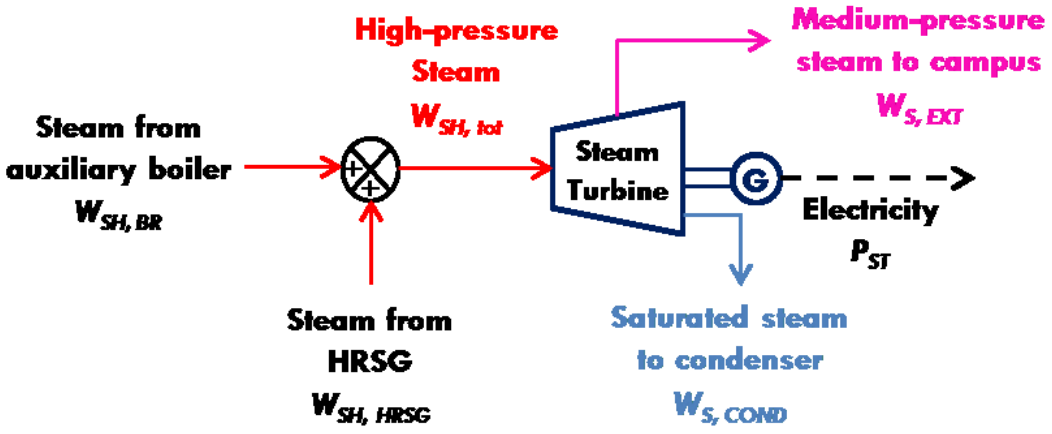

Figure 2.5: Schematic of the steam turbine.

A mass balance on the superheated steam header yields the throttling steam flow $W_{S,\,THR}$ entering the extraction steam turbine:

$$W_{S,\,THR} = W_{SH,\,HRSG} + W_{SH,\,BR} \tag{2.15}$$

This combined steam output is throttled through the steam turbine, generating additional electricity (see Figure 2.5 for the steam turbine schematic). The medium pressure steam is removed from the turbine and sent to campus to meet the heating demand. The rest of the steam that is not extracted is expanded in a number of stages and exits near saturated vapor conditions. The net energy supplied to the steam turbine P_{ST} is computed by applying mass and energy balances on the steam turbine as follows:

$$P_{ST} = \eta_{ST}\left(W_{S,\,THR}\cdot\hat{H}_{S,\,THR} - W_{S,\,EXT}\cdot\hat{H}_{S,\,EXT} - W_{S,\,COND}\cdot\hat{H}_{S,\,COND}\right) \tag{2.16}$$

subject to

$$W_{S,\,COND} = W_{S,\,THR} - W_{S,\,EXT} \tag{2.17}$$

$$\hat{H}_{S,\,COND} = q\cdot\hat{H}^{v}_{sat'd} + (1-q)\cdot\hat{H}^{l}_{sat'd} \tag{2.18}$$

where η_{ST} is the steam turbine efficiency, $W_{S,\,EXT}$ is the extraction steam flow, $W_{S,\,COND}$ is the condensate flow, and q is the vapor quality of the condensate. Table 2.5 summarizes the nominal values of the model parameters shown in (2.16)-(2.18).

Table 2.5: Steam turbines.

Symbol	Description	Unit	Value	
			ST7	ST9
$P_{n,\,ST}$	Steam turbine power output	MW_e	25	25
$\hat{H}_{S,\,THR}$	Enthalpy of the throttle steam	kJ/kg	3,197	3,198
$\hat{H}_{S,\,EXT}$	Enthalpy of the extraction steam	kJ/kg	3,060	3,052
$\hat{H}^{v}_{sat'd}$	Enthalpy of the saturated vapor	kJ/kg	2,567	2,567
$\hat{H}^{l}_{sat'd}$	Enthalpy of the saturated liquid	kJ/kg	153	153
$\hat{H}_{S,\,COND}$	Enthalpy of the condensate	kJ/kg	2,326	2,326
q	Vapor quality	-	0.9	0.9

2.3 MODEL VALIDATION

We validate the models using hourly measured data, which are obtained from the Department of Utility and Energy Management at UT Austin [80]. The goodness of fit (R^2) is used to quantify the quality of the models.

The model parameters (η_t and η_c) of gas turbines were estimated by applying least mean squares (LMS) nonlinear regression algorithm to match the generated power P_{GT} with the developed models. Figure 2.6 shows the power output match for the two gas turbines. Estimated model parameters with 95% confidence intervals and the goodness of fit of gas turbines are summarized in Table 2.6.

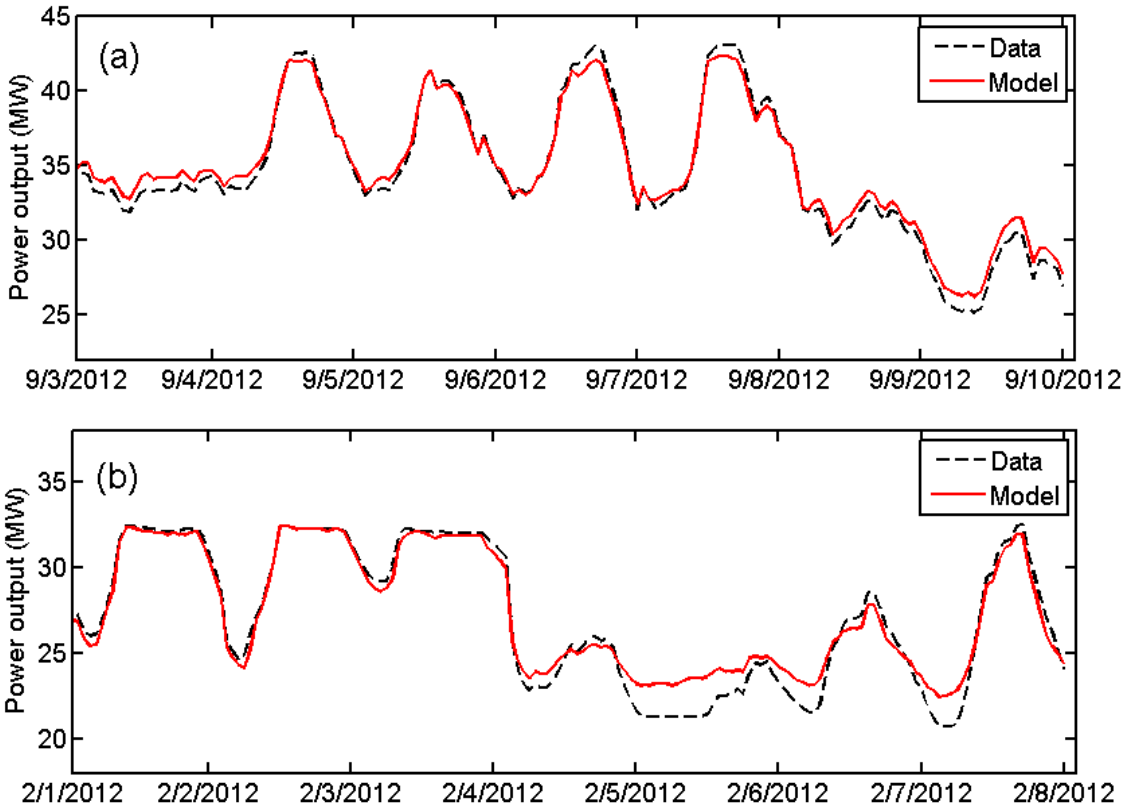

Figure 2.6: Data vs. model prediction of power outputs: (a) GT8, (b) GT10

Table 2.6: Model parameter estimates of the gas turbines.

Symbol	Description	Unit	Value	
			GT8	GT10
η_T	Turbine efficiency	%	90.3 ± 0.01[a]	80.0 ± 0.17[a]
η_C	Compressor efficiency	%	80.7 ± 0.07[a]	86.5 ± 0.06[a]
R^2	Goodness of fit	-	0.981	0.953

[a] 95% confidence intervals

As seen in Figure 2.6 the model fits the data well with large R^2 values for both GT8 and GT10 except during the time between February 5th and 7th for GT10. This discrepancy was caused by the fact that the fuel flow measurement device in GT10 is inaccurate at low flow rates. The fuel flow rates were overestimated than the actual ones

when the power outputs were lower than 24 MW. However, the 95% confidence intervals of the model estimates are narrow enough to conclude the regression coefficients are statistically significant.

Hourly data over a period of one week are plotted for HRSG8 and HRSG10 in Figure 2.7 illustrating the quality of the model fits compared to data. Estimated model parameters (α_{HRSG} and β_{HRSG}) with 95% confidence intervals and R^2 values of the HRSG model are listed in Table 2.7.

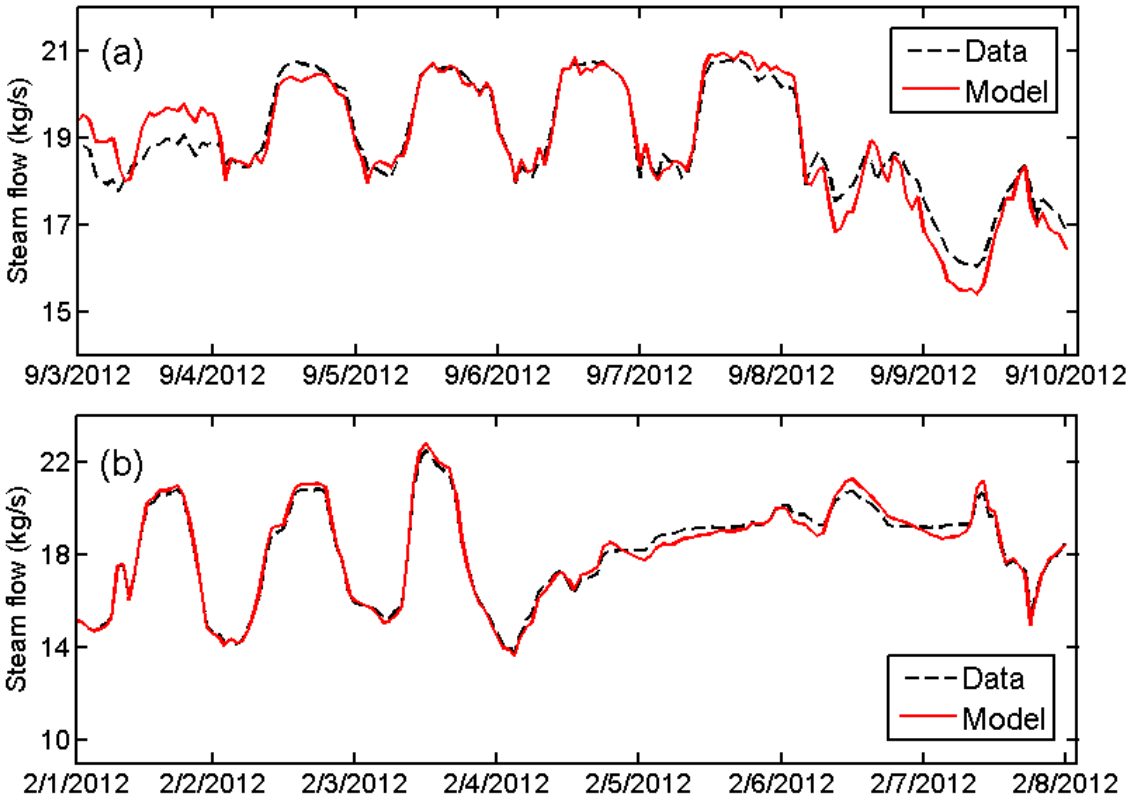

Figure 2.7: Data vs. model prediction of steam flows: (a) HRSG8, (b) HRSG10

Table 2.7: Model parameter estimates of the gas turbines.

Symbol	Description	Unit	Value	
			HRSG8	HRSG10
α_{HRSG}	$\eta_{HRSG} \cdot C_{ph}$	kJ/kg·K	1.27 ± 0.01[a]	0.819 ± 0.01[a]
β_{HRSG}	$\eta_{HRSG} \cdot \eta_{HRSG,\ comb} \cdot LHV$	kJ/kg	30,344 ± 4,987[a]	54,507 ± 783[a]
R^2	Goodness of fit	-	0.900	0.986

Notes: $\eta_{HRSG,\ comb}$ is the duct burner combustion efficiency. η_{HRSG} is the overall HRSG efficiency.
[a] 95% confidence intervals

The high R^2 values indicate good model fits. Narrow confidence intervals of the model parameters indicate that the regression coefficients are precisely estimated.

Regression results for the auxiliary boilers (BR3 and BR7) and steam turbines (ST7 and ST9) are plotted in Figures 2.8 and 2.9, respectively. Their estimated model parameters with 95% confidence intervals and R^2 values are summarized in Tables 2.8 and 2.9.

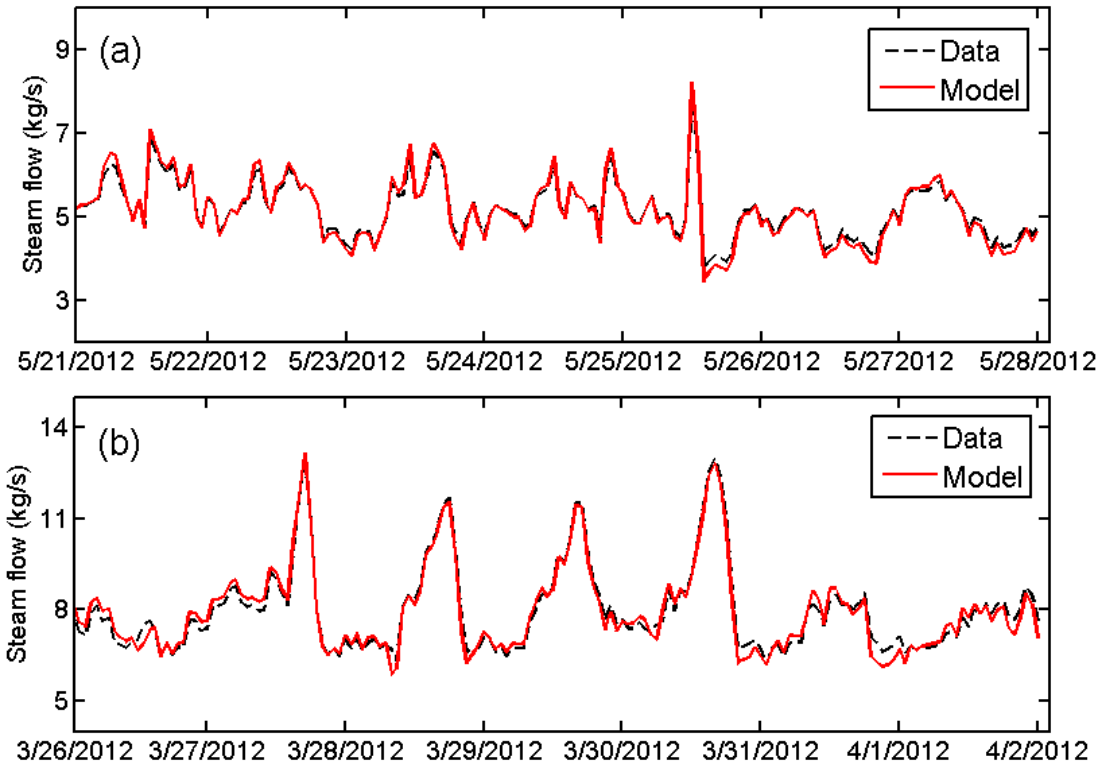

Figure 2.8: Data vs. model prediction of steam flows: (a) BR3, (b) BR7

Table 2.8: Model parameter estimates of the auxiliary boilers.

Symbol	Description	Unit	Value	
			BR3	BR7
α_{BR}	$\eta_{BR} \cdot \rho_{NG} \cdot LHV$	Btu/SCF	983 ± 2.1[a]	951 ± 4.5[a]
R^2	Goodness of fit	-	0.967	0.969

Notes: η_{BR} is the boiler efficiency. ρ_{NG} is the density of natural gas.
[a] 95% confidence intervals

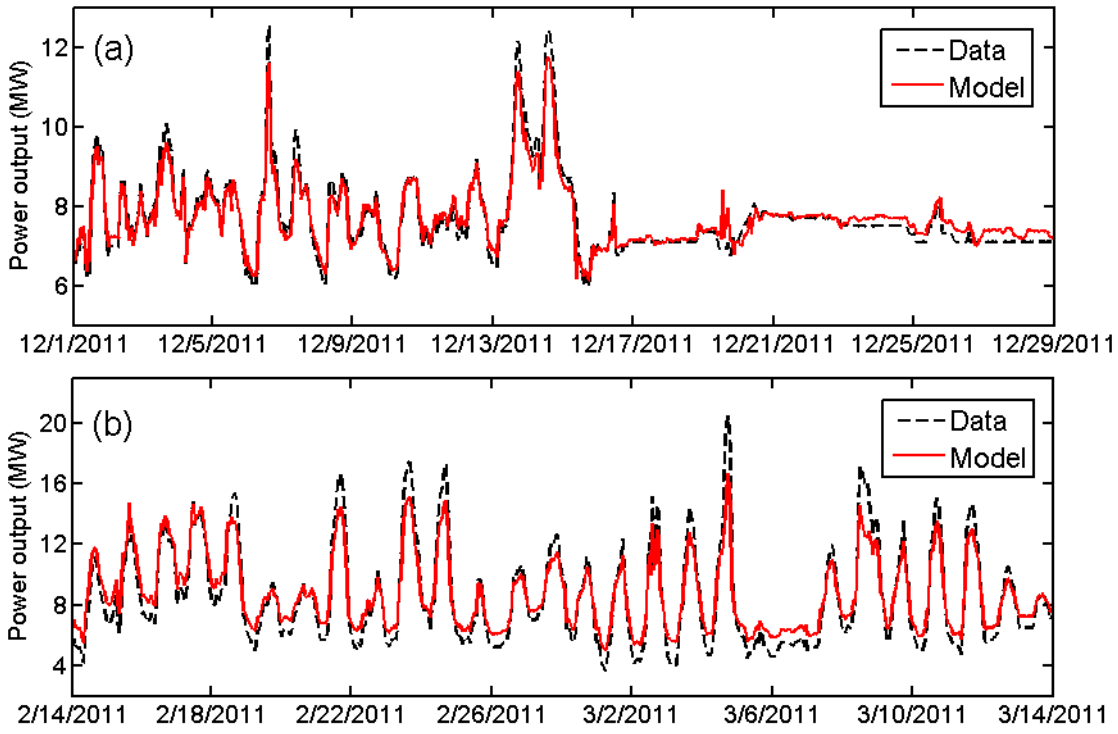

Figure 2.9: Data vs. model prediction of power outputs: (a) ST7, (b) ST9

Table 2.9: Model parameter estimates of the steam turbines.

Symbol	Description	Unit	Value	
			ST7	ST9
η_{ST}	Steam turbine efficiency	%	89.9 ± 0.06[a]	97.0 ± 0.17[a]
R^2	Goodness of fit	-	0.938	0.901

[a] 95% confidence intervals

The quality of the model fits compared to data as well as the high R^2 values indicate excellent model fits.

2.4 SUMMARY

In this section, the mathematical models of major pieces of equipment present in a CHP plant (gas turbine, HRSG, auxiliary boiler, and steam turbine) are developed and validated. The first principle models (on an individual component basis) being developed could capture the general trends of plant outputs (power and steam productions) at high accuracy over the entire range of operating conditions. The good model fits lead to meaningful solutions to the optimization formulations.

Chapter 3: Economic Dispatch of Combined Heat and Power Plants

In this section, the mathematical models developed in Chapter 2 are applied to the day-ahead wholesale energy market to evaluate three objectives: (1) maximizing revenue by selling/buying power (referred to as "Case 1"), (2) maximizing revenue by selling power only (referred to as "Case 2"), and (3) maximizing energy efficiency without participating in the wholesale energy markets (referred to as "Case 3"). The resulting problems are complex optimization problems because all the pieces of equipment present in a CHP plant are inter-related, i.e., the outputs of some components become the inputs of others.

3.1 Nonlinear Programming Formulation

In Cases 1 and 2, the objective is to maximize the net income of the CHP plant by participating in the day-ahead electricity market:

$$\max_{X_{C,t}} J = \sum_{t \in T} \left(C_{e,t}^{DAM} \cdot P_t^{DAM} - C_{e,t}^{DAM} \cdot \Delta P_{TIAC,t} - C_f \cdot W_{f,tot,t} \right) \cdot \Delta t \quad (3.1)$$

where

$$P_t^{DAM} = P_{GT,t} + P_{ST,t} - L_{E,t}, \quad \forall t \in T \quad (3.2)$$

$$\Delta P_{TIAC,t} = \frac{\Delta H_{TIAC,t}}{COP}, \quad \forall t \in T \quad (3.3)$$

$$W_{f,tot,t} = W_{f,GT,t} + W_{f,HRSG,t} + W_{f,BR,t}, \quad \forall t \in T \quad (3.4)$$

The objective function defined in (3.1) is the net income of a CHP plant including the revenue of selling/buying power to/from the grid, the cost associated with additional cooling from electrically-powered chillers due to the use of the TIAC system, and total fuel cost, where $C_{e,t}^{DAM}$ is the day-ahead electricity price at hour t, C_f is the fixed fuel cost, and Δt is the sampling rate. Equation (3.2) defines the power output accepted by the ISO at hour t in the day-ahead energy market (P_t^{DAM}), where $L_{E,t}$ is the electric load at the corresponding hour. In some cases, P_t^{DAM} can be negative (i.e., during the off-peak hours, it is more economical to buy the power from the wholesale electricity market rather than to self-generate). Equation (3.3) relates the cooling load of a gas turbine inlet air cooling system ($\Delta H_{TIAC,t}$) to the power consumption of an electrically-powered chiller at hour t ($\Delta P_{TIAC,t}$). The total fuel flow in the system at hour t ($W_{f,tot,t}$) is defined in (3.4).

In Case 3, the first term on the RHS in (3.1) is ignored as the plant does not participate in the wholesale energy markets ($P_t^{DAM} = 0$):

$$\min_{X_{C,t}} J = \sum_{t \in T} \left(C_{e,t}^{DAM} \cdot \Delta P_{TIAC,t} + C_f \cdot W_{f,tot,t} \right) \cdot \Delta t \tag{3.5}$$

In this case, the objective is to minimize the operating costs of the CHP plant.

The problems posed above ((3.1) and (3.5)) are NLP problems solved by changing a set of continuous decision variables (X_C). Table 3.1 summarizes the lower and upper bounds for the X_C.

Table 3.1: Constraint limits on continuous decision variables (X_C).

Decision variable	Unit	Bound	
		Lower	Upper
$F_{d,\ GT8}$, $F_{d,\ GT10}$	pu[a]	-0.1	1.5
$\theta_{IGV,\ GT8}$, $\theta_{IGV,\ GT10}$	degrees	52.2	88
$V_{w,\ TIAC,\ GT8}$	GPM	0	2,695
$V_{w,\ TIAC,\ GT10}$	GPM	0	1,902
$W_{f,\ HRSG8}$	kg/s	0	0.630
$W_{f,\ HRSG10}$	kg/s	0	0.583
$W_{f,\ BR3}$	kg/s	0.138	N/A
$W_{f,\ BR7}$	kg/s	0.254	N/A
$W_{S,\ EXT,\ ST7}$, $W_{S,\ EXT,\ ST9}$	kg/s	see (3.8)	see (3.8)

Note: Inequality constraints are imposed on the decision variables for all three case studies.
[a] per unit value

In Case 2, in addition to the constraints on the decision variables, (3.1) is also subject to satisfying the campus loads. In order to meet the electric load, (3.6) is proposed to ensure that the total electric power generated from the system is greater than the campus electric load (L_E).

$$L_{E,\ t} \leq P_{GT,\ t} + P_{ST,\ t}, \quad \forall t \in T \tag{3.6}$$

In Case 3, (3.6) is replaced by (3.7) to ensure that the power generation meets the campus electric loads at all times:

$$L_{E,\ t} = P_{GT,\ t} + P_{ST,\ t}, \quad \forall t \in T \tag{3.7}$$

In all case studies, the extraction steam flow ($W_{S,\ EXT}$) must be greater than the campus heating load (L_H) but is restricted to be less than the throttling steam flow in a steam turbine ($W_{S,\ THR}$), ensuring the mass balance on a steam turbine is not violated:

$$L_{H,\ t} \leq W_{S,EXT,\ t} \leq W_{S,THR,\ t}, \quad \forall t \in T \tag{3.8}$$

In addition to meeting the loads (electric loads in Cases 2 and 3 and heating loads in Cases 1, 2, and 3), the system is subject to a number of system operating constraints as follows:

$$T_c^{min} \le T_{c,\,t}, \quad \forall t \in T \tag{3.9}$$

$$P_{GT}^{min} \le P_{GT,\,t}, \quad \forall t \in T \tag{3.10}$$

$$T_{e,\,t} \le T_e^{ref}, \quad \forall t \in T \tag{3.11}$$

$$T_{f,\,t} \le T_f^{ref}, \quad \forall t \in T \tag{3.12}$$

$$T_{SH,\,HRSG} + \Delta T_{HRSG}^{min} \le T_{e,\,HRSG,\,in,\,t}, \quad \forall t \in T \tag{3.13}$$

$$W_{SH,\,HRSG,\,t} \le W_{SH,\,HRSG}^{max}, \quad \forall t \in T \tag{3.14}$$

$$W_{SH,\,BR}^{min} \le W_{SH,\,BR,\,t} \le W_{SH,\,BR}^{max}, \quad \forall t \in T \tag{3.15}$$

$$P_{\mathrm{ST}}^{min} \le P_{\mathrm{ST},\,t} \le P_{\mathrm{ST}}^{max}, \quad \forall t \in T \tag{3.16}$$

The lower limit on T_c in (3.9) is specified to be 7 °C to avoid the risk of freezing at the intake of the compressor [88]. Equation (3.10) ensures that the gas turbine power output is kept greater than its technical minimum (40% of its rated power output). Equation (3.11) enforces the maximum gas turbine's exhaust gas temperature so as not to damage the gas turbine [92]. In order to regulate Nitrogen Oxide (NOx) emissions, the turbine's

firing temperature also needs to be kept lower than a specified upper limit as shown in (3.12). The gas temperature entering the HRSG after duct burning must remain above the superheated steam temperature by a minimum differential (see (3.13)). The HRSG (3.14) and boiler (3.15) steam flows are constrained with lower and upper bounds. The steam turbine power output must also remain within bounds as shown in (3.16). Note that the upper bound on P_{GT} is dropped since it is bounded indirectly due to (3.11) or (3.12).

3.2 CASE STUDIES

The optimal operating strategies obtained by solving (3.1) for Cases 1 and 2, and (3.5) for Case 3 are compared with historical operating schedule (referred to as "base case") for 2 simulated time periods: (1) from February to November in 2011 and (2) from January to December in 2012. The two-month time periods (January and December) in 2011 are excluded in the analysis due to bad quality of data. When estimating the net incomes, savings in operating costs, and fuel costs, the electrical and heating loads on an annual basis, the January and December values are assumed to be the same as those in November. Required data that are not listed in Tables 2.2-2.4 in Chapter 2 are provided in Table 3.2.

Table 3.2: Parameter values used in the case studies.

Symbol	Description	Unit	Value
P_{GT8}^{min}	Minimum power output from GT8	MW_e	16.8
P_{GT10}^{min}	Minimum power output from GT10	MW_e	12.9
P_{ST7}^{min}	Minimum power output from ST7	MW_e	6
P_{ST9}^{min}	Minimum power output from ST9	MW_e	6
$W_{SH,\,BR3}^{min}$	Minimum steam output from BR3	kg/s	2.90
$W_{SH,\,BR7}^{min}$	Minimum steam output from BR7	kg/s	5.67
T_c^{min}	Minimum compressor inlet air temperature	°C (or K)	7
ΔT_{HRSG}^{min}	Minimum temperature differential in HRSG8	°C (or (K)	8
ε	Effectiveness of a heat transfer	-	0.9
MW_{air}	Molecular weight of air	g/mol	28.96
R_g	Ideal gas constant	J/mol·K	8.314
COP_8	Coefficient of performance of a chiller from May to October	MW_{th}/MW_e	6
COP_{10}	Coefficient of performance of a chiller from November to April in the following year	MW_{th}/MW_e	10
ρ_W	Density of water	kg/m^3	999.97
ρ_{NG}	Density of natural gas	lb/SCF	0.0438
$C_{f,\,2011}$	Fuel price in 2011	$/MMBtu	5.12
$C_{f,\,2012}$	Fuel price in 2012	$/MMBtu	3.96

Assumptions for the case studies are as follows:

(1) Operation and maintenance (O&M) costs are constant regardless of the operational strategy and do not affect the solution outcome.

(2) Accurate forecasting models for the loads and day-ahead electricity prices are available in advance.

(3) A price-taker producer is considered, i.e., a producer whose market actions do not alter the market clearing prices.

(4) The wholesale power prices are constant regardless of the fuel price, i.e., the fuel prices do not drive the wholesale electricity prices.

3.2.1 Case 1: Maximizing Revenue by Selling/Buying Power

In Case 1, the objective is to maximize the net income of the CHP plant by participating in the day-ahead energy market. Figure 3.1(a) compares the optimized total power production rates with historical power production rates (base case) on May 28, 2011. Figure 3.1(b) shows the day-ahead electricity prices during the corresponding hours, in the Austin Load Zone of the ERCOT grid. Optimized steam production rates vs. historical steam production rates (base case) are shown in Figure 3.2.

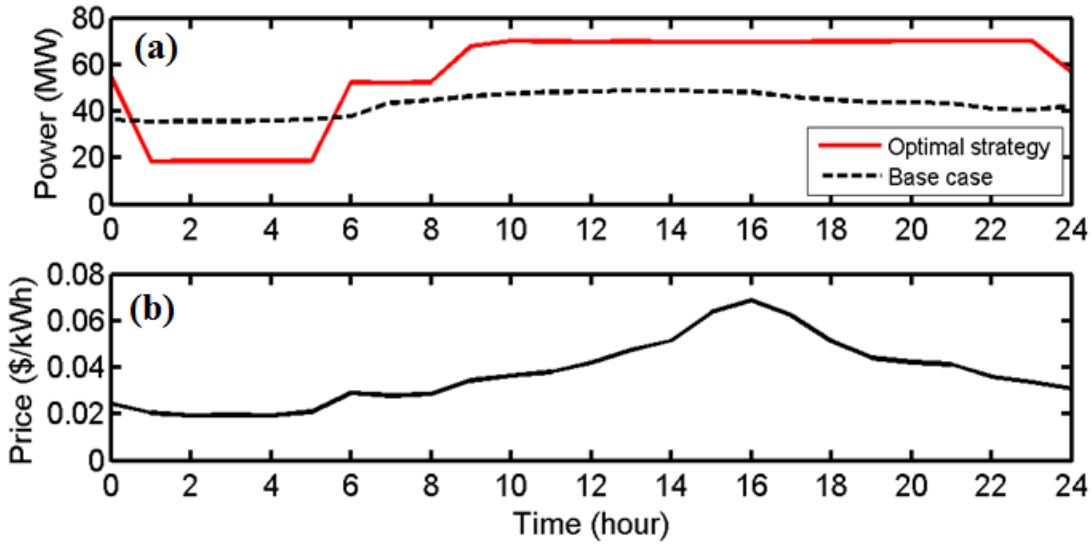

Figure 3.1: Case 1 results for May 28, 2011 – (a) total power outputs, (b) day-ahead electricity prices

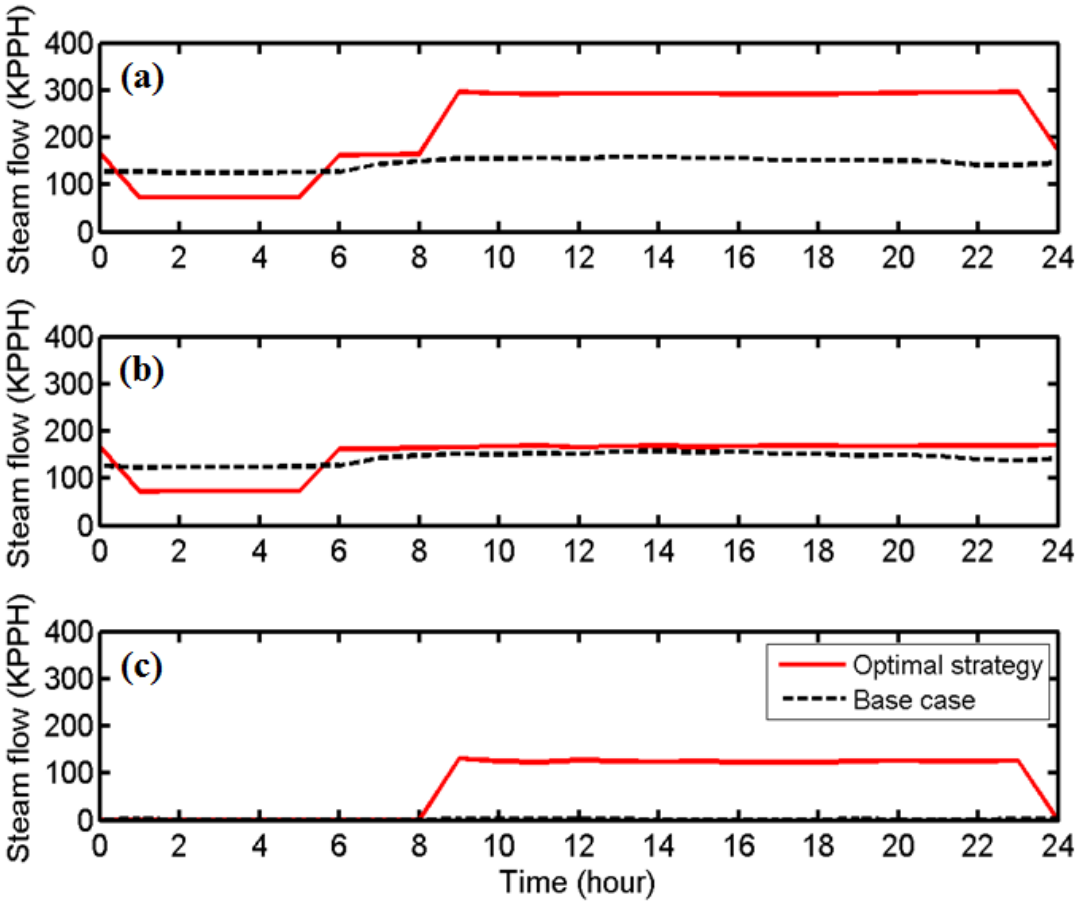

Figure 3.2: Case 1 results for May 28, 2011 – (a) total steam flow, (b) HRSG steam flow, (c) boiler steam flow

In hours 1-5, the total power production was limited to its technical minimum as it would have been more economical to buy the deficit power (difference between the power output in base case and that in Case 1) from the grid at off-peak electricity tariffs rather than to self-generate. In hours 6-8, the results show that the plant could increase the net income by selling the extra power to the grid when the electricity prices were above about \$0.03/kWh. In hours 9-23, the power production was maximized (67 MW_e), owing to high electricity prices of the late afternoon hours during the summer months (from May to October) in the ERCOT grid. Figure 3.2 witnesses that the overall HP

steam flow directed to the steam turbine has been maximized during the on-peak hours (hours 9-23), resulting in an increase in the power outputs from the steam turbine and bringing additional profits from electricity sales. The suggested plant's operating scheme was repetitive on a daily basis throughout the year (both in 2011 and 2012).

3.2.2 Case 2: Maximizing Revenue by Selling Power

In Case 2, the objective is to maximize the net income of the CHP plant by selling surplus power to the grid (buying power from the grid is not allowed). Figure 3.3(a) compares the optimized total power production rates with historical power production rates (base case) on May 28, 2011. Optimized steam production rates vs. historical steam production rates (base case) are shown in Figure 3.4. In Case 2, the results are similar to those observed in Case 1, except the plant did not buy the power from the grid during the off-peak hours (hours 1-8) but met the campus electric load.

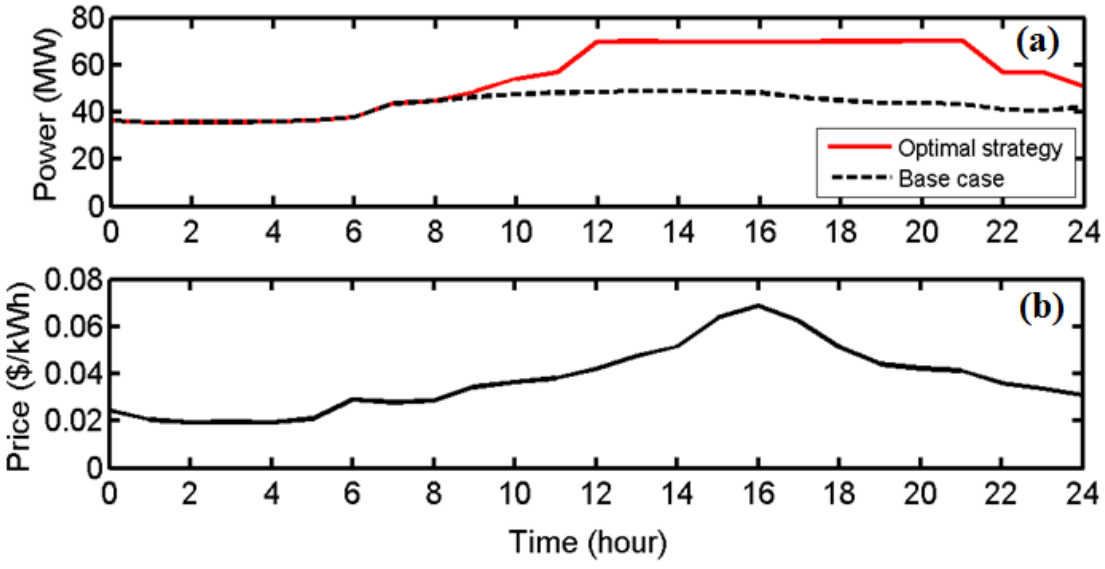

Figure 3.3: Case 2 results for May 28, 2011 – (a) total power outputs, (b) day-ahead electricity prices

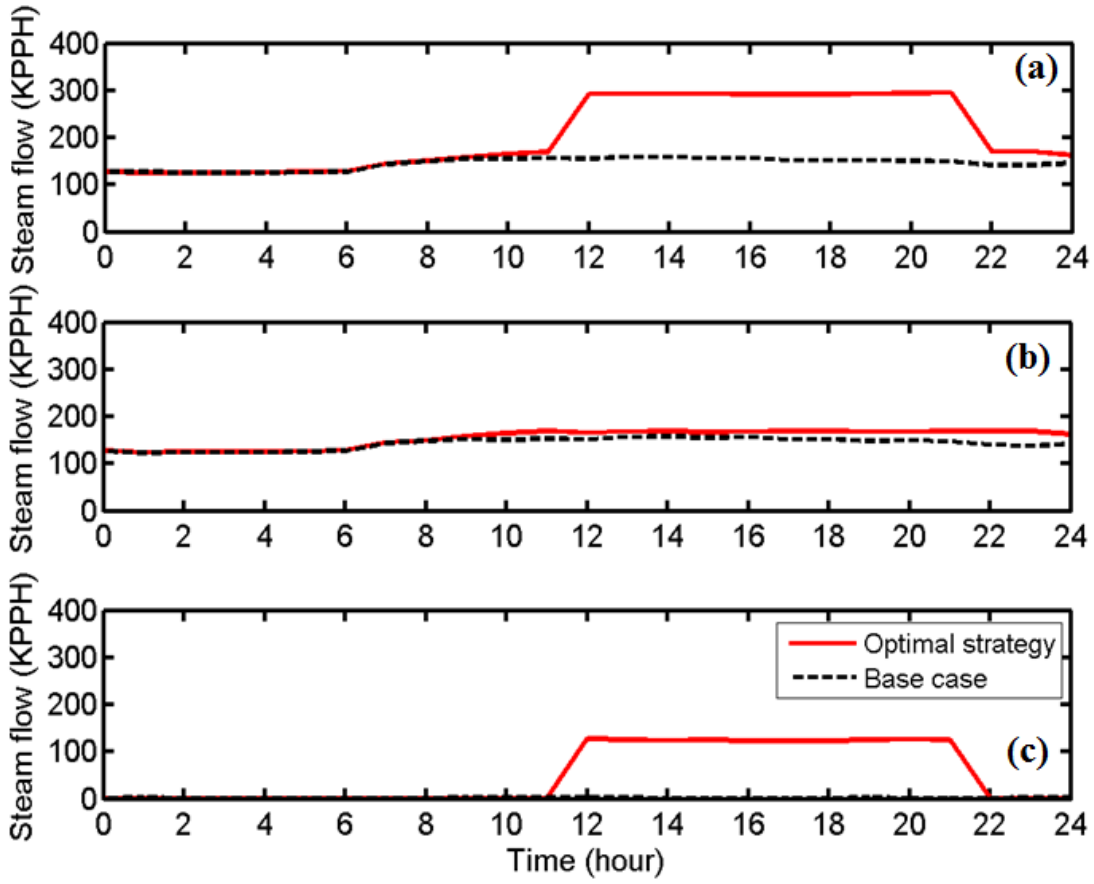

Figure 3.4: Case 2 results for May 28, 2011 – (a) total steam flow, (b) HRSG steam flow, (c) boiler steam flow

The annual power production schedules based on the optimal strategy are presented in Figure 3.5(a) and the day-ahead electricity prices for the year 2012 are shown in Figure 3.5(b). Figure 3.5 witnesses that electricity sales are highly recommended when electricity prices are high (especially from April to September), at which high profits are expected for wholesale market participants.

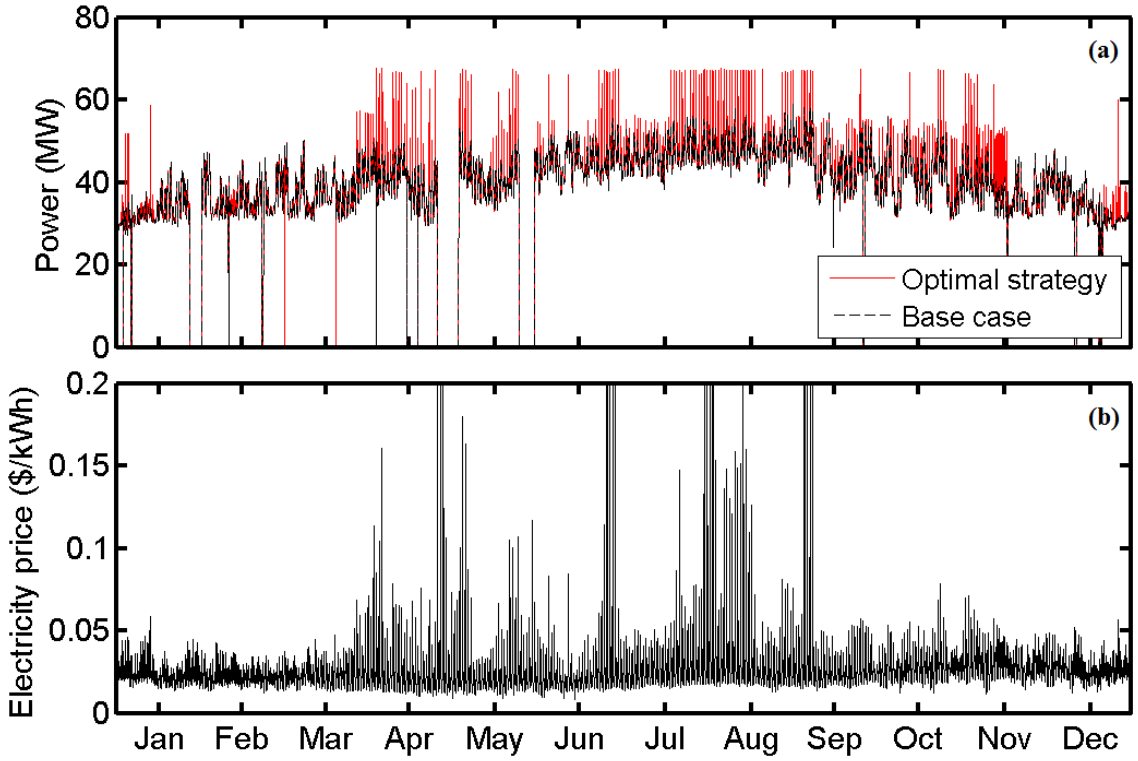

Figure 3.5: Case 2 results for year 2012 – (a) total power outputs, (b) day-ahead electricity prices. Optimized power outputs (red solid line) are highly correlated to the day-ahead electricity prices.

3.2.3 Case 3: Maximizing Energy Efficiency without Participating in the Wholesale Energy Markets

In Case 3, the goal is to determine a schedule of local energy production that minimizes the costs of providing the electrical and heating loads without participating in the wholesale energy markets. The results are shown in Figure 3.6 (power production) and Figure 3.7 (steam production).

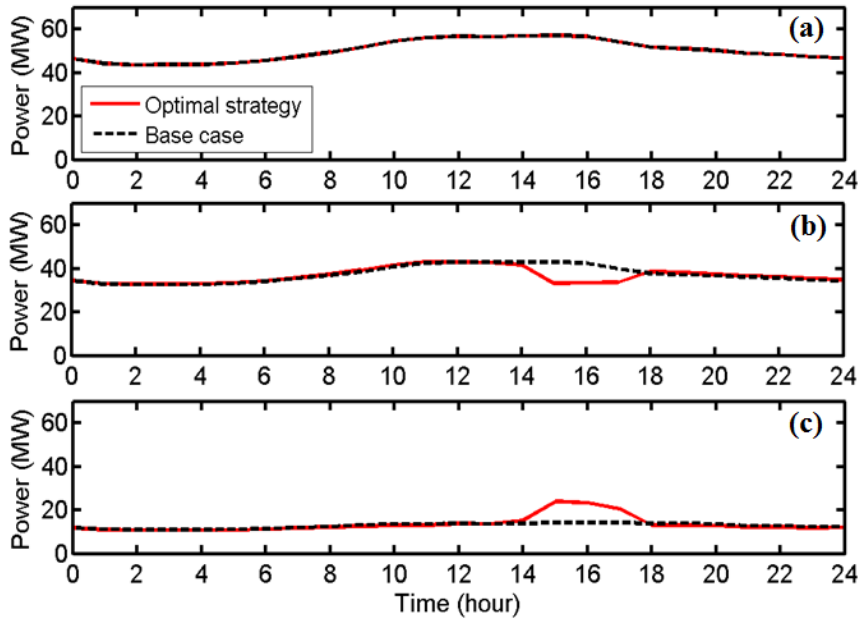

Figure 3.6: Case 3 results for August 22, 2011 – (a) total power outputs, (b) gas turbine power outputs, (c) steam turbine power outputs

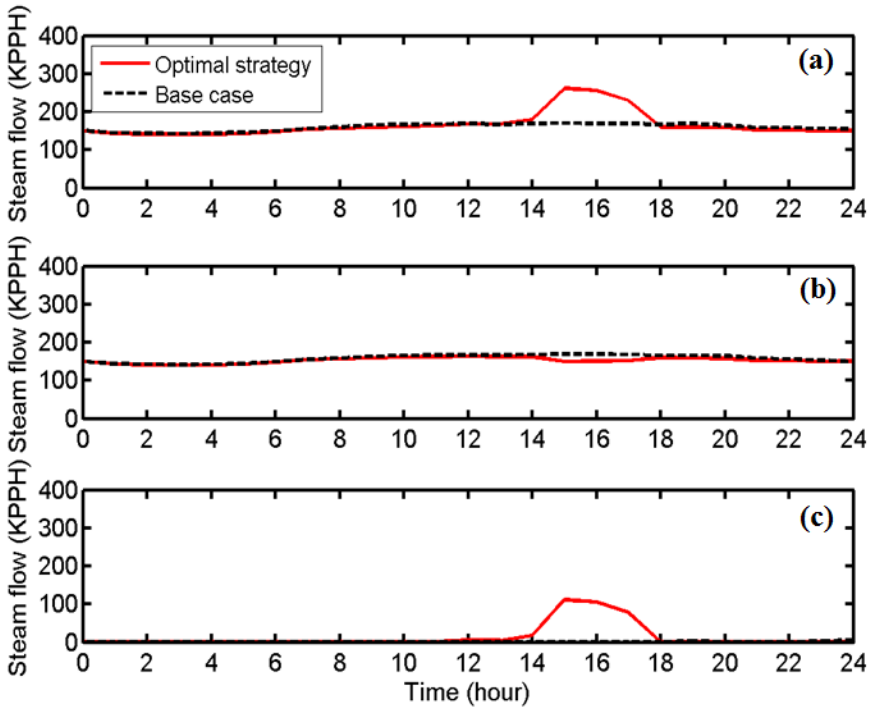

Figure 3.7: Case 3 results for May 28, 2011 – (a) total steam flow, (b) HRSG steam flow, (c) boiler steam flow

In hours 1-14 and 18-24, the optimized total power outputs (Figure 3.6(a)), gas turbine power outputs (Figure 3.6(b)), and steam turbine power outputs (Figure 3.6(c)) were the same as those observed in base case. In hours 15-17, the power outputs from the gas turbine were reduced and the steam turbine made up the deficit power. During these hours, the plant was able to generate the same power outputs at lower operating costs through the optimal allocation of the total power among the gas turbine (GT8) and steam turbine (ST9). Similar results in terms of the steam production were observed as seen in Figure 3.7.

Table 3.3 summarizes the total yearly cost for each case study performed for the year 2011. Figure 3.8 shows the same results as histograms.

Table 3.3: Summary of the cases studies performed for year 2011.

Scenarios	Operating costs ($ million)	Net income ($ million)	Net income (%)
Base case	**16.0[b]**	-	-
Case 1: sell/buy power	**12.6**	**3.42 (2.23[a])**	**21.4 (14.0[a])**
Case 2: sell power only	**13.7**	**2.34**	**14.6**
Case 3: No power sales or purchases	**15.7**	**0.27**	**1.7**

[a] net income by selling power to the grid
[b] net income in January and December are assumed to be the same as those in November

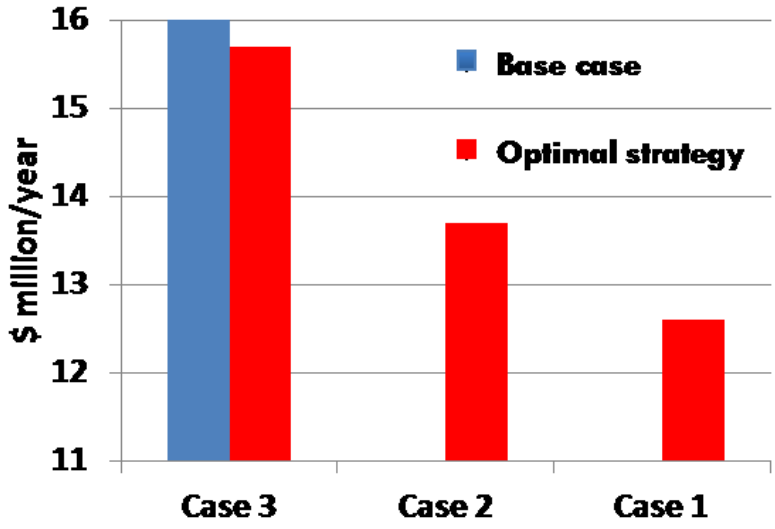

Figure 3.8: Annual operating costs for year 2011 for Cases 1, 2, and 3.

In Case 3, the plant could reduce annual operating costs by 1.7% (or $0.27 million per year) through the optimal allocations of the total power and total steam. The fact that only a marginal benefit was resulted in Case 3 indicates that the current operating scheme of the power plant at UT Austin campus is close its optimal operating scheme. In Case 2, revenue from selling surplus power helped to significantly offset an additional fuel costs, resulting in annual net income of $2.34 million (14.6% of the base case operating costs). As in Case 1, when power could be bought/sold from/to the grid, the net income was further increased. For instance, in Case 1, the simulated results show that the plant could achieve annual net income of $3.42 million (21.4% of the base case operating costs), of which $2.23 million (about two-thirds of the net income) came from by selling surplus power to the grid during the on-peak hours when electricity prices are highest, and the remainder came from the buying cheap power from the grid during the off-peak hours. While the gas and steam turbines must still be run to meet heating loads, their power productions were minimized by supplementing the electrical generation with imported power.

Figure 3.9 shows the monthly operating costs for Case 1 presented in histograms and Figure 3.10 represents the corresponding average electricity prices.

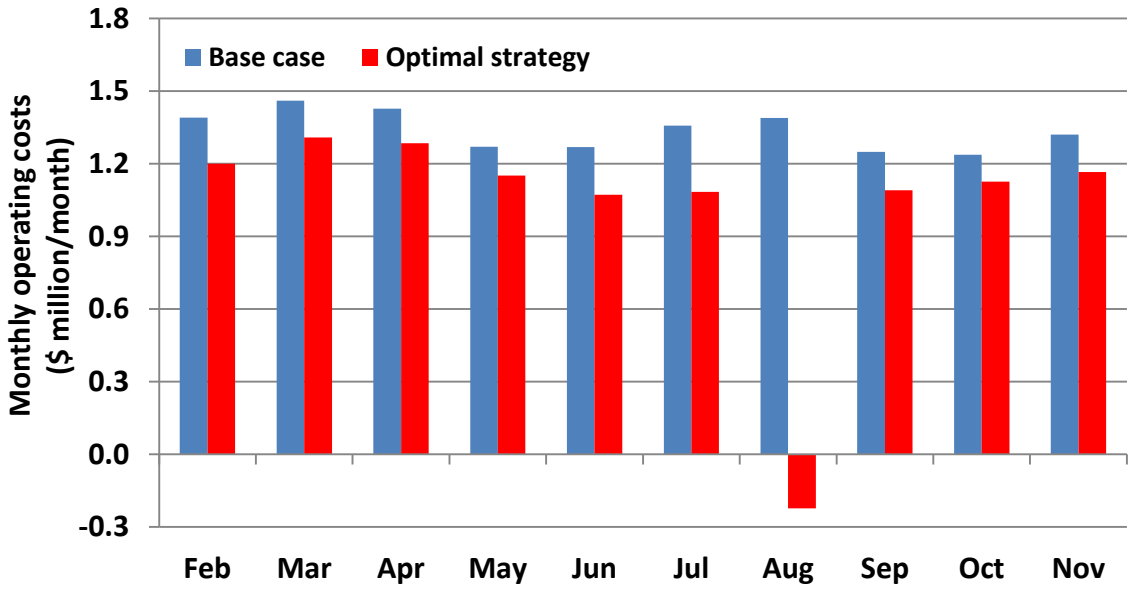

Figure 3.9: Case 1 results for year 2011 - monthly operating costs.

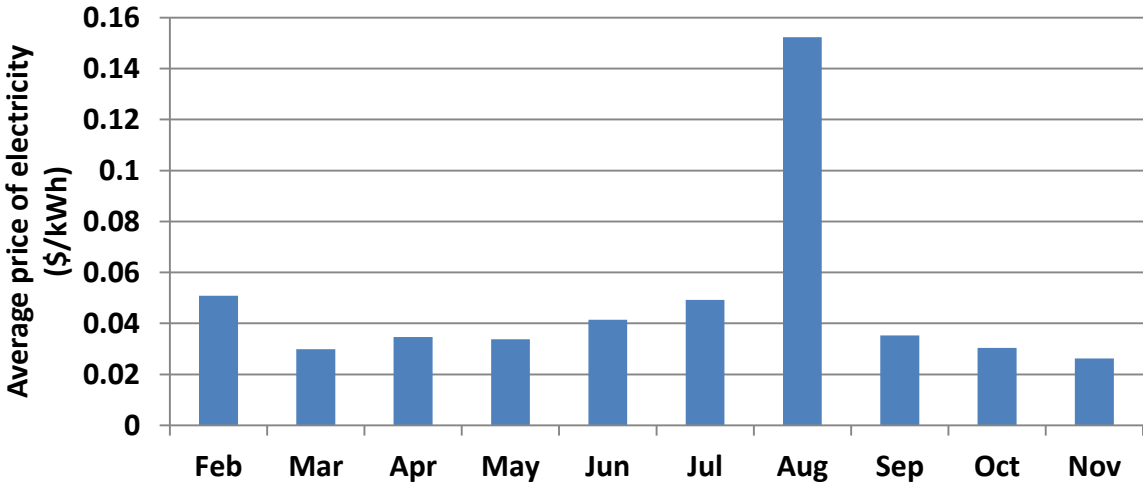

Figure 3.10: Average monthly day-ahead electricity prices for year 2011.

The results imply that higher overall profits are expected when electricity prices are higher as the profit by selling power at expensive on-peak rates outweighs that by

buying cheap power. Especially, in August, the highest monthly net income was observed ($1.61 million), which was about half of the annual net income, owing to extremely high electricity prices (average price of $0.15/kWh) observed in the corresponding month.

The same case studies were performed using 2012 historical data and day-ahead electricity prices, of which the ranges represent typical values. The optimized results are summarized in Table 3.4 and graphically represented in Figure 3.11.

Table 3.4: Summary of the cases studies performed for year 2012.

Scenarios	Operating costs ($ million)	Net income ($ million)	Net income (%)
Base case	**13.4**	**-**	**-**
Case 1: sell/buy power	**12.0**	**1.4 (0.71[a])**	**10.8 (5.3[a])**
Case 2: sell power only	**12.4**	**1.0**	**7.5**
Case 3: No power sales or purchases	**12.9**	**0.5**	**3.7**

[a] net income by selling power to the grid

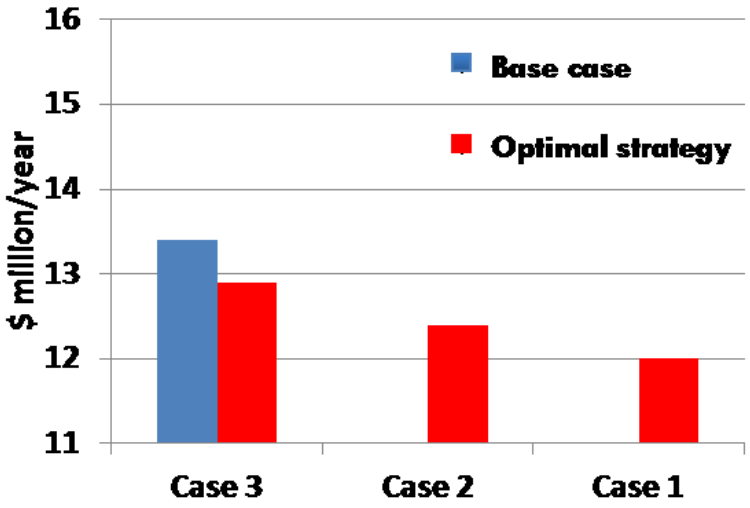

Figure 3.11: Annual operating costs for year 2012 for Cases 1, 2, and 3.

In comparison to the results obtained when 2011 historical data were used, annual net incomes calculated based on 2012 historical data were relatively lower, i.e., $1.4 million and $1.0 million for Case 1 and Case 2, respectively.

To better understand the effects of fuel prices on overall net incomes of the plant, sensitivity analysis was performed using various fuel prices using 2012 historical data. Figure 3.12 shows the optimized power productions under various fuel prices for Case 2 during a May week in 2011. Figures 3.13 and 3.14 show the changes in annual operating costs and net incomes, respectively, as a function of fuel prices.

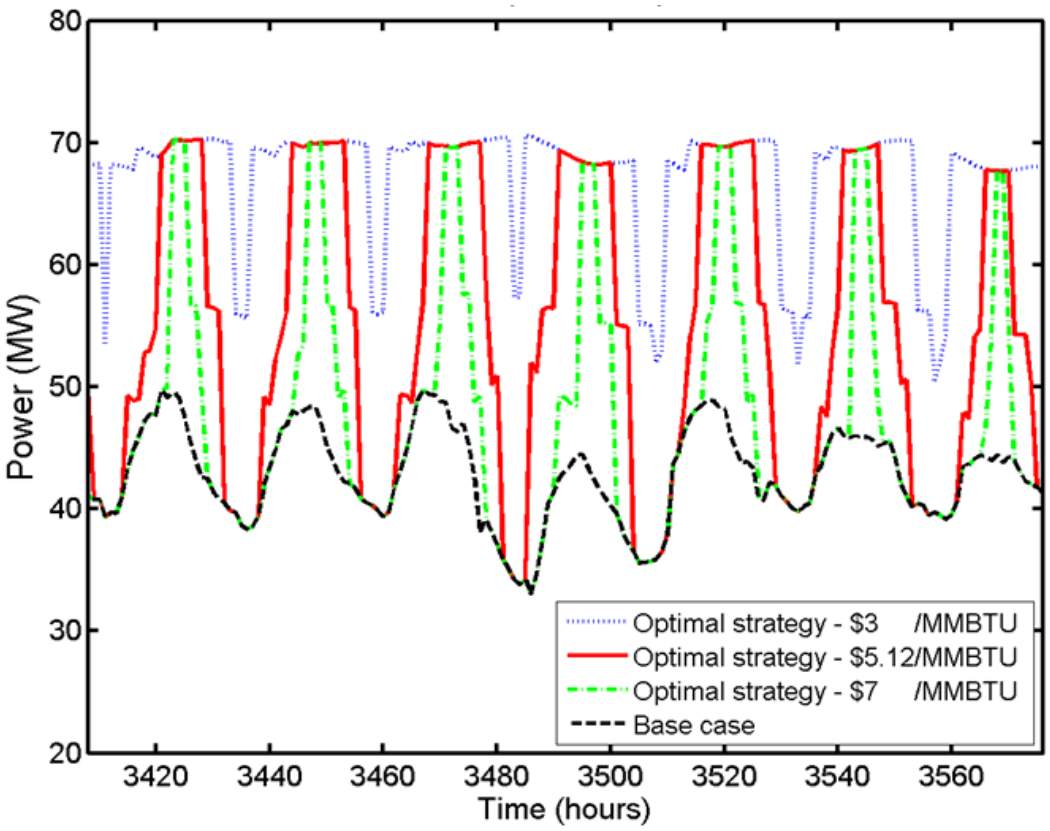

Figure 3.12: Case 2 results for a May week in 2011- optimized power outputs under various fuel prices.

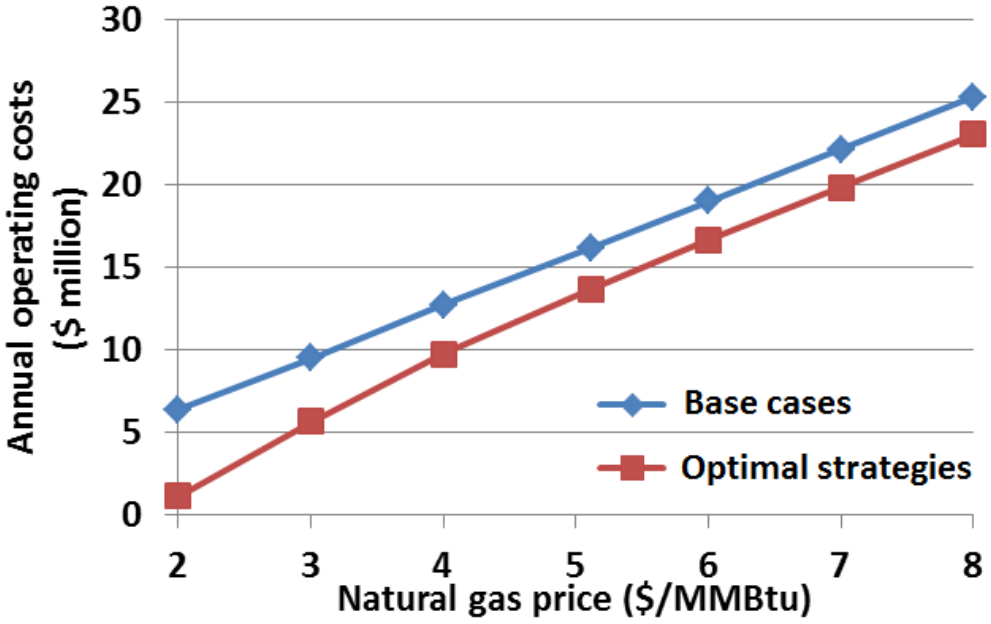

Figure 3.13: Evolution of expected annual operating cost for year 2011 vs. fuel prices.

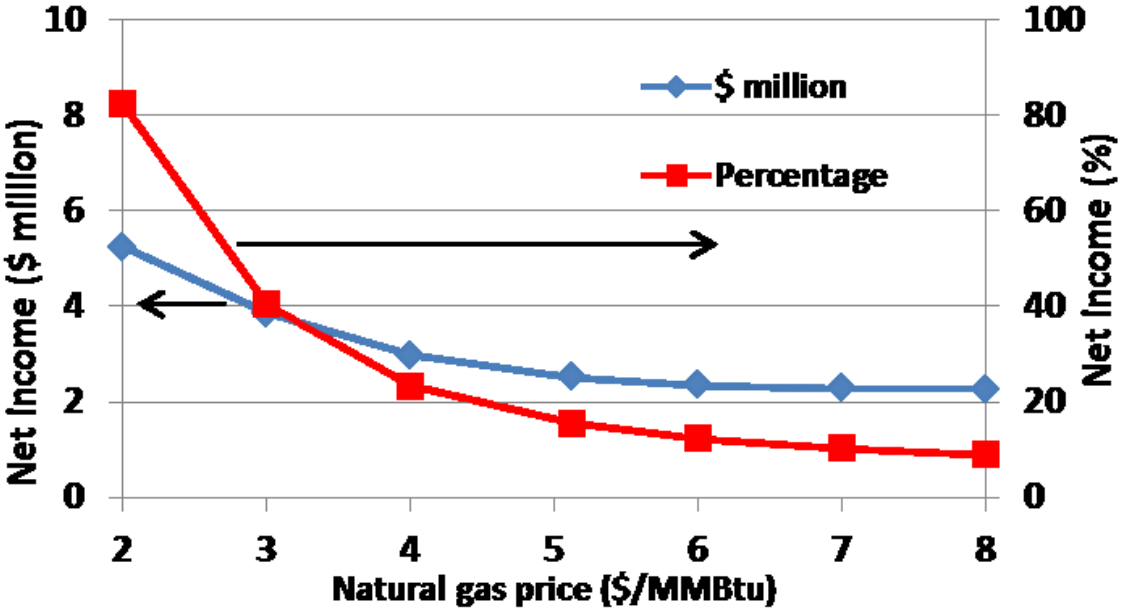

Figure 3.14: Evolution of expected annual net income for year 2011 vs. fuel prices.

In Figure 3.12, when the fuel price was low (i.e., $3/MMBtu), the power production was maximized during the most of the time periods as significant profits by selling extra power to the grid could offset an increased operating costs. As the fuel price increased (i.e., when going from $3/MMBtu to $5.12/MMBtu or/and from $5.12/MMBtu to$7/MMBtu), the amount of electrical energy sold to the grid decreased, resulting in reduced net income.

As seen in Figure 3.13, the plant's annual operating costs for both cases (base case and optimal strategy) increase as the fuel prices increase. But their differences for each fuel-price scenario (see Figure 3.14) decrease as the fuel prices increase. In order words, higher variations in electricity prices (or equivalently lower fuel costs when electricity prices are the same for each fuel-price scenario) allow achieving better economic results.

It should be noted that labor and other operational costs are not included in the costs discussed in this work. Also, the case studies performed in this chapter assume that the system is freely able to exchange electricity with the grid at wholesale market prices. Thus, the scenarios considered are idealized as there may be a number of regulatory hurdles (non-technical) to overcome when exporting/importing power to /from the grid. Nevertheless, the ability to sell/buy power to/from the grid can significantly offset operating costs although there may be regulatory constraints for district energy system freely to do so. From a purely technical point of view, the benefits of participating in the wholesale energy market are straightforward.

3.3 SUMMARY

This chapter has introduced the constrained nonlinear optimization approach to develop an optimal operating strategy for the CHP system in the competitive wholesale

energy markets. The ability to exchange power with the external grid gives the district energy system additional degrees of freedom, allowing it to export surplus power when electricity prices are high and to import when they are low. Ideal objectives (i.e., maximizing revenue by participating in the wholesale energy market or maximum energy efficiency) can be achieved by exploiting these degrees of freedom through optimization. Optimal solutions to the different objective functions provide insight into the best strategies for operating the systems.

Chapter 4: Economic Dispatch of Combined Heat and Power Plants that Provide the Emergency Response Service

The electricity grid experiences short-term, temporary changes in overall capacity even in the best of circumstances. For this reason grid operators and utilities must be prepared to account for contingencies, i.e., power plants or transmission lines that go out of service or unforeseen drastic changes in electric demand. Furthermore, as grid operators and utilities increase their reliance on intermittent renewable energy resources such as solar, photovoltaic, geothermal, and wind power, additional balancing resources are required to address any inconsistencies in power generation. Therefore ancillary services must be continuously sourced from generation or load resources and provided to the electricity grid to ensure the reliable operation of the transmission system and increase grid stability.

4.1 Background

In Texas, ERCOT periodically procures emergency response service (ERS) resources to provide ERS through qualified schedule entities (QSEs). QSEs are able to submit offers to sell and/or bids to buy energy in the wholesale energy markets (the day-ahead market (DAM) and the real-time market (RTM)) on behalf of entities that own or control potential ERS resources, i.e., resource entities (REs) or load serving entities (LSEs) [67]. Thus, they are responsible for settling financially with ERCOT.

ERS providers can receive a capacity payment based on MWs awarded for each hour in the contract periods. The payment to a QSE is made regardless of whether there is a deployment event. Participants may offer to provide the ERS for one or more non-overlapping contract periods. According to Standard Contract Term [96], the current four-month contract periods are as follows:

- February – May
- June – September
- October – January

Table 4.1 summarizes the average capacity payment per unit ERS load (MW) per hour in the ERCOT market during the contract periods from June to September in 2012.

Table 4.1: Capacity payments in the four different business hours in the June to September 2012 contract period.

Business Hours (*hrs* ϵ *BHs*)	**Time periods**	**Total hours (hours[b])**	**Capacity payment**	
			($/MWh[b])	**($/MW[b])**
Business Hours 1 (*BHs1*)	8 AM to 1 PM Monday - Friday[a]	420	8.7	3,654
Business Hours 2 (*BHs2*)	1 PM to 4 PM Monday - Friday[a]	252	9.67	2,437
Business Hours 3 (*BHs3*)	4 PM to 8 PM Monday - Friday[a]	336	9.97	3,350
Non-Business Hours (*NBHs*)	All other hours	1,920	8.83	16,954

[a] except ERCOT holidays
[b] from June to September, 2012

As seen in Table 4.1, the capacity payment is relatively higher during the late afternoon hours (from 1 PM to 8 PM) than the rest of the hours.

ERS providers will be called upon to provide the ERS into the ERCOT in an electric grid emergency for a maximum of 8 hours for each deployment event. If one or more ERS resources exhaust their obligation during a day, the contract period ends that night at midnight for all awarded resources. However, if ERS resources operate at less than 8 hours but greater than 4 hours for the first deployment event, then they are subject to obligation of being called the second time to provide the ERS for an additional 4 hours at maximum if needed. If ERS resources provide the ERS less than 4 hours for the first deployment event, then the remainder of their 8-hour obligation is carried over for the

second possible deployment event. In other words, they will still have a cumulative deployment obligation time of 8 hours prior to a next deployment event.

A QSE may schedule in advance with ERCOT periods of unavailability for an ERS load for up to 2 % of its total committed hours in an ERS contract period. These scheduled periods of unavailability must be communicated to ERCOT by an authorized representative of the QSE representing the ERS load at least five business days prior to the first day of the period of unavailability [96].

4.2 PROBLEM FORMULATION

The NLP model developed in Section 3.1 (Case 2) is adapted in this section. The objective is to maximize the net income of a CHP plant that not only sells surplus power to the grid at wholesale spot market prices but also participates in providing ERS, which is a significant additional income source.

The logic that determines whether to participate in the day-ahead market (DAM) is shown in Table 4.2. Equation (4.1a) states that generation resources (individual or aggregated) do not participate in the DAM because their total electric load will exceed the maximum generation capacity when required to provide the ERS in an electric grid emergency by the contract. They may participate in the RTM if it is profitable to sell surplus power to the grid, especially during the on-peak hours. If the total electric load is less than the maximum generation capacity (4.1b), then generation resources may participate in the DAM.

Table 4.2: Wholesale energy market participation under different logic conditions.

$L_{E,\,t} + L^{sold}_{ERS,\,hrs} \geq \sum_{i \in I} P_i^{max}$ $\Rightarrow$, $\forall t \in T, \quad \forall hrs \in BHs$	If the sum of the local electric load in hour t ($L_{E,\,t}$) and the ERS capacity sold to ERCOT in business hours hrs ($L^{sold}_{ERS,\,hrs}$) is equal to or greater than the maximum available generation capacity, then generation resources do not participate in the DAM.	(4.1a)
$L_{E,\,t} + L^{sold}_{ERS,\,hrs} < \sum_{i \in I} P_i^{max}$ $\Rightarrow$, $\forall t \in T, \quad \forall hrs \in BHs$	If the sum of $L_{E,\,t}$ and $L_{ERS,\,hrs}$ is less than the maximum available generation capacity, then regeneration resources may participate in the DAM.	(4.1b)

If (4.1a) holds, then (4.2) is solved:

$$\max_{X_{C,\,t}} J = \sum_{t \in T} \left(C^{RTM}_{e,\,t} \cdot P_t - C^{RTM}_{e,\,t} \cdot \Delta P_{TIAC,\,t} - C_f \cdot W_{f,\,tot,\,t} \right) \cdot \Delta t \tag{4.2}$$

$$P_t = \sum_{i \in I} \left(P_{it} \right) - L_{E,\,t} - L_{ERS,\,hrs}, \quad \forall t \in T, \quad \forall hrs \in BHs \tag{4.3}$$

subject to (3.3)-(3.4), (3.8)-(3.16), and (4.4):

$$L_{E,\,t} + L_{ERS,\,hrs} \leq \sum_{i \in I} \left(P_{it} \right), \quad \forall t \in T, \quad \forall hrs \in BHs \tag{4.4}$$

where $L_{ERS,\,hrs}$ is the ERS load in business hours hrs (see Table 4.1 for business hours). The total electric load (sum of the local electric load ($L_{E,\,t}$) and the ERS load ($L_{ERS,\,hrs}$) in case of a grid emergency) is satisfied by (4.4). Note that the power output accepted by the ISO in hour t (P_t) does not include $L_{E,\,t}$ and $L_{ERS,\,hrs}$. Equations (4.3) and (4.4) reduce to (3.2) and (3.6), respectively, if there is no electric grid emergency ($L_{ERS,\,hrs} = 0$).

The profit of selling surplus power to the grid in time t ($Profit_t^{wholesale}$) defined in (4.5) consists of two parts: power revenue from electricity sales in the RTM (4.6) and the operating cost of the system (4.7) as follows:

$$Profit_t^{wholesale} = \left(REV_{power,\,t} - Opr_{cost,\,t} \right) \cdot \Delta t \tag{4.5}$$

$$REV_{power,\,t} = C_{e,\,t}^{RTM} \cdot P_t \tag{4.6}$$

$$Opr_{cost,\,t} = C_{e,\,t}^{RTM} \cdot \Delta P_{TIAC,\,t} + C_f \cdot W_{f,\,tot,\,t} \tag{4.7}$$

where $C_{e,\,t}^{RTM}$ is the real-time electricity price in time t. Note that (4.5)-(4.7) are used only when (4.1a) holds.

When (4.1b) holds (i.e., the total electric load is less than the maximum available generation capacity), generation resources may participate in the DAM. In this case, the optimization procedure is divided into two steps. First, (3.1), the objective function defined in Section 3.1 for Case 2, is solved to determine the amount of electricity to be sold in the DAM subject to (3.2)-(3.4), (3.6), (3.8)-(3.16), and (4.8):

$$\sum_{i \in I} \left(P_{it} \right) \le \sum_{i \in I} \left(P_{it}^{max} \right) - L_{ERS,\,hrs}^{sold}, \quad \forall t \in T, \quad \forall hrs \in BHs \tag{4.8}$$

where $L_{ERS,\,hrs}^{sold}$ is the ERS capacity that is sold the ERCOT in business hours *hrs*. Ancillary service providers shall not bid the capacity that they have sold to ERCOT into the market for other capacity services. This is achieved by (4.8) to save the capacity to provide the ERS for a possible emergency deployment in the following day. By solving (3.1) an optimal amount of power to be sold is calculated and offered to bid to sell energy

in the DAM. Subsequently, an additional power to be sold in the RTM is calculated by (4.9):

$$\max_{X_{C,t}} J = \sum_{t \in T} \left(C_{e,t}^{RTM} \cdot P_t^{RTM} - C_{e,t}^{RTM} \cdot \Delta P_{TIAC,t} - C_f \cdot W_{f,tot,t} \right) \cdot \Delta t \quad (4.9)$$

$$P_t^{RTM} = \sum_{i \in I} \left(P_{it} \right) - P_t^{DAM} - L_{E,t} - L_{ERS,hrs}, \quad \forall t \in T, \quad \forall hrs \in BHs \quad (4.10)$$

subject to (3.3)-(3.4), (3.8)-(3.16), and (4.11):

$$P_t^{DAM} + L_{E,t} + L_{ERS,hrs} \leq \sum_{i \in I} \left(P_{it} \right), \quad \forall t \in T, \quad \forall hrs \in BHs \quad (4.11)$$

where $P_t{}^{RTM}$ and $P_t{}^{DAM}$ are the power outputs accepted by the ISO at hour t in the RTM and DAM, respectively. Equation (4.10) ensures that $P_t{}^{RTM}$ must exclude $P_t{}^{DAM}$, $L_{E,t}$, and $L_{ERS,hrs}$. As defined in (4.11), the total power output in time t should be equal to or greater than the sum of $P_t{}^{DAM}$, $L_{E,t}$, and $L_{ERS,hrs}$ to meet the loads. Equations (4.10) and (4.11) reduce to (4.3) and (4.4), respectively, if generating units do not participate in the DAM.

When (4.1b) holds, $Profit_t{}^{wholesale}$ consists of three parts: power revenue from electricity sales in the DAM (4.13), power revenue from electricity sales in the RTM (4.14), and the operating cost of the system (4.7) as follows:

$$Profit_t^{wholesale} = \left(REV_{power,t}^{DAM} + REV_{power,t}^{RTM} - Opr_{cost,t} \right) \cdot \Delta t \quad (4.12)$$

$$REV_{power,t}^{DAM} = C_{e,t}^{DAM} \cdot P_t^{DAM} \quad (4.13)$$

$$REV_{power,t}^{RTM} = C_{e,t}^{RTM} \cdot P_t^{RTM} \quad (4.14)$$

Finally, the net income of ERS resources ($Income_{net}$) is defined by

$$Income_{net} = \sum_{t \in T} Profit_t^{wholesale} + \sum_{hrs \in BHs} \left(C_{ERS,\,hrs} \cdot L_{ERS,\,hrs}^{sold} \cdot T_{ERS,\,hrs} \right) \quad (4.15)$$

where $C_{ERS,\,hrs}$ is the capacity payment per MWh in business hours *hrs*, and $T_{ERS,\,hrs}$ is the total number of hours in business hours *hrs* during the contract periods. The first term on the RHS of (4.15) accounts for the profit of selling surplus power in the wholesale energy markets (in the RTM or/and DAM) over the time span *T*. The second term on the RHS of (4.15) accounts for the ERS capacity payment.

4.3 CASE STUDIES

Case studies demonstrate how the net incomes of the CHP plant at UT Austin campus change as a function of MWs sold to the ERCOT for the ERS. The net income consists of the two parts: the ERS capacity payments based on MWs awarded for each hour during the contract periods and the power revenue by selling the extra power in the wholesale markets excluding the capacity that is sold to the ERCOT for the ERS. The net income of ERS resources by the end of the contract periods will depend on whether they are called to provide the ERS during the contract periods. This aspect is also examined in detail.

The same assumptions made for the case studies in Section 3.2 hold in this section. Additional assumptions are as follows:

(1) Ancillary service providers do not bid the capacity that they have sold to ERCOT into the market for other capacity services.

(2) $L_{ERS,\,hrs}$ is the same for all business hours in each case scenario for the sake of simplicity, so the subscript *hrs* is left off.

(3) The ERS is assumed to be procured for a four-month contract period (June to September of 2012) for deployment in an electric grid emergency.

(4) Sampling rate (Δt) of 1 hour is considered.

(5) Purchasing the power from the grid is not allowed.

4.3.1 Net Incomes under Various ERS Capacities Sold to the ERCOT without a Deployment Event

The case studies were performed under various ERS capacities that were sold to the ERCOT. In these cases, the ERCOT did not have to procure the ERS as there was no electric grid emergency observed during the contract periods. Table 4.3 summarizes the total power revenue and net income corresponding to a specific value of $L_{ERS,\,hrs}^{sold}$. Figure 4.1 shows the contribution of three power revenues: an ERS capacity payment, electricity sales in the RTM, and electricity sales in the DAM.

Table 4.3: Total power revenue and net income under various $L_{ERS,\,hrs}^{sold}$

$L_{ERS,\,hrs}^{sold}$ (MW)	Total power revenue ($)	Net income	
		($)	(%)
1	756,783 (26,394[a])	443,914	10.2 (0.6[a])
2	763,729 (52,789 [a])	458,909	10.5 (1.2[a])
3	769,543 (79,183 [a])	473,763	10.8 (1.8[a])
4	775,580 (105,580 [a])	488,380	11.2 (2.4[a])
5	781,600 (131,970 [a])	503,000	11.5 (3.0[a])
6	787,910 (158,370 [a])	517,370	11.8 (3.6[a])
8	799,170 (211,150 [a])	546,960	12.5 (4.8[a])
10	812,250 (263,940 [a])	577,110	13.2 (6.0[a])
15	883,047 (395,920[a])	668,110	15.3 (9.1[a])
20	980,885 (527,890[a])	788,840	18.1 (12.1[a])

[a] additional profit by providing the ERS

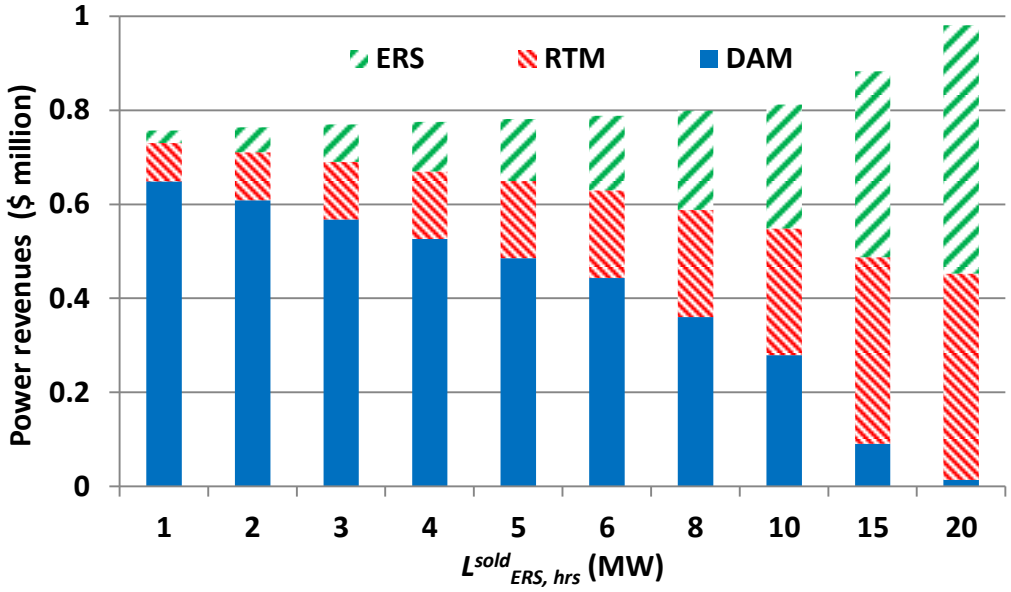

Figure 4.1: Power revenues as a function of $L^{sold}_{ERS,\,hrs}$: ERS capacity payment (top green), power revenue from the RTM (middle red), and power revenue from the DAM (bottom blue).

The results (see Figure 4.1) show that the power revenues from electricity sales in the RTM increased but those in the DAM decreased as $L^{sold}_{ERS,\,hrs}$ increased. A reduced total available power that could be sold to the DAM (if profitable) due to an increased $L^{sold}_{ERS,\,hrs}$ resulted in a reduction in power revenues from electricity sales in the DAM. However, this resulted in an increased available power that was sold to the RTM in the following day (if profitable), resulting in an increased power revenues from electricity sales in the RTM. In all cases, the power revenues from the DAM are greater than those obtained from the RTM due to two reasons: (1) the maximum amount of power that could be sold in the RTM equals to $L^{sold}_{ERS,\,hrs}$ (especially during the on-peak hours) and it is less than the amount of power sold in the DAM most of the times, and (2) the day-ahead electricity prices are usually greater than real-time electricity prices unless the electric grid is stressed by high demand. The combined revenues from electricity sales in

the wholesale energy markets (DAM and RTM) decreased as $L_{ERS,\,hrs}^{sold}$ increased; however, ERS capacity payments, which increased linearly with $L_{ERS,\,hrs}^{sold}$, could offset reduced power revenues. As a result, the net income of the plant (shown in Table 4.3) increased as the ERS capacity of generating units sold to the ERCOT increased.

4.3.2 Effect of Deploying the ERS on the Net Income

Day-ahead electricity prices are usually more expensive than real-time electricity prices, but the opposite happens when the electric grid is stressed due to weather, generator malfunctions, or loss of renewables often caused by lack of wind or cloud cover. In the Austin Load Zone on June 26, 2012, the grid experienced excessive demand, resulting in extremely high electricity prices in both the day-ahead and real-time markets as shown in Figure 4.2.

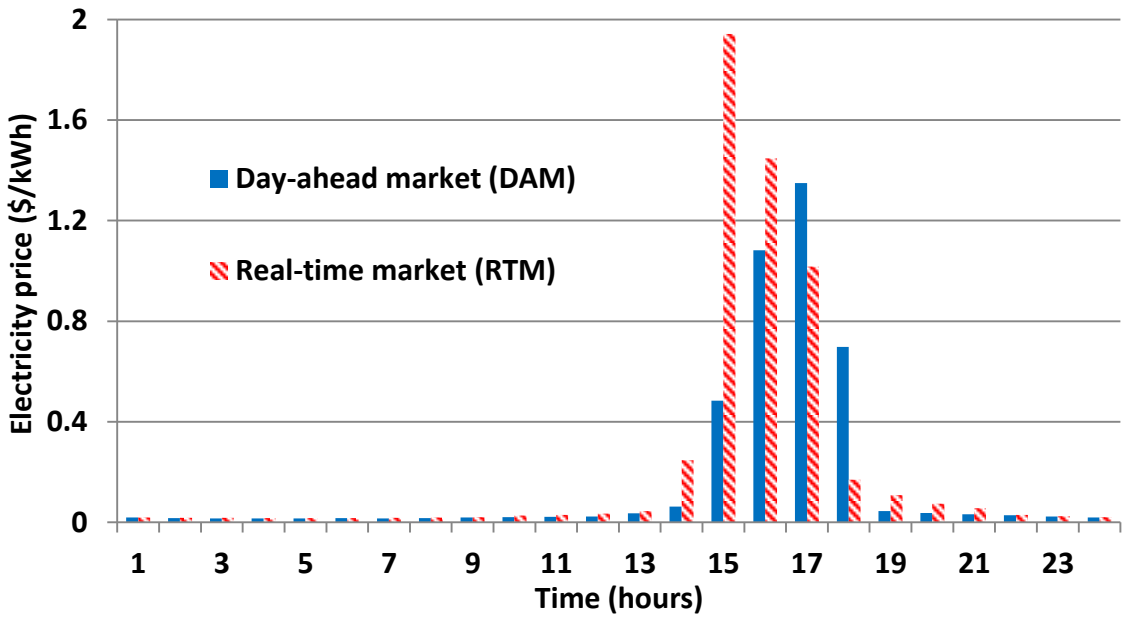

Figure 4.2: Day-ahead and real-time settlement point prices for the Austin Load Zone in the ERCOT market on June 26, 2012.

On this date, real-time electricity prices were higher than day-ahead electricity prices throughout the day (except hours from midnight to 1 AM and hours from 3 PM to 5 PM), requiring ERCOT to procure the ERS to balance electrical supply and demand. So, the case study was performed to demonstrate the effect of deploying the ERS on the net income as well as operating strategy of the plant in response to a grid emergency.

In hours 9-16 (from 8 AM to 3 PM), the generation resources were called to provide the ERS for 8 continuous hours, so they exhausted their 8-hour obligation with one deployment event. The capacity payments for four business hours are listed in Table 4.1. The ERS capacity sold to the ERCOT was 6 MW during the procurement cycle. Figures 4.3 and 4.4 show the power outputs on June 26 in 2012 with and without a deployment event, respectively.

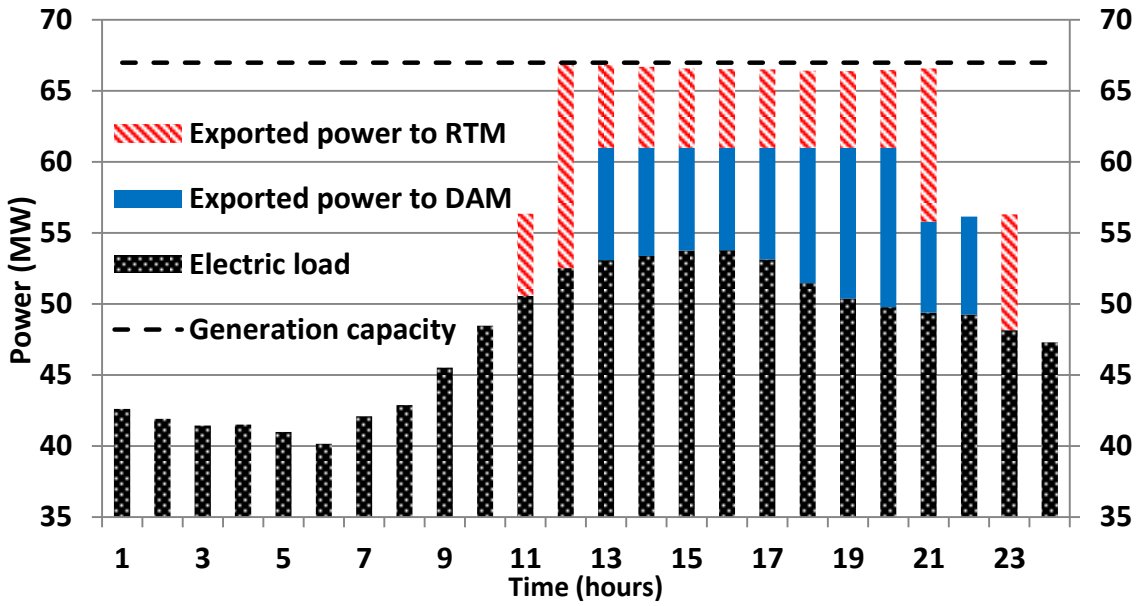

Figure 4.3: Power outputs on June 26 in 2012 without a deployment event.

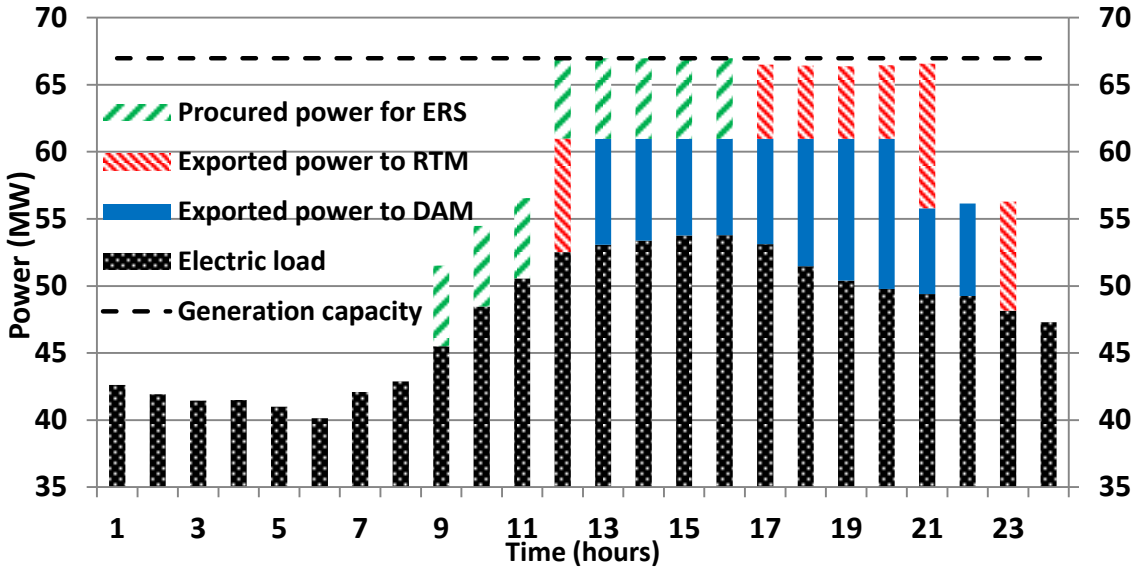

Figure 4.4: Power outputs on June 26 in 2012 with a deployment event.

When there was no deployment event, the plant did not participated in the DAM in hours 1-12 and 23 due to low day-ahead electricity prices but participated in the RTM in hours 11-12, owing to relatively high real-time electricity prices. In hour 22, the plant only participated in the DAM because the real-time electricity price during this hour was not attractive to sell the power. In hours 13-21, at least 6 MW was saved to provide the ERS in case of a grid emergency when participating in the DAM. As there was no deployment event observed, the remaining power could be sold to the RTM as well at expensive real-time market electricity prices. In the rest of the hours, the total power output met the load and did not participate in neither the DAM nor the RTM due to the low wholesale settlement point prices during these hours.

When a grid emergency occurred, the ERS of 6 MW was procured for 8 hours in hours 9-16 (see Figure 4.4). Compared to the case without a deployment event, the plant lost the profit of $21,326; however, this was significantly offset by the ERS capacity payment ($158,370), that amounted to 32% of the net income.

The optimal economic dispatch algorithm proposed is effective and safe to implement because the ERS capacity is always reserved to be procured in response to a possible grid emergency in the following day while maximizing the net income by participating in the wholesale energy markets. It is recommended to limit $L_{ERS,\,hrs}^{sold}$ to be less than 10% of the total generation capacity of the plant or/and the least surplus power based on the highest predicted local load of the contract periods to ensure that the local electric load is met. In this case study, the total generation capacity of the power plant at UT Austin was 67 MW, 10% of which was 6.7 MW, and the least surplus power observed during the contact periods was 13.2 MW. So, $L_{ERS,\,hrs}^{sold}$ of less than 6.7 MW was recommended.

4.4 SUMMARY

In this chapter, net incomes of generation resources by providing the ERS while participating in the wholesale energy markets have been evaluated. Case studies demonstrated that the ERS participants can achieve a significant additional profit since the capacity payment is (1) made regardless of there is a deployment event and (2) enough to offset the decrease in net income due to the ERS procurement in case of a grid emergency. The key-value of the proposed economic dispatch algorithm comes by its ability to save the ERS load when the ERS providers participating in the DAM, allowing them to procure the ERS if required in the following day or to sell the reserved ERS energy to the RTM.

Chapter 5: Optimal Scheduling of Combined Heat and Power Plants

The optimization problem addressed in this chapter is formulated as a scheduling problem. So, a producer (or a unit) needs to determine the best scheduling (most profitable), i.e., start-up and shut-down planning, of its production units in advance.

5.1 Mixed-Integer Nonlinear Programming Formulation

When the pieces of equipment in a CHP plant (referred to as "producers") to be committed to operation are known a priori, the scheduling problem is an NLP problem as no binary decision variables are required. On the other hand, if we assume multiple producers can be brought on-line to maximize the CHP plant's profit as many as they exist in the system, then the scheduling problem is formulated in an MINLP framework as both continuous (X_C) and binary decision variables (X_B) are required to solve an optimization problem. The optimal usage of generating resources during a scheduling period (T) is determined by solving the following objective function:

$$\max_{X_{C,\,it},\,X_{B,\,it}} J = \sum_{t\in T}\left[C_{e,\,t}^{DAM}\cdot P_t^{DAM} - \sum_{i\in I}\left(C_{e,\,t}^{DAM}\cdot \Delta P_{TIAC,\,it} + C_{prod,\,it}\right)\right]\cdot \Delta t \quad (5.1)$$

subject to

$$c\left(X_{C,\,it},\, X_{B,\,it}\right)\le 0, \quad \forall i\in I,\ \forall t\in T \quad (5.2)$$

$$c_{eq}\left(X_{C,\,it},\, X_{B,\,it}\right)= 0, \quad \forall i\in I,\ \forall t\in T \quad (5.3)$$

$$X_{C,\,it}^{min}\le X_{C,\,it}\le X_{C,\,it}^{max}, \quad \forall i\in I,\ \forall t\in T \quad (5.4)$$

$$X_{B,\,it} \in [0,1], \quad \forall i \in I,\ \forall t \in T \tag{5.5}$$

where $\Delta P_{TIAC,\,it}$ is the power consumption of a chiller associated with TIAC unit i in hour t and $C_{prod,\,it}$ is the production cost of unit i in hour t. Equations (5.2) and (5.3) enforce the inequality and equality constraints, respectively. The continuous (5.4) and binary (5.5) decision variables are also constrained with lower and upper bounds. These constraints represent the system operating constraints of the producers such as minimum/maximum power output and steam flow restrictions, minimum up/down times, start-up and shut-down procedures, fuel limits, etc. They are further described in the following sub-sections in greater details.

When the producer is committed to operation, it experiences a predefined sequence of modes (or phases), with a residence time specified for each mode. Figure 5.1 represents the different operating modes of the producer [97]. After being turned off (u_{it} = 0) for T_i^{off} hours, which should be greater than the minimum down time, i.e., $T_i^{min,down} \leq T_i^{off}$, the producer starts up at hour t_1 (y_{it} = 1) and continues committed for at least minimum up time ($T_i^{min,\,up,\,l}$) until the producer is shut-down at hour t_5 (z_{it} = 1). Once committed, the producer enters four consecutive operating phases: (1) synchronization, (2) soak, (3) dispatchable, and (4) desynchronization, denoted by binary variables u_{it}^{syn}, u_{it}^{soak}, u_{it}^{disp}, and u_{it}^{desyn}, respectively. The producer start-up phase consists of the two phases: (1) synchronization and (2) soak. After a type-l start-up decision is made ($y_{it}^{\,l}$ = 1), the producer enters the synchronization phase that lasts for $T_i^{syn,\,l}$ hours. No power is produced during the synchronization phase. Subsequently, the producer enters the soak phase that lasts for $T_i^{soak,\,l}$ hours. During the soak phase the producer's power ramps up from the synchronization load (P_i^{syn}) to the technical minimum power output ($P_i^{\,min}$).

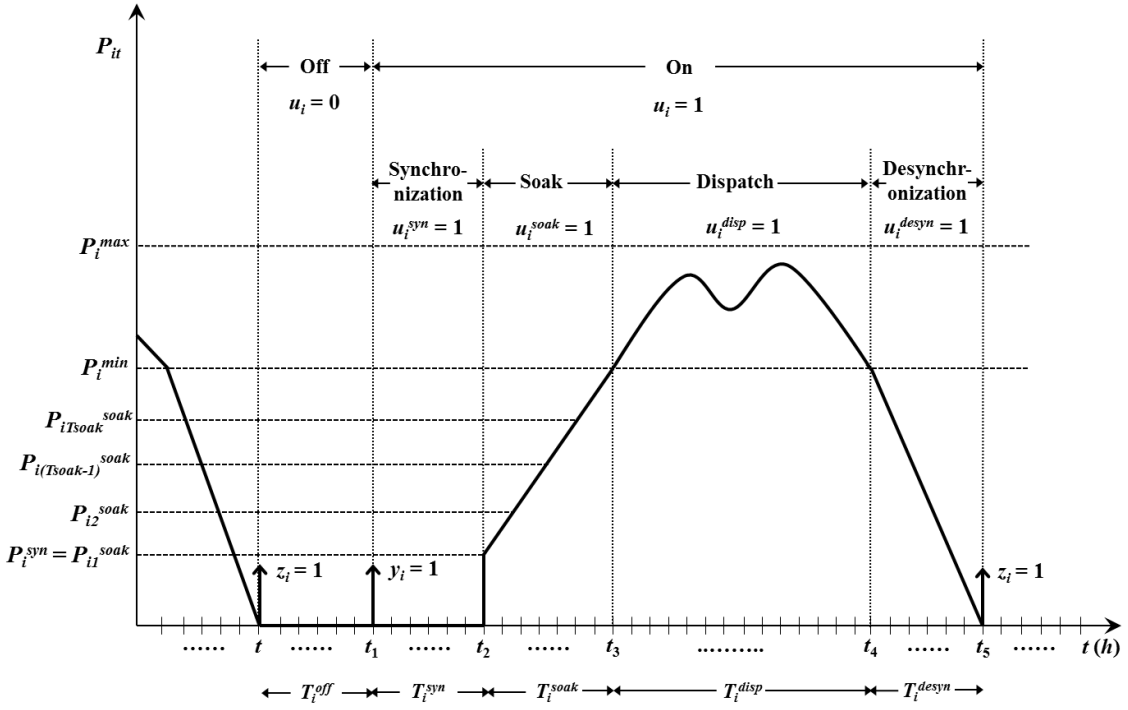

Figure 5.1: Operating modes of a unit. Image is adopted from [97].

Three start-up types are modeled: hot, warm and cold, each with distinct synchronization time ($T_i^{syn,\,l}$), soak time ($T_i^{soak,\,l}$), and start-up cost ($C_i^{start,\,l}$). These three model parameters depend on the producer's prior reservation time (T_i^{off}). For example, if T_i^{off} is greater than zero but less than $T_i{}^{w}$, than the start-up type is classified as the "hot" start-up. When T_i^{off} falls in between $T_i{}^{w}$ and $T_i{}^{c}$, then the start-up type is classified as the "warm" start-up. If T_i^{off} is greater than $T_i{}^{c}$, we classify the start-up type as the "cold" start-up.

Once the producer is bought on-line, it must complete the start-up sequence and enter the dispatchable phase during which it can receive dispatch instructions to vary its power output between its technical minimum and its nominal power output as many

hours as needed to satisfy the minimum up time requirement. Subsequently, the producer follows a predefined shut-down sequence, which we will describe later for each producer individually. In the following sub-sections, we adapt the notation and terminology from [97].

5.1.1 Start-up Type Constraints

$$y_{it}^{l} \leq \sum_{\tau=t-\overline{T}_i^l+1}^{t-\underline{T}_i^l} z_{i\tau}, \quad \forall i \in I,\ \forall t \in T,\ \forall l \in L \tag{5.6}$$

$$y_{it} \leq \sum_{l \in L} y_{it}^{l}, \quad \forall i \in I,\ \forall t \in T \tag{5.7}$$

Equation (5.6) chooses the distinct start-up type of the unit i depending on the unit's prior reservation time by constraining the type-l start-up of unit i during hour t ($y_{it}{}^{l}$) to be zero unless there has been a prior shut-down of the unit within the time window [$t-\overline{T}_i^l$, $t-\underline{T}_i^l$] (see Table 5.1). Equation (5.7) makes sure that only one start-up type per start-up is selected.

Table 5.1. Producer start-up model.

Start-up type	Prior reservation time $\underline{T}_i^l \leq T_i^{off} < \overline{T}_i^l$	Synchroni-zation time	Soak time	Start-up cost
Hot	$0 \leq T_i^{off} < T_i^{w}$	$T_i^{syn,\,h}$	$T_i^{soak,\,h}$	$C_i^{start,\,h}$
Warm	$T_i^{w} \leq T_i^{off} < T_i^{c}$	$T_i^{syn,\,w}$	$T_i^{soak,w}$	$C_i^{start,\,w}$
Cold	$T_i^{c} \leq T_i^{off} < T^{\infty}$	$T_i^{syn,\,c}$	$T_i^{soak,c}$	$C_i^{start,\,c}$

Note: T^{∞} is the maximum length of the planning horizon extended to the past (negative time).

5.1.2 Synchronization Phase Constraints

$$u_{it}^{syn,\,l} = \sum_{\tau=t-T_i^{syn,\,l}+1}^{t} y_{i\tau}^{l}, \quad \forall i \in I,\ \forall t \in T,\ \forall l \in L \tag{5.8}$$

$$u_{it}^{syn} \le \sum_{l \in L} u_{it}^{syn,\,l}, \quad \forall i \in I,\ \forall t \in T \tag{5.9}$$

After the type-*l* start-up decision is made ($y_{it}^{l} = 1$) for unit *i*, it must enter the synchronization phase immediately (see Figure 5.1). This is achieved in (5.8) by turning on the type-*l* synchronization phase binary variable ($u_{it}^{syn,\,l} = 1$), whenever a type-*l* start-up of the unit *i* is selected in the past $T_i^{syn,\,l}$ hours. Equation (5.9) ensures that only one synchronization phase type per start-up is selected.

5.1.3 Soak Phase Constraints

$$u_{it}^{soak,\,l} = \sum_{\tau=t-T_i^{syn,\,l}-T_i^{soak,\,l}+1}^{t-T_i^{syn,\,l}} y_{i\tau}^{l}, \quad \forall i \in I,\ \forall t \in T,\ \forall l \in L \tag{5.10}$$

$$u_{it}^{soak} \le \sum_{l \in L} u_{it}^{soak,\,l}, \quad \forall i \in I,\ \forall t \in T \tag{5.11}$$

The producer should enter a soak phase immediately after a synchronization phase as described in Figure 5.1. This is achieved in (5.10) by turning on the type-*l* soak phase binary variable ($u_{it}^{soak,\,l} = 1$), whenever a type-*l* start-up of the unit *i* is selected in the past time interval [$t - T_i^{syn,\,l} - T_i^{soak,\,l} + 1$, $t - T_i^{syn,\,l}$]. Equation (5.11) ensures that only one soak phase type per start-up is selected. During the soak phase, the power output

from turbines is fixed to the constant value ($\overline{P}_i^{soak}$) while in soak phase. So, the power output of unit *i* during the soak phase in hour *t* is defined by (5.12):

$$P_{it}^{soak} = \overline{P}_i^{soak} \sum_{l \in L} u_{it}^{soak,\, l}, \quad \forall i \in I,\ \forall t \in T \tag{5.12}$$

The duration of the soak phase so as the power output during the soak phase depends on the unit *i* start-up type.

5.1.4 Desynchronization Phase Constraints

$$u_{it}^{desyn} = \sum_{\tau=t+1}^{t+T_i^{desyn}} z_{i\tau}, \quad \forall i \in I,\ \forall t \in T \tag{5.13}$$

Before shutting down the unit *i*, it should operate in the desynchronization phase for T_i^{desyn} hours (see Figure 5.1). This is achieved by turning on the desynchronization phase binary variable ($u_{it}^{desyn} = 1$), whenever a shut-down of the unit *i* occurs in the future time interval [t +1 and $t + T_i^{desyn}$], as modeled in (5.13). The power output during the desynchronization phase decreases linearly from its technical minimum value (P_i^{min}) to zero:

$$P_{it}^{desyn} = \left[\sum_{\tau=t+1}^{t+T_i^{desyn}} z_{i\tau} \cdot (\tau - t) \right] \cdot \frac{P_i^{min}}{T_i^{desyn}}, \quad \forall i \in I,\ \forall t \in T \tag{5.14}$$

5.1.5 Minimum Up/Down Time Constraints

$$\sum_{\tau=t-T_i^{min,\, up,\, l}+1}^{t} y_{i\tau}^{l} \le u_{it}, \quad \forall i \in I,\ \forall t \in T,\ \forall l \in L \tag{5.15}$$

$$\sum_{\tau=t-T_i^{min,\,down}+1}^{t} z_{i\tau} \le 1-u_{it}, \quad \forall i \in I,\ \forall t \in T,\ l \in L \tag{5.16}$$

The unit must meet the minimum up time constraint once it is committed to operation. This is achieved in (5.15) by forcing the unit i committed at hour t ($u_{it} = 1$) if a unit's start-up started in the past time interval [t - $T_i^{min,\,up,\,l}$, t]. Similarly, if a unit's shut-down started in the past time interval [t - $T_i^{min,\,down}$, t], it should remain de-committed at hour t as described in (5.16) [98].

5.1.6 Logical Status of Commitment

$$u_{it} = u_{it}^{syn} + u_{it}^{soak} + u_{it}^{disp} + u_{it}^{desyn}, \quad \forall i \in I,\ \forall t \in T \tag{5.17}$$

$$y_{it} - z_{it} = u_{it} - u_{i(t-1)}, \quad \forall i \in I,\ \forall t \in T \tag{5.18}$$

$$y_{it} + z_{it} \le 1, \quad \forall i \in I,\ \forall t \in T \tag{5.19}$$

Equation (5.17) ensures that only one of the binary variables corresponding to the different commitment states, i.e., synchronization (u_{it}^{syn}), soak (u_{it}^{soak}), dispatchable (u_{it}^{disp}), and desynchronization (u_{it}^{desyn}), of the unit i to be equal to 1 at hour t. The logic of the start-up and shut-down status change is modeled in (5.18). Equation (5.19) is for prevention of a unit to be at start-up and shut-down at the same time in a given hour t.

5.1.7 Objective Function

In preparation for reformulating a scheduling problem as an MINLP problem, the objective function (5.1) needs to be rewritten in terms of the binary and continuous variables as the follow:

$$\begin{aligned}\max_{X_{C,it},\,X_{B,it}} J \;=& \sum_{t\in T}\left(C_{e,t}^{DAM}\cdot P_t^{DAM}\right)\cdot\Delta t-\sum_{t\in T}\sum_{i\in I}\left(C_{e,t}^{DAM}\cdot\Delta P_{TIAC,it}^{disp}\right)\cdot\Delta t \\ &-\sum_{t\in T}\sum_{i\in I}\left(C_{prod,it}\right)\cdot\Delta t\end{aligned} \tag{5.20}$$

$$P_t^{DAM}=\sum_{i\in I}\left(P_{it}^{soak}+P_{it}^{disp}+P_{it}^{desyn}\right)-L_{E,t},\quad \forall t\in T \tag{5.21}$$

$$P_{it}^{disp}=P_{it}\cdot u_{it}^{disp},\quad \forall i\in I,\ \forall t\in T \tag{5.22}$$

$$\Delta P_{TIAC,it}^{disp}=\frac{\Delta H_{TIAC,it}}{COP}\cdot u_{it}^{disp},\quad \forall i\in I,\ \forall t\in T \tag{5.23}$$

$$C_{prod,it}=\sum_{l\in L}\left(C_i^{start,l}\cdot y_{it}^{l}+C_i^{shut}\cdot z_{it}+C_f\cdot W_{f,it}^{disp}\right),\quad \forall i\in I,\ \forall t\in T \tag{5.24}$$

$$W_{f,it}^{disp}=W_{f,it}\cdot u_{it}^{disp},\quad \forall i\in I,\ \forall t\in T \tag{5.25}$$

The surplus power sold to the grid (P_t^{DAM}) comprises the power outputs during the soak phase (P_{it}^{soak}), dispatchable phase (P_{it}^{disp}), and desynchronization phase (P_{it}^{desyn}), and the electric load. The production cost of unit i in hour t ($C_{prod,it}$) defined in (5.24) consists of three parts: the unit's start-up type dependent start-up cost ($C_i^{start,l}$), shut-down cost

(C_i^{shut}), and the time dependent fuel cost. Note that P_{it}^{disp} in (5.22) and $\Delta P_{TIAC,\,it}^{disp}$ in (5.23) are nonzero only during the dispatchable phase ($u_{it}^{disp} = 1$). Likewise, the fuel cost $W_{f,it}^{disp}$ (the last term) in (5.24) is accounted for during the unit's dispatchable phase only as that during synchronization, soak, and desynchronization is included in the unit start-up and shut-down costs.

The start-up cost in (5.24) is discretized into three levels, each of which corresponds to the distinct start-up type (see Figure 5.2). However, the start-up cost can be an exponential or linear function of the number of hours a unit has been off [99].

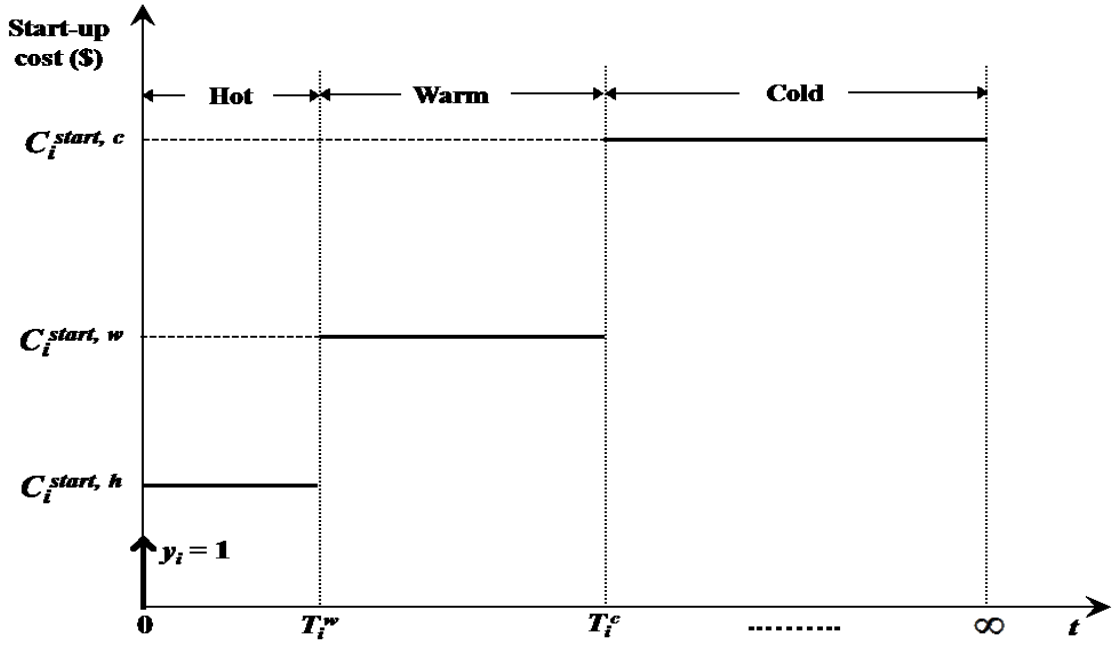

Figure 5.2: Producer start-up cost depending on the start-up types: hot (*h*), warm (*w*), and cold (*c*).

5.1.8 System Operating Constraints

As the producer experiences predefined start-up (synchronization and soak phases) and shut-down schedules, the constraints defined in Section 3.1 are accounted during its dispatchable phase only. Therefore, the constraints become active only during

the dispatchable phase. This is achieved by using the binary variable u_{it}^{disp} to enable/disable the constraints associated with each producer.

Inequality constraints imposed on the total power output and steam flow are redefined as follows:

$$L_{E,\,t} \le \sum_{i \in I} \left(P_{it}^{soak} + P_{it}^{disp} + P_{it}^{desyn} \right), \quad \forall t \in T \tag{5.26}$$

$$L_{H,\,t} \le \sum_{st \in EST} W_{S,\,EXT,\,(st)t}^{disp}, \quad \forall t \in T \tag{5.27}$$

where

$$W_{S,\,EXT,\,(st)t}^{disp} = W_{S,\,EXT,\,(st)t} \cdot u_{(st)t}^{disp}, \quad \forall st \in EST,\ \forall t \in T \tag{5.28}$$

Equations (5.26) and (5.27) state that the sum of power and extraction steam (defined in (5.28)) generations in the system should be greater than the campus electric and heating loads, respectively, during the dispatchable phase.

Equations (5.29)-(5.39) comprise the number of system operating constraints in the system:

$$T_c^{min} \cdot u_{(gt)t}^{disp} \le T_{c,\,(gt)t} \cdot u_{(gt)t}^{disp}, \quad \forall gt \in HDGT,\ \forall t \in T \tag{5.29}$$

$$T_{e,\,(gt)t} \cdot u_{(gt)t}^{disp} \le T_{e,\,gt}^{ref} \cdot u_{(gt)t}^{disp}, \quad \forall gt \in HDGT,\ \forall t \in T \tag{5.30}$$

$$T_{f,\,(gt)t} \cdot u_{(gt)t}^{disp} \le T_{f,\,gt}^{ref} \cdot u_{(gt)t}^{disp}, \quad \forall gt \in HDGT,\ \forall t \in T \tag{5.31}$$

$$P_i^{min} \cdot u_{it}^{disp} \le P_{it} \cdot u_{it}^{disp} \le P_i^{max} \cdot u_{it}^{disp}, \quad \forall i \in I, \ \forall t \in T \tag{5.32}$$

$$\left(T_{SH,\,(gt)t} + \Delta T_{HRSG}^{min}\right) \cdot u_{(gt)t}^{disp} \le T_{e,\,in,\,(gt)t} \cdot u_{(gt)t}^{disp}, \quad \forall gt \in HDGT, \quad \forall t \in T \tag{5.33}$$

$$W_{SH,\,i}^{min} \cdot u_{it}^{disp} \le W_{SH,\,it} \cdot u_{it}^{disp} \le W_{SH,\,i}^{max} \cdot u_{it}^{disp}, \quad \forall i \in I, \ \forall t \in T \tag{5.34}$$

$$W_{S,\,THR,\,(st)t}^{disp} = W_{SH,\,tot,\,t}^{disp} \cdot SFR_{(st)t}, \quad \forall st \in EST, \ \forall t \in T \tag{5.35}$$

$$W_{SH,\,tot,\,t}^{disp} = \sum_{i \in I} \left(W_{SH,\,it} \cdot u_{it}^{disp}\right), \quad \forall t \in T \tag{5.36}$$

$$0 \le SFR_{(st)t} \le 1, \quad st \in EST, \ \forall t \in T \tag{5.37}$$

$$\sum_{st \in EST} SFR_{(st)t} \le 1, \quad \forall t \in T \tag{5.38}$$

$$0 \le W_{S,\,EXT,\,(st)t}^{disp} \le W_{S,\,THR,\,(st)t}^{disp}, \quad \forall st \in EST, \ \forall t \in T \tag{5.39}$$

Equations (5.29)-(5.34) are equivalent to Equations (3.9)-(3.16) defined in Section 3.1. Equation (5.35) states that the throttling steam flow fed to a steam turbine ($W_{S,\,THR,\,(st)t}^{disp}$) is regulated through the steam flow regulator (*SFR*) by allocating the total HP steam available in the system, which is defined in (5.36), to an individual steam turbine. The $SFR_{(st)t}$, an additional decision variable besides those listed in Table 3.1, is the fraction of the total HP steam to be allocated to the steam turbine *st* at hour *t*. Equation (5.37)

imposes lower and upper bounds on *SFR*. The sum of $SFR_{(st)t}$ should be one at any given time (5.38) to ensure that the mass balance of the HP steam is conserved. Equation (5.39) restricts the extraction steam flow during the dispatchable phase to lie between zero and throttling steam flow in a steam turbine.

In order to assess the system efficiency on a wide range of operating conditions, the overall plant heat rate (HR_t) in hour *t* is calculated by

$$HR_t\left(\frac{\text{Btu}}{\text{kWh}}\right)=\sum_{i\in I}\left(\frac{W_{f,it}\left(\frac{\text{SCF}}{\text{h}}\right)}{P_{it}\left(\text{kW}\right)}\right)\cdot LHV\left(\frac{\text{Btu}}{\text{SCF}}\right),\quad \forall t\in T \tag{5.40}$$

where W_f is the total fuel flow in hour *t*. *LHV* of natural gas is assumed to be 1,020 Btu/SCF in this work.

It should be noted that a scheduling problem (MINLP problem) reduces to an economic dispatch problem (NLP problem) when producers to be committed are known prior to operation.

5.2 CASE STUDIES

The developed methods in Sections 3.1 and 5.1 have been applied to the day-ahead energy market of the ERCOT interconnection for scheduling of the CHP plant located at UT Austin. Table 5.2 presents the technical and economic data of the producers used for the objective function, i.e., type-*l* start-up time and corresponding start-up cost, minimum up/down times, duration of the operating phases, etc. They have been selected from [97, 100] and scaled appropriately to match the rated capacity of designated run units, which are depicted in Figure 5.3. Note that the optimal start-up trajectory of the producer can be calculated offline through the deployment of nonlinear model predictive

control (NMPC) as shown in [79], and then can be included in the proposed optimization model.

Table 5.2: Technical and economic data of the producers.

Unit name $(\forall i \in I)$	T_i^w (h)	T_i^{desyn} (h)	Start-up time $T_i^{syn,l}$ (h), $T_i^{soak,l}$ (h)						$T_i^{min,up,l}$ (h) / $C_i^{start,l}$ ($)			$T_i^{min,down}$ (h)
	T_i^c (h)	C_i^{shut} ($)	l = hot		l = warm		l = cold		l = hot	l = warm	l = cold	
			syn	soak	syn	soak	syn	soak				
GT8 & HRSG8 (1)	3	2	0	1	0	2	0	3	2	3	4	2
	8	1,467							558	1,115	1,673	
GT10 & HRSG10 (2)	3	2	0	1	0	2	0	3	2	3	4	2
	8	1,048							396	793	1,189	
ST7 (3)	3	1	0	1	1	2	2	3	2	4	6	1
	8	440							272	816	1,360	
ST9 (4)	3	1	0	1	1	2	2	3	2	4	6	1
	8	440							272	816	1,360	
BR3 (5)	3	-	-	1	-	2	-	3	2	3	4	1
	8	390							321	643	964	
BR7 (6)	3	-	-	1	-	2	-	3	2	3	4	1
	8	964							611	1,223	1,834	

Note: The gas turbine and HRSG are assumed to operate together, so they are lumped as one producer.

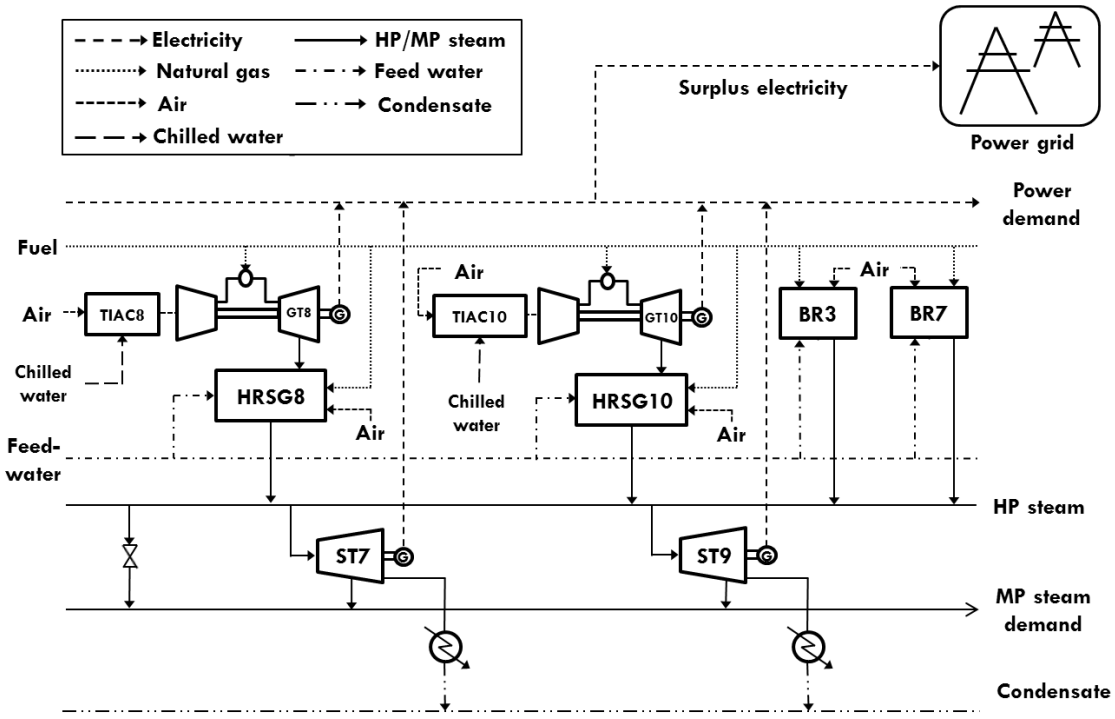

Figure 5.3: Flowsheet of Hal C. Weaver Power Complex at UT Austin.

In case studies, hourly data over a period of 4 months (from June to September, 2012) are used to illustrate the effectiveness of the proposed frameworks. Two case studies are considered. In Case 1, the operating units are known in advance to follow the heuristic unit commitment approach. In this case, only GT8, HRSG8, ST7, and BR3 are in service throughout the entire time horizon, resulting in an economic dispatch problem formulated in an NLP framework. In Case 2, in addition to the economic dispatch, the unit commitment is also taken into account as multiple generating units can be bought in service when needed. In this case, the scheduling problem is formulated in an MINLP framework. Required data that are not listed in Tables 2.2-2.5, 2.1, and 3.1 are provided in Table 5.3.

Table 5.3: Parameter values used in the case studies.

Symbol	Description	Unit	Value
$\overline{P}_{GT8}^{soak}$	Fixed power output from GT8 while in soak phase	MW_e	8.4
$\overline{P}_{GT10}^{soak}$	Fixed power output from GT10 while in soak phase	MW_e	6.4
$\overline{P}_{ST7}^{soak}$	Fixed power output from ST7 while in soak phase	MW_e	3
$\overline{P}_{ST9}^{soak}$	Fixed power output from ST9 while in soak phase	MW_e	3

In Case 2, the scheduling period (T) of 24 hours (i.e., scheduling adjustments are performed on a daily basis) with sampling rate (Δt) of 1 hour is considered. The sizes of the NLP and MINLP problems expressed as the number of continuous variables, binary variables, and constraints are provided in Table 5.4.

Table 5.4: Problem sizes of the case studies

Case study	Number of decision variables		Number of constraints
	Continuous	Binary	
Case 1: NLP problem	144	0	552
Case 2: MINLP problem	336	2,304	3,000

Note: For equivalent comparison, each entry associated with Case 1 is multiplied by the length of the scheduling period (24 hours).

The MINLP problem is solved in MATLAB environment using the SQP algorithm in conjunction with solver SCIP (Solving Constraint Integer Programs) [101].

The same assumptions made for the case studies in Section 3.2 hold in this section. Additional assumptions are as follows:

(1) The gas turbine and HRSG are treated as one producer.

(2) Initially, GT8, HRSG8, ST7, and BR3 have completed the unit start-up phase ($u_{i0}^{disp} = 1$).

(3) Initially, the GT10, HRSG10, ST9, and BR7 have been reserved for more than T_i^c ($u_{it} = 0$), above which the start-up type of unit i is cold start-up.

(4) Ramp up/down limits can be imposed on plant outputs, i.e., power output and steam flow, as in [11, 63, 97]. However, they can ramp up (down) from (to) the minimum value to (from) nominal value within the sampling rate in our case studies. Therefore, ramping constraints are not used.

(5) Purchasing the power from the grid is not allowed.

5.2.1 Case 1: Economic Dispatch of the CHP Plant Formulated as an NLP Problem

Figure 5.4 shows the day-ahead electricity prices for July 20, 2012, in the Austin Load Zone of the ERCOT grid. Figure 5.5 demonstrates how the plant operating schedules change responding to the hourly changing electricity prices on July 20, 2012.

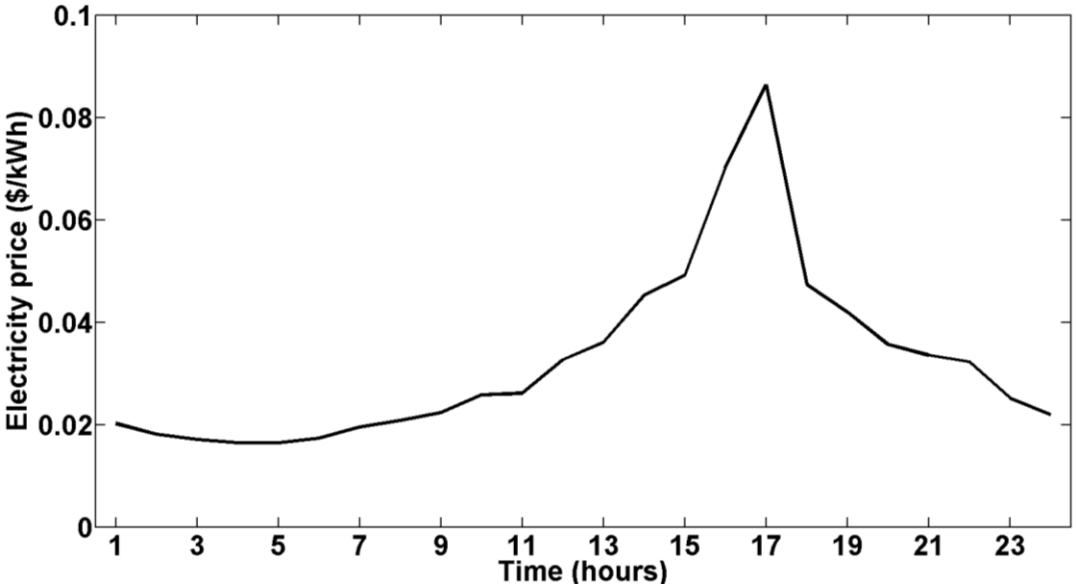

Figure 5.4: Day-ahead settlement point prices for the Austin Load Zone in the ERCOT market on July 20, 2012. Electricity prices are specified at one-hour intervals in the day-ahead market.

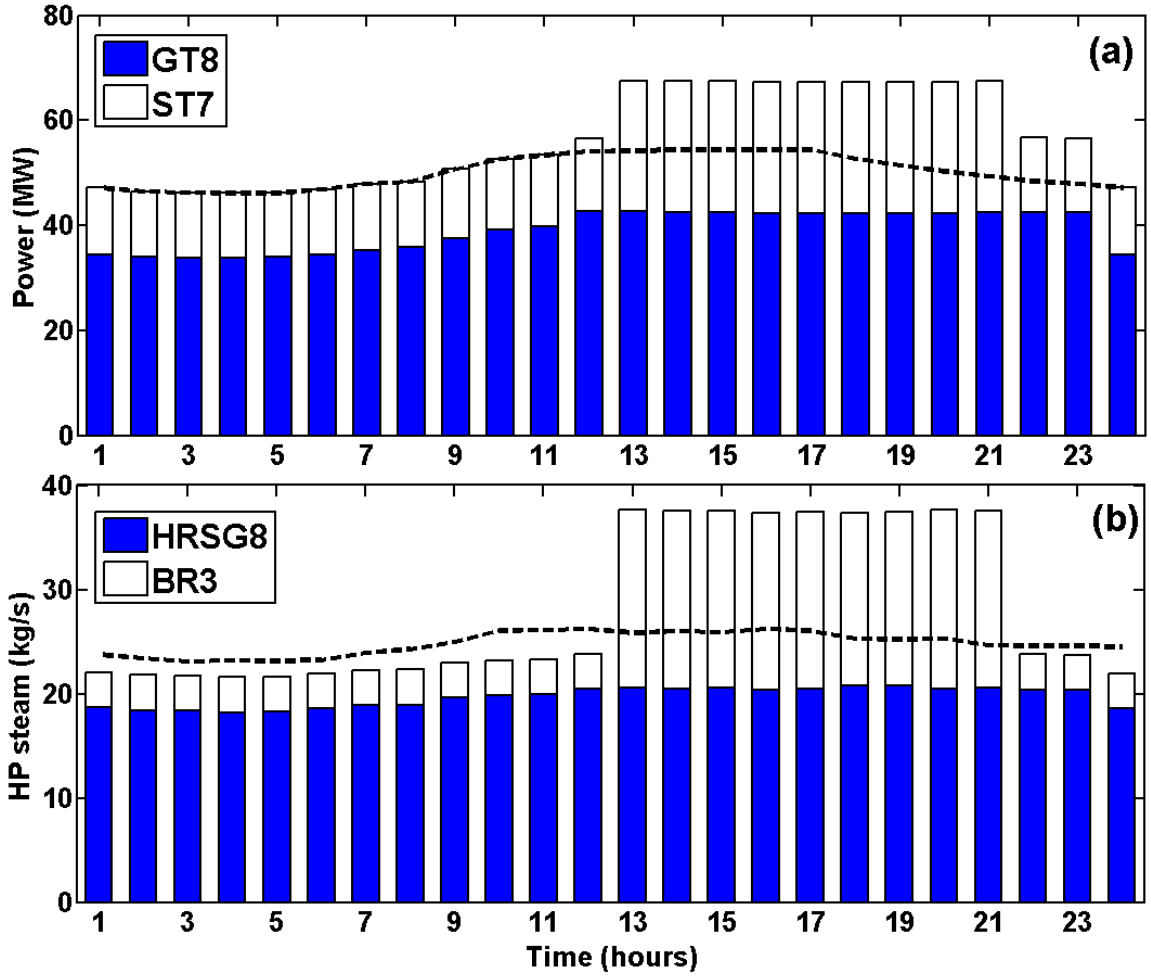

Figure 5.5: Case 1 results for July 20, 2012 - (a) power, (b) HP steam. Optimized operating schedules are shown as histograms and historical operating schedule s are shown as black dashed lines.

As seen in Figure 5.5(a), in hours 1-11 and 24, the plant power outputs increased (decreased) as the electricity prices increased (decreased), without participating in the wholesale energy market. During these hours, the plant was able to generate the same power outputs at lower operating costs through the optimal allocation of the total power among GT8 and ST7. This was achieved by reducing the power from ST7 (less efficient and more expensive producer) and increasing the power from GT8 (more efficient and

less expensive producer) to make up the deficit power. Figure 5.5(b) witnesses that the overall HP steam flow directed to ST7 in Case 1 has been reduced compared to that in base case, resulting in a reduction in the power outputs from ST7.

In hours 12-23, it would have been more profitable to sell surplus power to the grid when the electricity prices were above about $0.03/kWh. In hours 12, 22-23, the power production from GT8 was maximized (42 MW) but that from ST7 remained at about half of its nominal power (12.5 MW). In hours 13-21, the power production from both GT8 and ST7 were maximized, owing to the high electricity prices of the late afternoon hours during the summer months in the ERCOT grid.

The overall thermodynamic efficiency decreases for supplementary firing in HRSG due to the fact that the generated heat is only used in the steam turbines to generate power. For this reason, in Case 1, the duct burner fuel flows in HRSG8 were zero during the whole scheduling period. Likewise, the steam production from the auxiliary boiler (BR3) was limited to its technical minimum in hours 1-12 and 22-24 in order to maintain the high thermal efficiency of the system.

5.2.2 Case 2: Unit Commitment and Economic Dispatch of the CHP Plant Formulated as an MINLP Problem

Figure 5.6 shows the optimal power generation schedules in Case 2 during the same day (July 20, 2012). In Case 2, GT8 and ST9 were “base-load” units, which ran for 24 hours, as opposed to GT8 and ST7 in Case 1. The reason for this is that ST9 is more efficient and less expensive generating unit than ST7 (see Table 2.9 for their efficiency comparison).

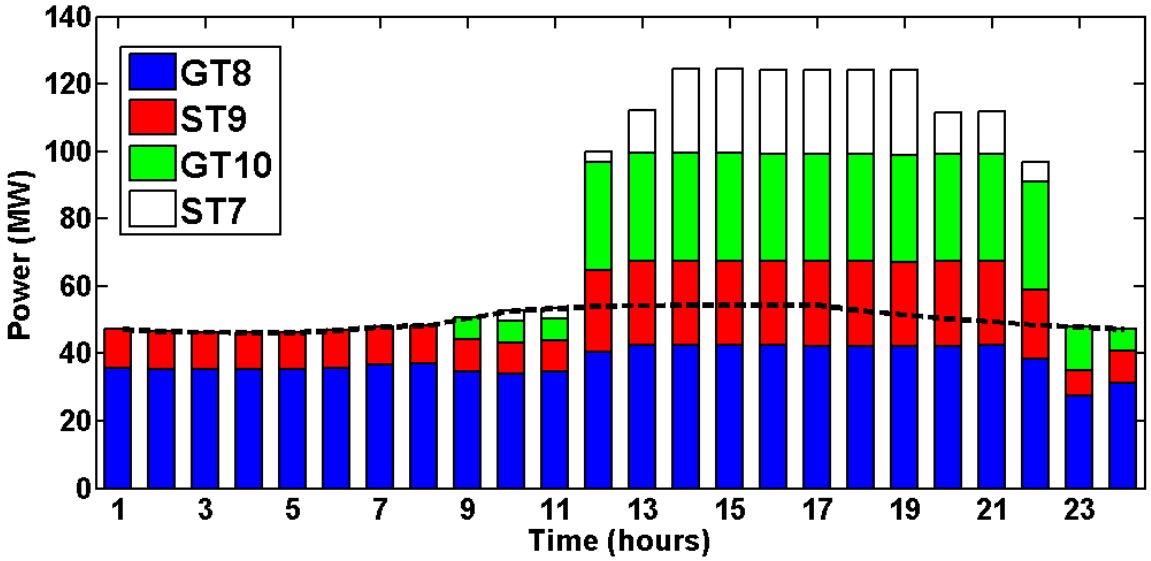

Figure 5.6: Case 2 results for July 20, 2012 - Optimized operating schedules are shown as histograms and historical operating schedules are shown as a black dashed line.

When only GT10, which is more efficient than GT8, and ST9 are committed to operation, the combined-cycle power output from the CHP plant at nominal operating condition is 44 MW_e, without utilizing supplementary firing in HRSG10. However, the lowest electric load observed was 46 MW_e, so the power generation cannot meet the load if GT10 and ST9 were used. The load can be met if more units are bought in service, but this will decrease the overall thermodynamic efficiency and incur additional operating costs due to their start-ups/shut-downs. For this reason, although GT8 is less efficient than GT10, the plant prefers to operate GT8 and ST9, with which the combined-cycle power output at nominal condition is 56 MW_e (sufficient to meet the load during all 24 hours of the scheduling horizon).

In hours 1-8, the power output from GT8 and ST9 met the load and did not participate in the wholesale electricity market due to the low electricity prices during these hours. In hour 7, a cold start-up of ST7 has been initiated and after 2 hours (time to

synchronize), during which the power output was zero, it entered the soak phase for 3 hours during which the power output was maintained at 3 MW (fixed power output from ST7 while in soak phase). In hour 9, a cold start-up of GT10 has been initiated and entered the soak phase immediately for 3 hours during which the power output was maintained at 6.4 MW (fixed power output from GT10 while in soak phase). Note that the time to synchronize with the gas turbine (peak load unit) is zero. The plant did not participate in the wholesale electricity market until hour 11 but started selling the surplus power to the grid at hour 12. In hours 13 and 20-21, the power outputs from GT9, GT10, and ST9 were maximized as it was profitable to sell the extra power at attractive wholesale electricity prices (~ $ 0.035/kWh). In hours 14-19, all the power generating units maximized their productions and sold as much power as possible to the grid, owing the expensive electricity prices of the late afternoon hours (< $ 0.042/kWh) as shown in Figure 5.4. Finally, after being in the dispatchable phase for several hours, which are greater than the minimum down times, ST7 and GT10 entered the desynchronization phase for 1 (hour 22) and 2 hours (hours 23-24), respectively, and followed a predefined sequence of the power output values as denoted in (5.14) and shown in Figure 5.6. In hours 23-24, the plant did not contribute to selling the power to the grid but met the campus electric load. Note that GT10 and HRSG10 started up prior to the start-up of ST7 due to the associated low operating cost of co-generation of steam and electricity.

Table 5.5 summarizes the start-up costs, shut-down costs, and committed operating hours of the producers during the four-month time periods for Case 2 expressed in terms of percentage.

Table 5.5: Start-up costs, shut-down costs, and committed operating hours of the individual plant components for Case 2 expressed in terms of percentage.

Unit index i	Unit name	Start-up cost, C^{start} ($)	Shut-down cost, C^{shut} ($)	Unit Commitment (%)
1	GT8 & HRSG8	0	0	100
2	GT10 & HSRG10	158,500	104,670	33
3	ST7	115,460	46,697	22
4	ST9	0	0	100
5	BR3	118,580	35,969	22
6	BR7	199,810	60,548	13

GT8, HRSG8, and ST9 operated continuously since they could meet the heating and electrical demands during the off-peak hours with minimum operating costs. GT10 and HRSG10 operated about 33 % of the tested time periods. BR3 and ST7 (the least efficient generating unit) operated about 22 % of the tested time periods during which BR3 provided additional HP steam to the steam turbines. The fact that the start-up cost of BR7 is the most expensive due to its largest steam production capacity among all the boilers resulted in its lowest contribution to operation (13 %). However, during these hours all the generating units reached at their rated capacity because market conditions favored the production of surplus electricity. It should be noted that the start-up procedures involved mostly cold start-ups because the reservation times of the producers were mostly greater than T_i^c (8 hours) but less than the duration of continuous off-peak hours in typical days (16 hours). Therefore, even if a longer, i.e., 48 hours, scheduling horizon is considered, the producers' profitability from participating in the wholesale energy market would be the same as the case where a short-sighted day-ahead profit maximization model is used as in this study.

Table 5.6 presents the total electrical energy produced, operating costs, and net income estimated for two cases studies.

Table 5.6: Net income by selling surplus power to the grid from June to September in 2012.

Scenarios	Electrical energy produced (GWh)	Operating costs ($ million)	Net income	
			($ million)	(%)
Base case	142	4.37	-	-
Case 1: NLP problem	154	3.95	0.42	9.5
Case 2: MINLP problem	200	3.23 (0.84[a])	1.14	26

[a] additional operating costs incurred due to the unit start-ups and shut-downs

In Case 1, the simulated results show that the plant could achieve net income of $ 0.42 million from June to September in 2012 by selling surplus energy of 12 GWh to the grid. In Case 2, the plant could achieve net income of $ 1.14 million by selling surplus energy of 58 GWh to the grid. In the second case, the profit was considerably higher than in the first case because more energy (46 GWh) could be sold to the grid with multiple-generating units operating although additional operating costs of $ 0.84 million were incurred due to the unit start-ups and shut-downs.

The system efficiencies expressed in terms of the plant heat rate (the inverse of efficiency) for July 20, 2012 are shown in Figure 5.7(a) and the power outputs during the corresponding hours are shown in Figure 5.7(b).

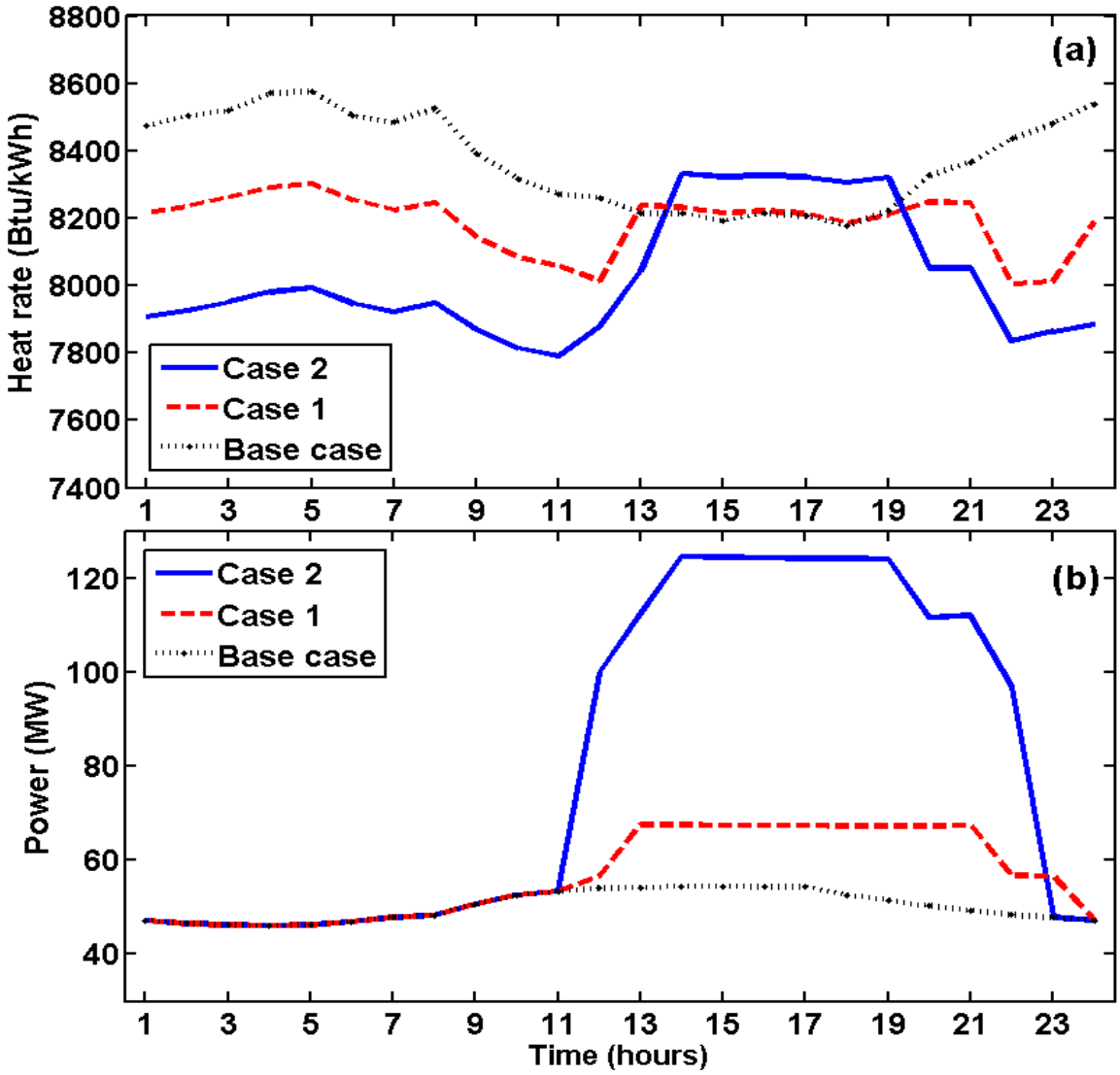

Figure 5.7: Plant heat rates (a) and power outputs (b) for July 20, 2012

In hours 1-11 and 23-24, during which there were no power sales, the results show that the heat rates decreased as the power production rates increased for all three cases. The reason for this is that a gas turbine experiences a reduced efficiency at part-load conditions. During these hours, in Case 1, the heat rates were lower than in the base case as less efficient units were operating at their technical minimum, i.e., steam production from BR3 was limited to its minimum. In Case 2, the heat rates were lower

than in Case 1, because more efficient units were brought in to operation and replaced less efficient units, i.e., ST9 was used instead of ST7. In hours 12-22, the heat rates in base case were considerably lower than those observed in neighboring hours because GT8 was operating near its nominal capacity [102]. On the other hand, during the same hours, the heat rates observed in Case 1 and Case 2 were higher than neighboring hours. Especially, during the on-peak hours (hours 13-18 in Case 1 and hours 14-19 in Case 2) the heat rates were higher than those observed in the base case. However, increased operating costs associated with the increased fuel consumption during the on-peak hours were compensated by the additional power revenues from day-ahead energy market for both cases.

5.3 SUMMARY

This chapter presented a mixed-integer nonlinear programming approach that provides optimal scheduling of combined heat and power plants in day-ahead electricity markets. The maximum profit of the plant from selling surplus power to the grid is realized by committing more efficient generating units while satisfying local loads and system operating constraints and dispatching the committed units economically. The proposed model takes into account of different start-up types (hot, warm, and cold) as well as different operating modes (or phases) of generating units. From the case studies involving a real-world commercial CHP plant at UT Austin, when compared to the base case, the day-ahead profit maximization model was able to achieve net income up to 26%.

Chapter 6: Nonlinear Model Predictive Control of a Heavy-Duty Gas Turbine Power Plant

In this chapter, a nonlinear model predictive control (NMPC) scheme is applied to a heavy-duty gas turbine (HDGT) power plant for frequency and temperature control. This scheme is compared to a classical PID/logic based control scheme.

The model used to describe the physical behavior of the gas turbine power plant (GTPP) is based on a Detailed model [75]. The air flow dynamics described in [74] is also applied in conjunction with the Detailed model. It is expected that the model is valid for variations in shaft speed between 95% to 105% and for unit loading above about 50% load [74]. Typical ISO conditions are assumed for this study (i.e. 1 atm ambient pressure, 15 °C and 60% relative humidity [93]). A gas turbine shows a very fast dynamic response due to small time constants, some of which are less than 0.2 sec, so a steady state assumption is made for the gas turbine dynamics [69-75]. Therefore, the gas turbine model developed in Section 2.2.2 is adapted in this chapter. The details of the model parameters of HDGT at nominal condition selected for modeling, which have been adapted from [93], are shown in Table 6.1.

Table 6.1: Nominal data of the gas turbine selected for modeling (adapted from [93]).

Model Parameter	Symbol	Unit	Value
Plant power output	P_m	MW	166
Nominal frequency	f	Hz	50
Rotation speed of the rotor shaft in the gas turbine	N	RPM	3000
Exhaust mass flow	W	kg/s	537
Fuel flow	W_f	kg/s	10.2
Gas turbine firing temperature	T_f	°C	1096
Exhaust gas temperature	T_e	°C	522
Pressure ratio	PR	-	15.4
Turbine efficiency	η_T	%	89
Compressor efficiency	η_C	%	86
Combustion efficiency	η_{comb}	%	99
Specific heat of air flow	C_{pc}	kJ/kg·K	1.005
Specific heat of exhaust gas flow	C_{ph}	kJ/kg·K	1.157
Cold end ratio of specific heats	γ_c	-	1.4
Hot end ratio of specific heats	γ_h	-	1.33

6.1 CONTROL SYSTEM OF THE GAS TURBINE POWER PLANT

The three main controlled variables (CVs) in gas turbine power plant are the rotor speed N, exhaust gas temperature T_e, and turbine firing temperature T_f. Once the generator is synchronized and connected to the power grid, the power imbalance between the generator power output P_m and electric load P_l will cause the deviation of the grid frequency unless it is controlled properly. Therefore, the rotation speed (frequency) of the rotor shaft in the gas turbine must be controlled at its nominal frequency all the time. The turbine's exhaust gas temperature needs to be kept lower than its reference temperature so as not to damage the gas turbine, yet high enough to achieve high efficiency. In order to regulate Nitrogen Oxide (NOx) emissions, the turbine firing temperature also needs to be kept lower than a specified upper limit as well. These CVs are controlled by manipulating two variables: fuel demand F_d to vary the fuel flow and compressor inlet guide vanes

(*IGVs*) to schedule air flow. Possible disturbance variables (DVs) are ambient air conditions, i.e. temperature, pressure, and relative humidity, and electric load.

6.1.1 Classical Feedback Control

Figure 6.1 shows a simplified block diagram for a single-shaft heavy-duty gas turbine together with its classical feedback control system used in this study.

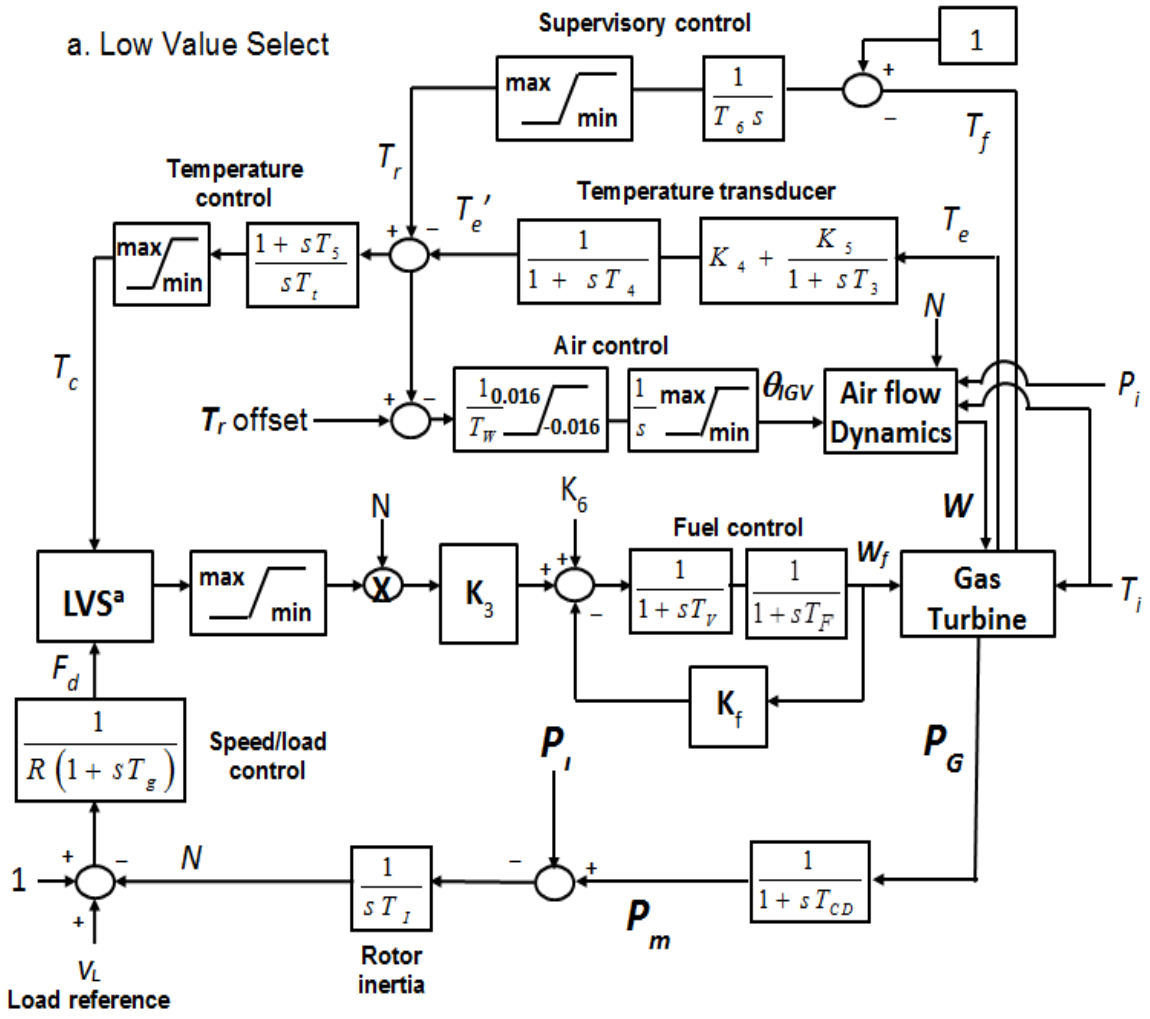

Figure 6.1: Simplified gas turbine simulation block diagram [74, 75].

Variables shown in Figure 6.1 are normalized by their rated values at nominal operating condition and expressed in per unit values, pu (per unit values are the decimal equivalents of percent values). In the percent system, 100 equals the design value, while in the per unit system 1.00 equals the design value [69, 70].

First-order dynamic models are used to represent the pneumatic valve positioner and valve actuator in the fuel control system as well as the radiation shield and thermocouple in the exhaust gas temperature measuring system. Also, a time lag that exists in the compressor discharge path to the turbine inlet is modeled as a first-order transfer function.

The speed/load control block determines the fuel demand F_d according to the rotor speed deviation from the rated value (1-N) and the load reference V_L. The temperature control block prevents the turbine's exhaust temperature T_e from exceeding its reference temperature T_r. The measured exhaust gas temperature T_e' is compared with the reference temperature T_r. The temperature control signal T_c is compared with the fuel demand F_d, and the lower value is selected by the low value selector (LVS), which determines the fuel flow W_f into the combustor. The fuel flow is proportional to the rotor speed N. Supervisory control defines the reference temperature T_r for the exhaust gas temperature T_e [75]. When the turbine firing temperature T_f exceeds its rated value, supervisory control reacts by decreasing T_r.

The air control block regulates the air flow W so as to achieve the desired exhaust gas temperature. The exhaust gas temperature T_e is kept lower than T_r, by an offset, i.e. 1% of its rated value [72]. The air flow is adjusted by the compressor inlet guide vanes (*IGVs*). Nonlinear dependency of a rotor speed of a gas turbine, ambient air temperature, and ambient air pressure on air flow is given as the followings [74]:

$$W = u\left(\Delta N_c\right)\frac{P_{amb}}{P_{a0}}\sqrt{\frac{T_{a0}}{T_{amb}}}\,\frac{\sin\left(\theta_{IGV}-\theta_{\min}\right)}{\sin\left(\theta_{\max}-\theta_{\min}\right)} \tag{6.1}$$

$$u\left(\Delta N_c\right) = 1 + A_0\Delta N_c + A_1\Delta N_c^2 + A_2\Delta N_c^3 \tag{6.2}$$

$$\Delta N_c = N\sqrt{\frac{T_{a0}}{T_{amb}}} - 1 \tag{6.3}$$

The parameters (P_{a0}, T_{a0}, $\theta_{\min}$, $\theta_{\max}$, A_0, A_1, and A_2) in (6.1)-(6.3) as well as those shown in Figure 6.1 are summarized in Table 6.2. The maximum rate of change in air flow is assumed to be 1.6 %/sec [103].

Table 6.2: Model parameters of the system shown in Figure 6.1.

Model parameter	**Symbol**	**Unit**	**Value**
Ambient air pressure reference	P_{a0}	atm	1
Ambient air temperature reference	T_{a0}	K	288.15
Minimum IGV angle	$\theta_{\min}$	degrees	11.6
Maximum IGV angle	$\theta_{\max}$	degrees	85.0
Air flow speed factor	A_0	-	0.945
Air flow speed factor	A_1	-	-7.8
Air flow speed factor	A_2	-	39
Speed governor gain	R	1/pu[a]	0.04
Speed governor time constant	T_g	sec	0.05
Gain of radiation shield	K_4	pu	0.85
Gain of radiation shield	K_5	pu	0.15
Radiation shield time constant	T_3	sec	12.2
Thermocouple time constant	T_4	sec	1.7
Exhaust gas temp. upper limit	T_{cmax}	pu	1.1
Exhaust gas temp. lower limit	T_{cmin}	pu	0.0
Fuel control upper limit	F_{dmax}	pu	1.5
Fuel control lower limit	F_{dmin}	pu	-0.112
Ratio of fuel adjustment	K_3	pu	0.8938
Fuel valve lower limit	K_6	pu	0.1062
Valve positioner time constant	T_V	sec	0.04
Fuel system external feedback constant	K_f	pu	0
Fuel system time constant	T_F	sec	0.26
Time constant of T_f control	T_6	sec	60
Rated exhaust gas temp. upper limit	T_{rmax}	pu	1.01
Rated exhaust gas temp. lower limit	T_{rmin}	pu	0.9772
Air control time constant	T_W	sec / pu	0.4789
Air valve upper limit	g_{max}	pu / sec	1.0
Air valve lower limit	g_{min}	pu / sec	0.73
Compressor discharge lag time constant	T_{CD}	sec	0.16
Temperature offset	$T_{r\ offset}$	pu	0.01
Turbine's rotor time constant	T_I	sec	18.5

[a] per unit value

The shaft The shaft dynamic model considers the torque inputs/outputs from each unit (turbine, compressor, starter motor, and generator), as well as friction [104]. Newton's law is applied to the torque balance yielding the shaft speed expression:

$$\frac{dN}{dt} = \frac{60}{2\pi J_R}\left(Q_M - Q_I\right) \tag{6.4}$$

where

- N is the rotational speed of the rotor shaft in RPM (revolution per minute)
- J_R is the lumped polar moment of inertia of compressor, turbine, starter motor, and generator
- Q_T is the developed torque, and
- Q_I is the load torque.

Equation (6.4) shows that the rotor speed changes with time unless the developed torque Q_T and the load torque Q_I are balanced to each other at any moment. The torque equation is accurate to within 5 percent at part load and is significantly more accurate at the 100 percent design rating [69].

6.1.2 NMPC Formulation

The model predictive controller is formulated as an NLP problem. The objective function associated with the model described in Figure 6.1is formed to minimize the sum of squared residuals at each sampling time k as shown in (6.5):

$$\begin{aligned}\min_{\substack{F_d(k+j)\\ \theta_{IGV}(k+j)}} \mathrm{J} = \sum_{i=k+1}^{P}\Big[& Q_N\left(\hat{N}_i - N^{sp}\right)^2 + R_{F_d}\left(\Delta F_d\right)^2 + R_{\theta_{IGV}}\left(\Delta\theta_{IGV}\right)^2 \\ & + Q_{T_e,i}\left(\hat{T}_{e,i} - T_e^{ref}\right)^2 + Q_{T_f,i}\left(\hat{T}_{f,i} - T_f^{ref}\right)^2\Big],\ j = 0,\ 1,\ \ldots,\ M\ \text{-}1\end{aligned} \tag{6.5}$$

where

$$\Delta F_d = F_d(k+j) - F_d(k+j-1), \quad j = 0,\ 1,\ \ldots,\ M\ \text{-}1 \tag{6.6}$$

$$\Delta\theta_{IGV} = \theta_{IGV}(k+j) - \theta_{IGV}(k+j-1), \quad j = 0, 1, \ldots, M\text{-}1 \tag{6.7}$$

$$Q_{T_{e,i}} \begin{cases} Q_{T_e}^{hi} \text{ if } \hat{T}_{e,i} > T_e^{ref} \\ Q_{T_e}^{low} \text{ otherwise} \end{cases}, \quad j = 0, 1, \ldots, M\text{-}1 \tag{6.8}$$

$$Q_{T_{f,i}} \begin{cases} Q_{T_f}^{hi} \text{ if } \hat{T}_{f,i} > T_f^{ref} \\ Q_{T_f}^{low} \text{ otherwise} \end{cases}, \quad j = 0, 1, \ldots, M\text{-}1 \tag{6.9}$$

subject to

$$F_d^- \le F_d(k+j) \le F_d^+, \quad j = 0, 1, \ldots, M\text{-}1 \tag{6.10}$$

$$\theta_{IGV}^- \le \theta_{IGV}(k+j) \le \theta_{IGV}^+, \quad j = 0, 1, \ldots, M\text{-}1 \tag{6.11}$$

$$\left|\theta_{IGV}(k+j) - \theta_{IGV}(k+j-1)\right| \le \Delta\theta_{IGV}^{\max}, \quad j = 0, 1, \ldots, M\text{-}1 \tag{6.12}$$

where P is the prediction horizon, M is the control horizon, N^{sp} is the set point of N, and T_e^{ref} and T_f^{ref} are the reference temperatures for T_e and T_f, respectively. A perfect model is assumed, so an output feedback term (bias correction) is not included in (6.5). The output weighting factors for the temperatures (Q_{Te}, Q_{Tf}) shown in (6.5) depend on the conditional statements ((6.8) and (6.9)). Relatively higher weighting factors are chosen in the case of T_e and/or T_f exceed their reference temperatures. On the other hand, lower weighting factors are specified to achieve high exhaust gas temperature by increasing the air flow, thus increasing the thermal efficiency of the gas turbine as long as T_e and/or T_f remain lower than their upper bounds. Constraints on the manipulated variables (MVs) as

shown in (6.10)-(6.12) ensure that the optimal solution to (6.5) lies within the feasible region. Their values used for this study are summarized in Table 6.3.

Table 6.3: Constraint limits on manipulated variables.

Constraint limits	Values
Lower limit on F_d, F_d^-	-0.1123 pu
Upper limit on F_d, F_d^+	1.5 pu
Lower limit on θ_{IGV}, θ_{IGV}^-	0.6588 pu
Upper limit on θ_{IGV}, θ_{IGV}^+	1.00 pu
Maximum change allowed in θ_{IGV}, $\Delta\theta_{IGV}^{\max}$	0.0176 pu

A good rule of thumb is to choose the sampling period Δt so that the sampling rate is less than one-tenth of the process time constant [105]. The largest time constant observed in the GTPP is the rotor inertia time constant (18.5 sec), so the sampling period of 1 second was selected. Considering the Δt of 1 sec, reasonable computation time, and frequent change in load demands, it has been found that the best performance could be obtained with M of 4 (4 sec) and P of 8 (8 sec). MPC tuning parameters and their values are listed in Table 6.4

Table 6.4: MPC tuning parameters.

Tuning parameters	Values
Sampling rate, Δt	1 sec
Control horizon, M	4
Prediction horizon, P	8
Output weighting factor for N, Q_N	10
Conditional output weighting factors[a], $Q_{T_e}^{hi}$, $Q_{T_f}^{hi}$	5
Conditional output weighting factors[a], $Q_{T_e}^{low}$, $Q_{T_f}^{low}$	1
Move suppression factor for F_d, R_{F_d}	1
Move suppression factor for θ_{IGV}, $R_{\theta_{IGV}}$	3

[a] see (6.8) and (6.9) for the conditional statements

6.2 SIMULTANEOUS SOLUTION METHOD

Figure 6.2 presents a schematic illustrating collocation on finite elements discretization with a first-order assumed for inputs (u) in each element (k). The differential state variables (x) are approximated at each of the collocation points, denoted by i [106].

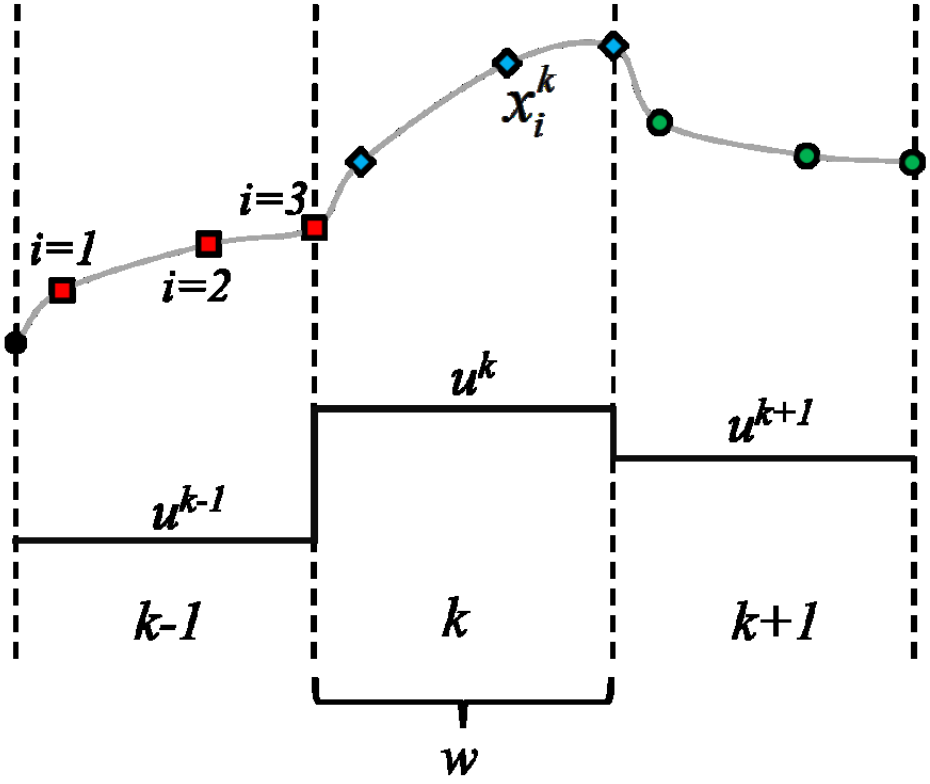

Figure 6.2: A schematic illustrating the orthogonal collocation on finite elements discretization with a first-order hold assumed for inputs (u) in each element (k). The differential state variables (x) are approximated at each of the collocation points, denoted by i. The points are represented using different shapes and colors, which help distinguish one finite element from another.

Using orthogonal collocation on finite elements, differential equations are converted to algebraic equations using Lagrange interpolation polynomials (Ω), which

are used to represent derivatives at select points, known as the collocation points [107]. A set of derivatives given by

$$\frac{dx(\tau)}{d\tau} = f\left(x(\tau), y(\tau), u(\tau), p(\tau)\right) \tag{6.12}$$

is represented by (Ω) using the following relationship

$$\frac{dx(\tau_i)}{d\tau} = \sum_{j=1}^{N_C} \Omega_j(\tau_i) f\left(x(\tau_j), y(\tau_j), u(\tau_j), p(\tau_j)\right) \tag{6.13}$$

where τ is a normalized time variable, x represents the differential states, y the algebraic states, u the user-defined inputs, and p the external inputs or disturbances. The Lagrange polynomials are given by:

$$\Omega_j(\tau) = \prod_{k=1,k\neq j}^{N_C} \frac{\tau - \tau_k}{\tau_j - \tau_k} \tag{6.14}$$

where N_c is the number of collocation points used in the approximation. With this representation, approximations of the state variables themselves are given by integrating (6.13) as shown in (6.15), where w is the width of the time intervals used and $\hat{\Omega}$ is the integral of Ω over w.

$$x(\tau_i) = x_0 + w\sum_{j=1}^{N_C} \hat{\Omega}_j(\tau_i) f\left(x(\tau_j), y(\tau_j), u(\tau_j), p(\tau_j)\right) \tag{6.15}$$

Using this method, the differential algebraic equation (DAE) system is converted to a set of algebraic equations so that the objective function can be minimized simultaneously to the constraints being satisfied using NLP. Simultaneous methods are generally much more efficient for solving NMPC problems as compared to sequential

methods, which rely on forward integration of the differential states subject to a set of pre-determined trial inputs. For further reading on this methodology, see [106, 108].

6.3 CASE STUDIES

The proposed classical feedback control (or PID control) was modeled dynamically with MATLAB/Simulink. The same controller settings in [72] were used in this work. NMPC system was implemented using Advanced Process Monitor (APM) [109]. APM uses orthogonal collocation on finite elements to covert the dynamic problem to a NLP problem. This NLP problem was then solved using analytical derivatives and an interior-point (IP) algorithm to provide fast solution times. In this work, ambient air temperature and pressure were assumed to have constant values (15 °C and 1 atm). Thus, the only disturbance considered in this study was the load P_I. Two case studies are considered to compare the simulated results between MPC and PID control.

6.3.1 Case 1: Plant Responses to Random Variations in P_I

Figure 6.3 and Figure 6.4 show the MVs and CVs responses to random variations in demand load. Figure 6.5 compares the random variations in P_I to the power output P_M from the plant simulated for 100 seconds. For practical cases, variations in demand load are less dramatic than those shown in Figure 6.5. However, during the island mode operation, a sudden large increase in demand load for a particular power generation unit could occur in case of one of the generators failing [72].

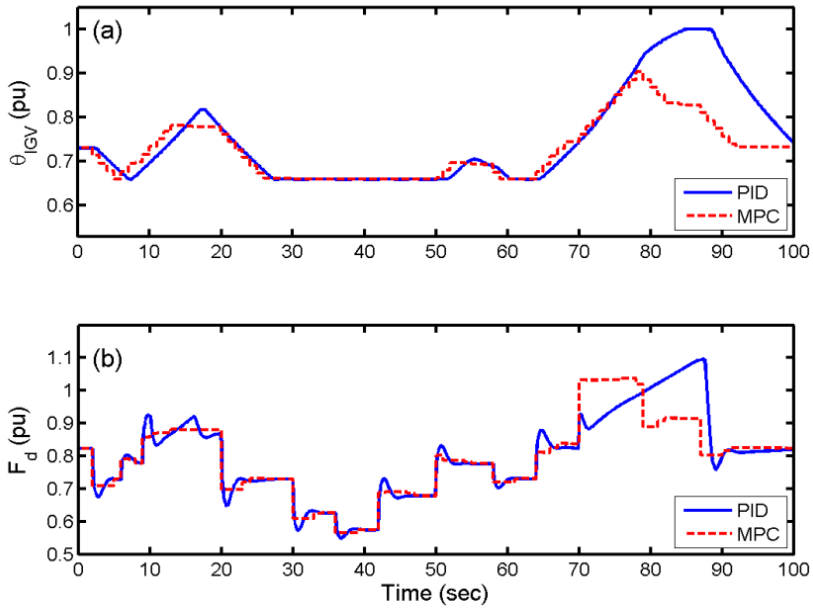

Figure 6.3: Controller responses to random variations in P_I: (a) *IGV* angle, (b) Fuel demand F_d

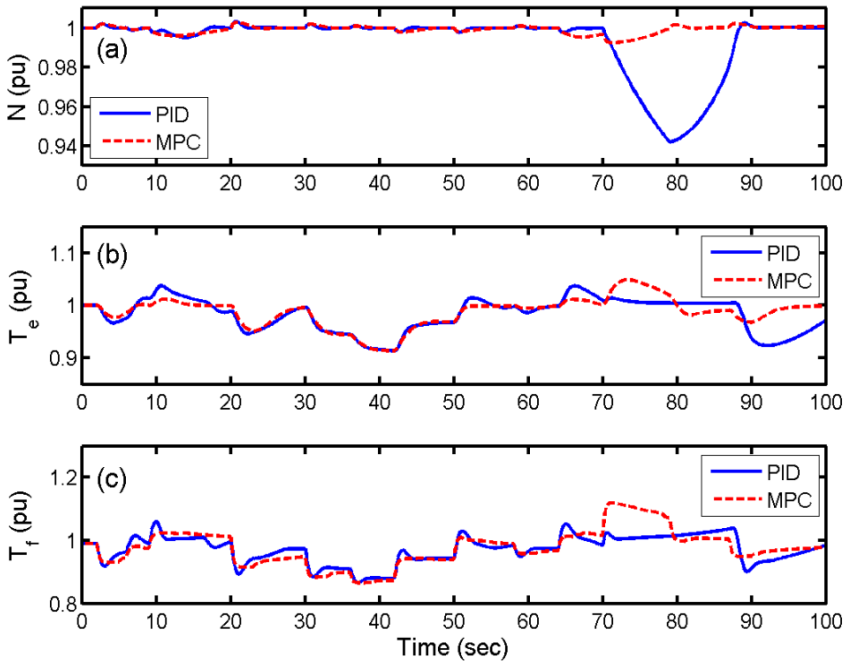

Figure 6.4: Output responses to random varations in P_I: (a) Rotor speed N, (b) Exhaust gas temperature T_e, (c) Turbine firing temperature T_f

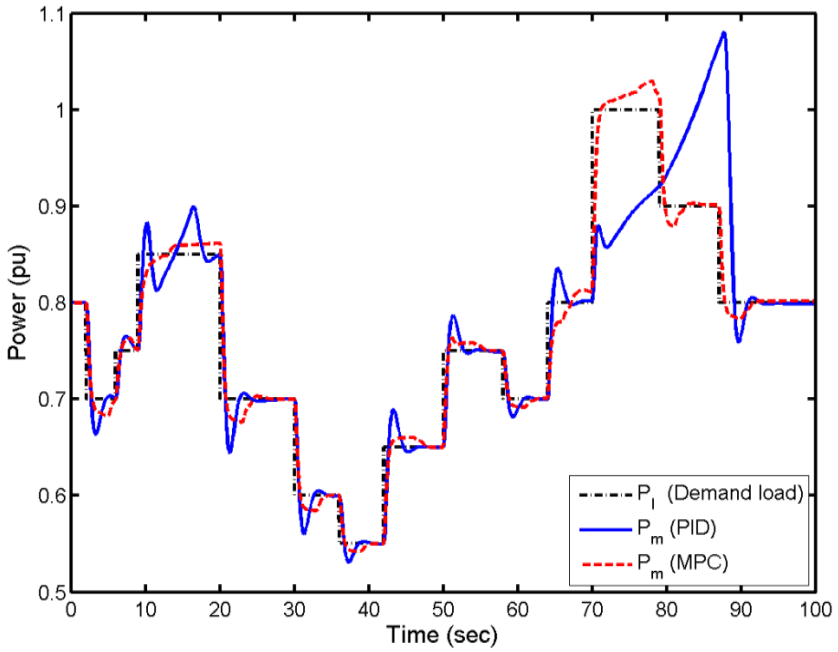

Figure 6.5: Demand load (P_l) vs. plant power ouput (P_m)

During the time between zero and 70 seconds, both the PID and MPC controllers were able to maintain the CVs at their set points (see Figure 6.4). In Figure 6.3, the control movements resulted from the MPC controller show smoother variations in MVs than those resulting from the PID controller. In Figure 6.5, the power outputs simulated by the MPC controller show relatively less oscillatory behavior than those simulated with the PID controller.

During the time between 70 and 100 seconds, the MPC controller provided superior output responses with small settling times. In comparison to the controller outputs from the PID controller, input changes of F_d calculated by the MPC controller were more aggressive. The main disadvantage of the PID controller is that it is not capable of predicting the future performance of the process. On the other hand, the MPC controller is able to predict the future values of the outputs based a reasonably accurate dynamic model of the process and current measurements. In Figure 6.4 and Figure 6.5,

the time period between 70 and 80 seconds well illustrates the drawback of PID control. During this period of time, a high demand load was sustained causing the frequency to drop continuously. The frequency drop through the speed governor control immediately resulted in an increase of fuel demand F_d in order to bring the frequency back to its nominal frequency (see Figure 6.3(b)). However, an increased fuel flow resulted in a temperature increase (see Figure 6.4(b)) that activated temperature control. This limits the fuel flow and power production as shown in Figure 6.5. On the other hand, the MPC controller was able to control the both frequency and turbine's exhaust gas temperature at their desired set points over the whole time horizon.

Figure 6.6 shows the time required to solve a NLP problem using the finite element method. The computation time significantly increased with an increase in prediction horizon P. However, the effect of control horizon M on the computation time was less significant. The computation time at each control step was sufficiently faster than the sampling rate (1 sec), allowing real-time implementation of NMPC for the GTPP. This problem was solved on a PC with Intel® Core™2 Duo processor 2.54 GHz and 4.00 GB of RAM.

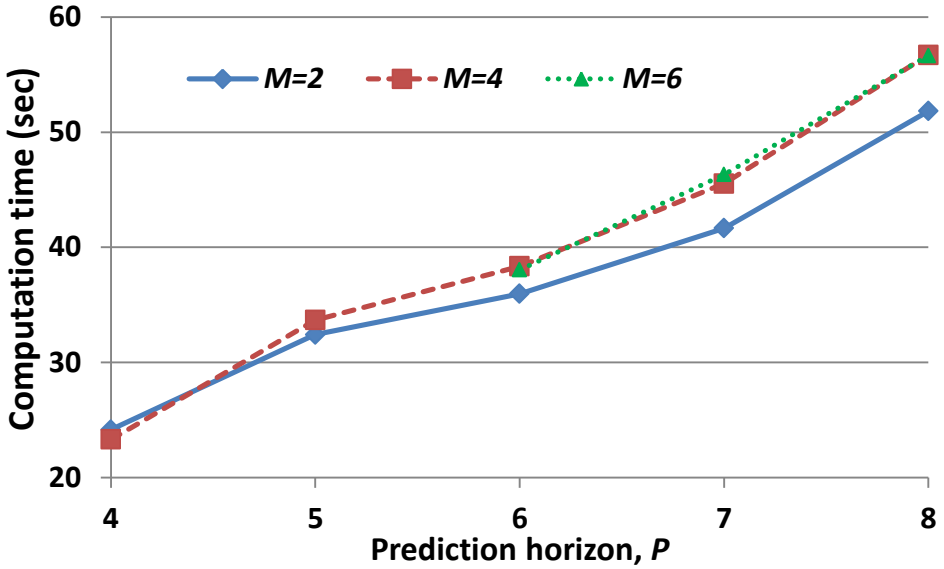

Figure 6.6: Computation time required to solve a NLP problem. *M* is the control horizon.

6.3.2 Case 2: Plant Responses to the Step Change Made in P_l

Figure 6.7 shows the output responses to the step change made in the electric load. The initial power output from the plant was 0.8 pu, and an additional electric load of 0.2 pu was introduced at the time of 2 seconds.

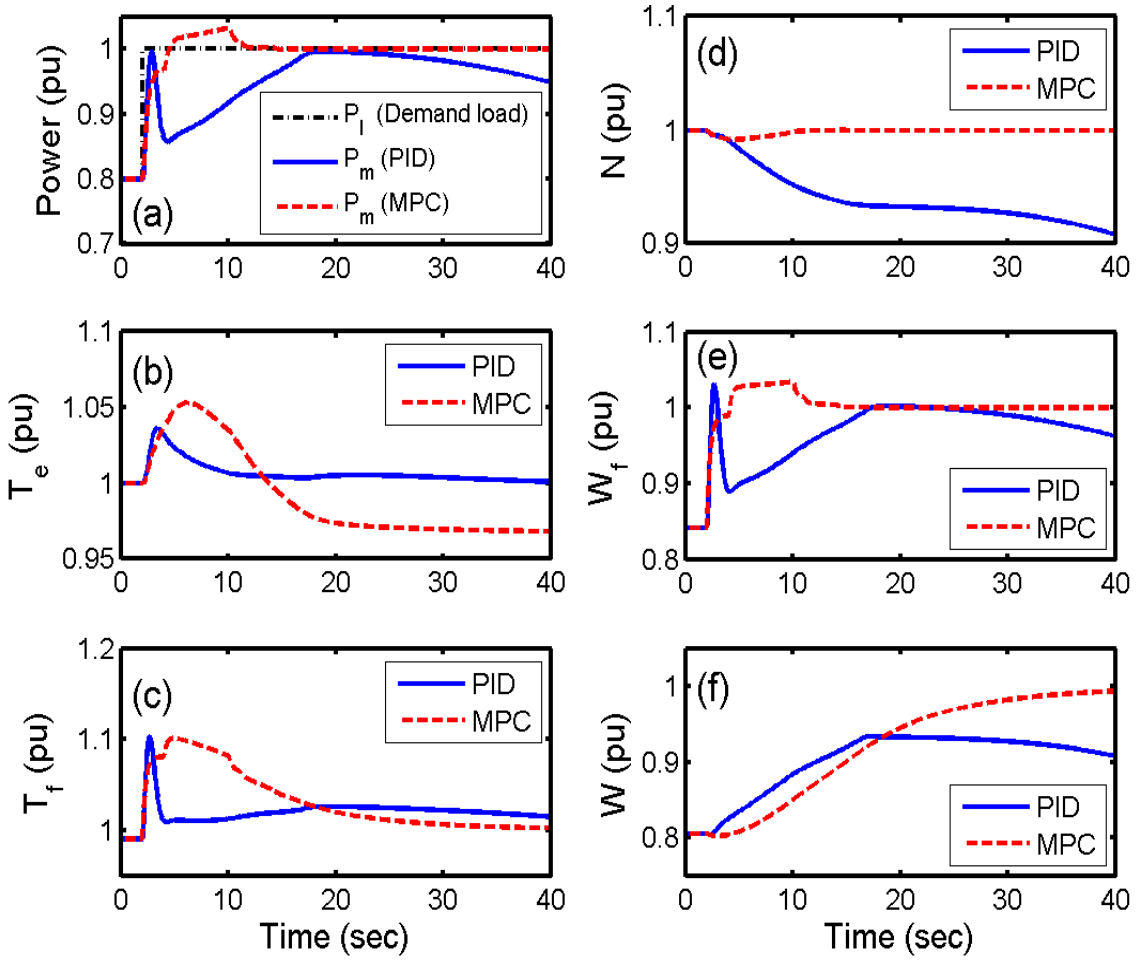

Figure 6.7: Output responses to P_l change from 0.8 to 1.0 pu: (a) Power output, (b) Exhaust gas temperature T_e, (c) Turbine firing temperature T_f, (d) Rotor speed N, (e) Fuel flow W_f, (f) Air flow W

In this case, the plant could not recover the frequency with the PID control system. As seen in Figure 6.7(a), after the first post-disturbance period of two seconds, the power generation was reduced to avoid overheating of gas turbine blades by decreasing the fuel flow (see Figure 6.7(e)). The activation of the temperature control resulted in a decrease in both T_e (Figure 6.7(b)) and T_f(Figure 6.7(c)). The temperature control made it possible to increase power generation without exceeding the upper limits of T_e and T_f by increasing the fuel and air (Figure 6.7(f)) flows. However, the frequency

experienced a continuous drop, and the plant went out of control (see Figure 6.7(d)). Unlike the PID controller, the MPC controller could maintain the rotor speed at its set point and keep T_e and T_f lower than their upper limits even when a large disturbance was introduced to the system instantaneously.

6.4 SUMMARY

In this study, both PID and MPC controllers were implemented to analyze the stability of a heavy-duty gas turbine power plant. The plant model was identified using two models (Detailed model and FD model) in order to simulate the gas turbine's rotor speed (frequency), exhaust gas temperature, firing temperature, and the power output. The plant responses to the major disturbance (demand load) were studied in both control systems. By comparison, the MPC controller provided superior output responses with smaller settling times, less oscillatory behavior and more aggressive control actions to the random variations in the electric load than those observed in the PID control system. When a sudden large step change was made in the load, the PID controller could not recover the rotor speed as opposed to the MPC controller was able to bring the rotor speed back to its nominal speed. When obtaining the NMPC solution, the computation time required to solve an optimization problem was sufficiently faster than the sampling rate by applying orthogonal collocation on finite elements. This efficient scheme would allow NMPC to be implemented via real-time optimization for gas turbine power plants in a fast and robust manner.

Chapter 7: Conclusions and Future Work

Optimization can be one of the most cost-effective methods to improve a utility network. The results of the analysis of plant-wide utility optimization led to improve the system energy efficiency and minimize operating costs and carbon footprint by optimal allocations of available resources. With the assumption that a combined heat and power (CHP) plant is allowed to exchange electricity with the external grid at wholesale market prices, operational decisions on whether to self-generate or buy power depend on prices of various energy commodities (electricity, fuel, etc.) as well as changes in the weather. The case studies provided insights into how different types of utility pricing, fuel costs, and various operational and ambient conditions affect the power output, energy efficiency, and total revenue. The ability to provide the emergency response service (ERS) has proven to be a compelling potential profit opportunity for ERS participants. For a power plant with multiple generating units, the proposed optimal scheduling technique, which determines unit commitment and economic dispatch relative to wholesale market prices and local electric loads, provides operational decision support to yield the highest net income during scheduling periods. As the solution of the scheduling problem strongly depends on the accuracy of the plant models used for simulations, mathematical models that are simple but accurately represent the complexity of a CHP system have been developed and validated. This work also highlighted the application of a nonlinear model predictive control (NMPC) scheme to a heavy-duty gas turbine power plant for frequency and temperature control. The case studies demonstrate that a NMPC scheme provides superior output responses with smaller settling times and less oscillatory behavior compared to a classical PID/logic based control scheme in response to disturbances in electric loads.

The case studies illustrated in this work are based on deterministic cases; therefore, the ability to forecast loads and electricity prices in advance is a valuable tool, which allows real-time implementation of the proposed method for a CHP plant. Powell et al. [106] developed a nonlinear autoregressive model with exogenous inputs (NARX) to accurately forecast hourly loads (electrical, heating, and cooling) for a district energy system up to 24 hours in advance using weather and time variables (month, hour, and day). They provided case studies involving the Hal C. Weaver power plant complex at UT Austin campus (the same power plant used for case studies throughout this work) to demonstrate the effectiveness of their forecasting model. So, incorporation of this load forecasting tool into the optimal scheduling model developed in this work is recommended. Also, the modeling of uncertainties in forecasted loads and electricity prices in a scheduling problem under the stochastic MINLP framework is the scope of proposed future work.

The model parameters in Chapter 2 once estimated were assumed to be constant over prediction horizons, of which spanned for the entire year. However, daily and seasonal changes in the weather will affect the model outputs and the efficiency of the system. Therefore, more up-to-date model must be used to account for changes in those conditions and provide a more accurate prediction. Updating the model using the most recently measured data on more frequent basis, i.e., a daily basis, is recommended.

The optimal scheduling algorithm developed in this work has proven to be an effective cost and energy saving methodology, so implementing optimal operational scheme on real systems and in real-time is recommended. The system studied in this work only involved six units, resulting in reasonable computation time of few hours to determine the optimal operation in 24-hour ahead. When this methodology is extended for solving a large- and commercial-scale problem with hundreds of generating units, it

would be difficult to find the optimal solution (or impractical to find the global solution) within the scheduling period. To overcome computational expense issues associated with solving such large-scale MINLP problems, intelligent initialization routines and novel solution methods are recommended for future work.

A thermal energy storage (TES) tank, when added to a CHP system, can provide extra flexibility. A TES tank stores chilled water so that it can be used later for cooling. This allows the system to produce extra cooling when capacity exceeds demand (typically at night) and then extract this energy when demand exceeds capacity, which is the current purpose of the thermal energy storage system. It essentially provides an extra chiller, thus extra electricity for electrically-powered chillers as in the UT Austin power plant, for hot summer days when cooling demands are at their peak. However, a TES tank can also be used to increase efficiency by shifting cooling demand to times when chillers operate more efficiently and by maximizing the use of the most efficient equipment. Thus, a TES tank gives the district energy system additional degrees of freedom which can be exploited through optimization to determine optimal operation. UT Austin campus also has the TES tank in use. So, an economic analysis on incorporating the TES system into the CHP plant is recommended.

Appendix: Establishment of Confidence Intervals on Fitted Parameters

To establish the confidence intervals about the fitted parameters, the sum of the squares of the fitted function from the actual data points is defined first:

$$S_r = \sum_{i=1}^{N} (f_i - f(x_i, y_i))^2 \tag{A.1}$$

where S_r is the sum of the squared residuals, f_i is the actual (or measured) data points, and $f(x_i,y_i)$ is the proposed linear regression function with two independent variables (x and y) evaluated at the i^{th} x and y values [110]. Next, the effective standard deviation about a regression curve is calculated by (A.2),

$$S_{y/x} = \sqrt{\frac{S_r}{N-m}} \tag{A.2}$$

where, $S_{y/x}$ is the standard error, S_r is defined by (A.1), N is the total number of data points, and m is the total number of coefficients in the fitted equation [110].

To construct confidence intervals about the fitted parameters, the inverse of the covariance matrix C is defined by (A.3),

$$C^{-1} = \left[Z^T Z \right]^{-1} \tag{A.3}$$

where C^{-1} is the inverse of covariance matrix C and Z is the matrix that consists of M columns, one for each coefficient in the proposed regression function, and N rows, one for each of the data points. Z^T is the transpose of the matrix in which the rows and columns are switched [110].

Finally, the 95% confidence interval about a fitted parameter is given below as a function of the variance value (C_{ii}) for that coefficient and the standard error of fit:

$$a_i \pm t_{0.95}(\nu = N - m) S_{y/x} \sqrt{C_{ii}^{-1}} \tag{A.4}$$

where a_i is a fitted parameter, $t_{0.95}(\nu = N - m)$ is the student's t-distribution at 95% confidence limits in which ν is the degree of freedom, and $\sqrt{C_{ii}^{-1}}$ is the square root of the off-diagonal elements of C^{-1} [110].

Nomenclature

Acronyms

AGC	automatic generation control
APC	advanced process control
APM	advanced process monitor
BHs	business hours
CCCT	combined cycle combustion turbine
CHP	combined heat and power
CVs	controlled variables
DAE	differential algebraic equation
DAM	day-ahead market
DP	dynamic programming
ERCOT	electric reliability council of Texas
ED	economic dispatch
GA	genetic algorithm
GTPP	gas turbine power plant
HDGT	heavy-duty gas turbine
HP	high-pressure
HRSG	heat recovery steam generator
IGVs	inlet guide vanes
IP	interior-point
ISOs	independent system operators
LMS	Least mean squares
LR	Lagrangean relaxation
LSEs	load serving entities
LVS	low value selector
MILP	mixed-integer linear programming
MINLP	mixed-integer nonlinear programming
MIP	mixed-integer programming
MP	Medium-pressure
MPC	model predictive control
MVs	manipulated variables

NARX	nonlinear autoregressive model with exogenous inputs
NERC	North America electric reliability council
NMPC	nonlinear model predictive control
NOx	nitrogen oxide
PID	proportional-derivative-integral
PSO	particle swarm optimization
QSEs	qualified scheduling entities
REs	resource entities
RHS	right-hand side
RTM	real-time market
SQP	sequential quadratic programming
TES	thermal energy storage
TIAC	turbine inlet air cooling
UC	unit commitment
UT Austin	University of Texas at Austin

Sets

gt (*HDGT*)	index (set) of gas turbines *HDGT* = {*GT_HRSG8*, *GT_HRSG*10}, where "*GT_HRSG8*" is gas turbine 8 coupled with HRSG 8, "*GT_HRSG10*" is gas turbine 10 coupled with HRSG 10
hrs (*BHs*)	index (set) of business hours *BHs* = {*BHs1*, *BHs2*, *BHs3*, *NBH*}, where "*BHs1*" is from 8 AM to 1 PM during weekdays, "*BHs2*" is from 1 PM to 4 PM, "*BHs3*" is from 4 PM to 8 PM, and "*NBHs*" is all other hours. *BHs1*, *BHs2*, and *BHs3* only include hours during weekdays, except ERCOT holidays.
i (*I*)	index (set) of units
l (*L*)	index (set) of unit start-up type *L* = {*h*, *w*, *c*}, where "*h*" is hot, "*w*" is warm, and "*c*" is cold
st (*EST*)	index (set) of steam turbines *EST* = {*ST7*, *ST9*}, where "*ST7*" is steam turbine 7, "*ST9*" is steam turbine 9
t (*T*)	index (set) of hours of the planning horizon

Binary variables

u_{it}	1 if a unit *i* is committed during hour *t* ; and 0 otherwise

u_{it}^{n}	1 if unit *i* is in operating phase *n* during hour *t*, where *n* = *syn*: synchronization, *n* = *soak*: soak, *n* = *disp*: dispatchable, and *n* = *desyn*: desynchronization; and 0 otherwise	
$u_{it}^{n,\,l}$	1 if a type-*l* start-up of unit *i* is in operating phase *n* during hour *t*, where *n* = *syn*: synchronization, *n* = *soak*: soak, *n* = *disp*: dispatchable, and *n* = *desyn*: desynchronization; and 0 otherwise	
X_B	binary decision variables	
y_{it}	1 if unit *i* is started-up during hour *t*	
y_{it}^{l}	1 if a type-*l* start-up of unit *i* is initiated during hour *t*	
z_{it}	1 if unit *i* is shut-down during hour *t*	

Continuous variables

$F_{d,\,t}$	gas turbine fuel demand at time *t*	, in pu[a]
$SFR_{(st)t}$	steam flow regulator of the steam turbine *st* during hour *t*	
$V_{w,\ TIAC,\,t}$	volumetric flow rate of chilled water entering the TIAC system at time *t*	, in GPM
$W_{f,\ BR,\,t}$	auxiliary boiler fuel flow at time *t*	, in kg/sec
$W_{f,\ HRSG,\,t}$	HRSG duct burner fuel flow at time *t*	, in kg/sec
$W_{S,\ EXT,\ (st)t}$	extraction steam flow of the steam turbine *st* at time *t*	, in kg/sec
X_C	continuous decision variables	
θ_{IGV}	angular position of the *IGVs*	, in degree

[a] per unit value

Parameters

A_0	air flow speed factor	
A_1	air flow speed factor	
A_2	air flow speed factor	
$C_{e,\,t}^{DAM}$	day-ahead electricity price at hour *t*	, in $/kWh
$C_{e,\,t}^{RTM}$	Real-time electricity price at hour *t*	, in $/kWh
C_f	fixed fuel cost	, in $/kg
C_i^{shut}	shut-down cost of unit i	, in $
$C_i^{start,\,l}$	start-up cost of unit *i* under type-*l* start-up	, in $
C_{pc}	specific heat of air flow	, in kJ/kg·K

C_{ph}	specific heat of exhaust gas flow	, in kJ/kg·K
$C_{prod,\ it}$	production cost of unit *i* in hour *t*	, in $
COP	coefficient of performance of a chiller	, in MW_{th}/MW_e
f	frequency	, in H_Z
F_{dmax}	Fuel control upper limit	, in pu
F_{dmin}	Fuel control lower limit	, in pu
g_{max}	air valve upper limit	, in pu/sec
g_{min}	air valve lower limit	, in pu/sec
$\hat{H}_{EC,\ BR}$	specific enthalpy of the feedwater entering the auxiliary boiler	, in kJ/kg
$\hat{H}_{EC,\ HRSG}$	specific enthalpy of the feedwater entering the economizer	, in kJ/kg
HR_t	overall plant heat rate	, in Btu/kWh
$\hat{H}^{l}_{sat'd}$	specific enthalpy of the saturated liquid	, in kJ/kg
$\hat{H}^{v}_{sat'd}$	specific enthalpy of the saturated vapor	, in kJ/kg
$\hat{H}_{S,\ COND}$	specific enthalpy of the condensate	, in kJ/kg
$\hat{H}_{S,\ EXT}$	specific enthalpy of the extraction steam	, in kJ/kg
$\hat{H}_{SH,\ BR}$	specific enthalpy of the superheated steam exiting the auxiliary boiler	, in kJ/kg
$\hat{H}_{SH,\ HRSG}$	specific enthalpy of the superheated steam exiting the HRSG	, in kJ/kg
$\hat{H}_{S,\ THR}$	specific enthalpy of the throttle steam	, in kJ/kg
K_f	fuel system external feedback constant	, in pu
K_5	gain of radiation shield	, in pu
K_4	gain of radiation shield	, in pu
K_{NL} or K_6	fuel valve lower limit	, in pu
K_3	ratio of fuel adjustment	, in pu
$L_{E,\ t}$	electric load at during hour *t*	, in MW_e
$L_{ERS,\ hrs}$	ERS load in business hours *hrs*	, in MW_e
$L^{sold}_{ERS,\ hrs}$	ERS capacity that is sold the ERCOT in business hours *hrs*	, in MW_e
$L_{H,\ t}$	heating load in time *t*	, in kg/sec
LHV	lower heating value of the fuel	, in kJ/kg

M	control horizon	
MW_{air}	molecular weight of the air	, in kg/kmol
N	rotation speed of the rotor shaft in the gas turbine	, in RPM
P	prediction horizon	
P_{amb}	ambient pressure	, in bar
P_{a0}	ambient air pressure reference	, in bar
P_c	pressure of air at the compressor inlet	, in bar
$P_{EC,\ BR}$	pressure of the auxiliary boiler feedwater at the inlet of the economizer	, in bar
$P_{EC,\ HRSG}$	pressure of the HRSG feedwater at the inlet of the economizer	, in bar
$P_{GT,\ t}$	net energy supplied to HDGT at time t	, in MW_e
P_I	electric load	, in MW_e
$\overline{P}_i^{soak}$	fixed power output of unit i while in soak phase	, in MW_e
P_{it}	power output of unit i at time t	, in MW_e
P_{it}^{desyn}	power output of unit i during the desynchronization phase in time t	, in MW_e
P_{it}^{disp}	power output of unit i during the dispatchable phase	, in MW_e
P_{it}^{soak}	power output of unit i during the soak phase in time t	, in MW_e
P_m	net power output from a HDGT	, in MW_e
$P_{ST,\ t}$	net energy supplied to the steam turbine at time t	, in MW_e
$P_{SH,\ BR}$	pressure of the auxiliary boiler steam at the outlet of the superheater	, in bar
$P_{SH,\ HRSG}$	pressure of the HRSG superheated steam at the outlet of the superheater	, in bar
P_t	power output accepted by the ISO during time t	, in MW_e
P_t^{DAM}	power output accepted by the ISO during time t in the DAM	, in MW_e
P_t^{RTM}	power output accepted by the ISO during time t in the RTM	, in MW_e
PR	gas turbine compression ratio	
q	vapor quality	
Q_N	output weighting factor for N	
Q_{T_e}	output weighting factor for T_e	

Q_{T_f}	output weighting factor for T_f	
R	speed governor gain	, in 1/pu[a]
R_{F_d}	move suppression factor for F_d	
R_g	ideal gas constant	, in J/mol·K
R^2	goodness of fit	
$R_{\theta_{IGV}}$	move suppression factor for θ_{IGV}	
T_{amb}	ambient temperature	, in °C
$T_{air,\,TIAC,\,out}^{min}$	minimum possible air temperature at the outlet of the TIAC system	, in °C
T_{a0}	ambient air temperature reference	, in K
T_{CD}	compressor discharge lag time constant	, in sec
T_{cmax}	Exhaust gas temperature upper limit	, in pu
T_{cmin}	Exhaust gas temperature lower limit	, in pu
$T_{c,\,t}$	temperature at compressor inlet at time t	, in K
$T_{d,\,t}$	temperature at compressor outlet at time t	, in K
$T_{e,\,t}$	gas turbine's exhaust gas temperature at time t	, in K
$T_{e,\,HRSG,\,in,\,t}$	post duct burner HRSG air temperature at time t	, in K
$T_{e,\,HRSG,\,out,\,t}$	exhaust gas temperature at the outlet of the HRSG at time t	, in K
$T_{EC,\,BR}$	temperature of the auxiliary boiler feedwater at the inlet of the economizer	, in K
$T_{EC,\,HRSG}$	temperature of the HRSG feedwater at the inlet of the economizer	, in K
T_F	fuel system time constant	, in sec
T_4	thermocouple time constant	, in sec
$T_{f,\,t}$	gas turbine's firing temperature at time t	, in K
T_g	speed governor time constant	, in sec
T_I	turbine's rotor time constant	, in pu
$T_i^{\,l}$	Time off-load before going into longer standby conditions ($l = w$: hot to warm, $l = c$: hot to cold) of unit i	, in hour
$T_i^{min,down}$	minimum down time of unit i	, in hour
$T_i^{min,\,up,\,l}$	minimum up time of a type-l start-up of unit i	, in hour

T_i^{off}	prior reservation time of unit i	, in hour
T_i^{desyn}	time from desynchronize unit i	, in hour
$T_i^{soak,\ l}$	soak time of unit i under type-l start-up	, in hour
$T_i^{syn,\ l}$	time to synchronize unit i under type-l start-up	, in hour
T_r	reference temperature	, in K
$T_{r\ offset}$	temperature offset	, in pu
T_{rmax}	rated exhaust gas temperature upper limit	, in pu
T_{rmin}	rated exhaust gas temperature upper limit	, in pu
$T_{SH,\ BR}$	temperature of the auxiliary boiler superheated steam at the outlet of the superheater	, in K
$T_{SH,\ HRSG}$	temperature of the HRSG superheated steam at the outlet of the superheater	, in K
T_6	time constant of T_f control	, in sec
T_3	radiation shield time constant	, in sec
T_V	valve positioner time constant	, in sec
T_W	Air control time constant	, in sec/pu
$T_{w,\ TIAC,\ in}$	temperature of chilled water entering the TIAC system	, in °C
$T_{w,\ TIAC,\ out}$	temperature of chilled water exiting the TIAC system	, in °C
T^{∞}	maximum length of the planning horizon extended to the past (negative time)	, in hour
V_c	volumetric air flow at the compressor inlet	, in m^3/sec
W_t	actual dry-air mass flow at time t	, in kg/sec
W_f	fuel flow in the HDGT	, in kg/sec
$W_{f,\ GT,\ t}$	gas turbine fuel flow at time t	, in kg/sec
$W_{f,\ it}$	fuel flow of unit i during time t	, in kg/sec
$W_{f,\ tot,\ t}$	total fuel flow during time t	, in kg/sec
$W_{g,\ t}$	gas turbine exhaust flow at time t	, in kg/sec
$W_{S,\ COND,\ t}$	condensate flow at time t	, in kg/sec
$W_{SH,\ BR,\ t}$	auxiliary boiler steam flow rate at time t	, in kg/sec
$W_{SH,\ HRSG,\ t}$	HRSG steam flow rate at time t	, in kg/sec
$W_{SH,\ tot,\ t}$	total steam flow rate at time t	, in kg/sec
$W_{S,\ THR,\ t}$	throttling steam flow entering the steam turbine at time t	, in kg/sec
α_{BR}	lumped parameter for an auxiliary boiler	, in Btu/SCF

α_{HRSG}	lumped parameter for an HRSG	, in kJ/kg·K
β_{HRSG}	lumped parameter for an HRSG	, in kJ/kg
γ_c	cold end ratio of specific heats	
γ_h	hot end ratio of specific heats	
$\Delta H_{FWHTR,\,t}$	HRSG feedwater heat duty at time t	, in kW_{th}
$\Delta H_{TIAC,\,t}$	cooling load of a TIAC system during hour t	, in kW_{th}
ΔP_{TIAC}	average pressure drop across the TIAC	, in PSI
$\Delta P_{TIAC,\,t}$	power consumption of an electrically-powered chiller at hour t	, in kW_e
Δt	sampling rate	, in hour or sec
ΔT_{HRSG}^{min}	Minimum temperature differential between $T_{e,\,HRSG,\,in,\,t}$ and $T_{SH,\,HRSG}$	, in °C
$\Delta\theta_{IGV}^{\max}$	Maximum change allowed in θ_{IGV}	, in pu
ε	effective of a heat exchanger	
η_c	compressor efficiency	
$\eta_{comb,\,GT}$	gas turbine combustor efficiency	
η_{ST}	steam turbine efficiency	
η_t	turbine efficiency	
θ_{max}	maximum *IGV* angle	, in degree
θ_{min}	minimum *IGV* angle	, in degree
ρ_{NG}	density of natural gas	, in lb/SCF
ρ_w	density of water	, in kg/m^3

[a] per unit value

Subscripts

i	unit
n	at nominal condition

Superscripts

disp	during the dispatchable phase
max	maximum
min	minimum
ref	reference
sp	set point

References

[1] Siirola JJ, Edgar TF. Process energy systems: Control, economic, and sustainability objectives. Computers & Chemical Engineering 2012;47:134-44.

[2] Verbruggen A, Dewallef P, Quoilin S, Wiggin M. Unveiling the mystery of Combined Heat & Power (cogeneration). Energy 2013;61:575-82.

[3] Northeast CHP Technical Assistance Partnership. Combined Heat & Power, available: http://www.northeastchptap.org/whatischp/About-CHP.php. [Accessed: 11-Mar-2014].

[4] Thornton A, Monroy CR. Distributed power generation in the United States. Renewable and Sustainable Energy Reviews 2011;15(9): 4809-17.

[5] Lin F, Yi JA. Optimal operation of a CHP plant for space heating as a peak load regulating plant. Energy 2000;25(3):283-98.

[6] Bogdan Z, Kopjar D. Improvement of the cogeneration plant economy by using heat accumulator. Energy 2006;31(13):2285-92.

[7] United States Enviornmental Protection Agency. Ethanol Fact Sheet, available: http://www.epa.gov/chp/markets/ethanol_fs.html. [Accessed: 11-Mar-2014].

[8] Akorede MF, Hizam H, Pouresmaeil E. Distributed energy resources and benefits to the environment. Renewable and Sustainable Energy Reviews 2010;14(2);724-734.

[9] Newborough M. Assessing the benefits of implementing micro-CHP systems in the UK. Proceedings of the Institution of Mechanical Engineers, Part A: Journal of Power and Energy 2004;218(A4):203-218.

[10] Bracco S, Delfino F, Pampararo F, Robba M, Rossi M. A mathematical model for the optimal operation of the University of Genoa Smart Polygeneration Microgrid: Evaluation of technical, economic and environmental performance indicators. Energy 2014;64:912-22.

[11] Wang C, Shahidehpour S. Effects of ramp-rate limits on unit commitment and economic dispatch. IEEE Transactions on Power Systems 1993;8(3):1341-50.

[12] Fragaki A, Andersen AN, Toke D. Exploration of economical sizing of gas engine and thermal store for combined heat and power plants in the UK. Energy 2008;33(11):1659-70.

[13] Ristic M, Brujic D, Thoma K. Economic dispatch of distributed combined heat and power systems participating in electricity spot markets. Proceedings of the Institution of Mechanical Engineers, Part A: Journal of Power and Energy 2008;222(A7):743-52.

[14] Rolfsman B. Combined heat-and-power plants and district heating in a deregulated electricity market. Applied Energy 2004;78(1):37-52.

[15] Streckiene G, Martinaitis V, Andersen AN, Katz J. Feasibility of CHP-plants with thermal stores in the German spot market. Applied Energy 2009;86(11):2308-16.

[16] Ito K, Yokoyama R, Shiba T. Optimal Operation of a Diesel Engine Cogeneration Plant Including a Heat Storage Tank. Journal of Engineering for Gas Turbines and Power 1992;114(4): 687-94.
[17] Yokoyama R, Ito K. Optimal operational planning of cogeneration systems with thermal storage by the decomposition method. Journal of Energy Resources Technology 1995;117(4): 337-42.
[18] Siddiqui AS. Firestone R, Ghosh S, Stadler M, Edwards JL, Marnay C. Distributed Energy resources wtih combined heat and power applications. Technical report. Ernest Orlando Lawrence Berkeley National Laboratory; 2003, available: http://certs.lbl.gov/pdf/52718.pdf. [Accessed: 11-Mar-2014].
[19] Stoppato A, Mirandola A, Meneghetti G, Lo CE. On the operation strategy of steam power plants working at variable load: Technical and economic issues. Energy 2012;37(1):228-36.
[20] Happ H. Optimal power dispatch A comprehensive survey. IEEE Transactions on Power Apparatus and Systems 1977;96(3): 841-54.
[21] Chowdhury BH, Rahman S. A review of recent advances in economic dispatch. IEEE Transactions on Power Systems 1990;5(4):1248-59.
[22] Orero S, Irving M. Economic dispatch of generators with prohibited operating zones: a genetic algorithm approach. In: IEE Proceedings - Generation, Transmission and Distribution, p. 529-34, 1996.
[23] Walters DC, Sheble GB. Genetic algorithm solution of economic dispatch with valve point loading. IEEE Transactions on Power Systems 1993;8(3):1325-32.
[24] Shoults R, Venkatesh S, Helmick S, Ward G, Lollar M. A dynamic programming based method for developing dispatch curves when incremental heat rate curves are non-monotonically increasing. IEEE Transactions on Power Systems 1986;1(1):10-16.
[25] Whitley D. A review of models for simple genetic algorithms and cellular genetic algorithms. Department of Computer Science, available: http://citeseerx.ist.psu.edu/viewdoc/download?doi=10.1.1.18.8518&rep=rep1&type=pdf. [Accessed: 11-Mar-2014].
[26] Bakirtzis A, Petridis V, Kazarlis S. Genetic algorithm solution to the economic dispatch problem. In: IEE Proceedings - Generation, Transmission and Distribution, p. 377-82, 1994.
[27] Chen PH, Chang HC. Large-scale economic dispatch by genetic algorithm. IEEE Transactions on Power Systems 1995;10(4):1919-26.
[28] Sheblé GB, Brittig K. Refined genetic algorithm-economic dispatch example. IEEE Transactions on Power Systems 1995;10(1):117-24.
[29] Sewtohul LG, Ah King RTF. Rughooputh HCS. Genetic algorithms for economic dispatch with valve point effect. In: 2004 IEEE International Conference on Networking, Sensing and Control, p. 1358-63, 2004. Taipei, Taiwan, March 21-23 2004.
[30] Sheblé GB, Maifeld TT, Brittig K, Fahd G, Fukurozaki-Coppinger S. Unit commitment by genetic algorithm with penalty methods and a comparison of

Lagrangian search and genetic algorithm—economic dispatch example. International Journal of Electrical Power & Energy Systems 1996;18(6):339-46.
[31] Wang J, Zhai ZJ, Jing Y, Zhang C. Influence analysis of building types and climate zones on energetic, economic and environmental performances of BCHP systems. Applied Energy 2011;88(9): 3097-112.
[32] Chaturvedi KT, Pandit M, Srivastava L. Particle swarm optimization with time varying acceleration coefficients for non-convex economic power dispatch. International Journal of Electrical Power & Energy Systems 2009;31(6):249-57.
[33] Dotzauer E, Holmström K, Ravn HF. Optimal unit commitment and economic dispatch of cogeneration systems with a storage. In: 13th PSCC Proceedings, p. 738-744, 1999. Trondheim, Norway, June 1999.
[34] Rong A, Hakonen H, Lahdelma R. A dynamic regrouping based sequential dynamic programming algorithm for unit commitment of combined heat and power systems. Energy Conversion and Management 2009;50(4):1108-15.
[35] Cohen AI. Modeling unit ramp limitations in unit commitment. In: Proceedings of the Tenth Power systems and Computing Conference, 1990. PSCC '90, p. 1107-14, 1990.
[36] Innorta M, Marannino P, Granelli G, Montagna M, Silvestri A. Security constrained dynamic dispatch of real power for thermal groups. IEEE Transactions on Power Systems 1988;3(2):774-81.
[37] Wood WG. Spinning reserve constrained static and dynamic economic dispatch. IEEE Transactions on Power Apparatus and Systems 1982;PAS-101(2):381-8.
[38] Kerr R, Scheidt J, Fontanna A, Wiley J. Unit commitment. IEEE Transactions on Power Apparatus and Systems 1966;PAS-85(2):417-21.
[39] Lee FN. Short-term thermal unit commitment - A new method. IEEE Transactions on Power Systems 1988;3(2):421-8.
[40] Shoults RR, Chang SK, Helmick S, Grady WM. A practical approach to unit commitment, economic dispatch and savings allocation for multiple-area pool operation with import/export constraints. IEEE Transactions on Power Apparatus and Systems 1980;PAS-99(2):625-35.
[41] Lauer G, Sandell N, Bertsekas D, Posbergh T. Solution of large-scale optimal unit commitment problems. IEEE Transactions on Power Apparatus and Systems 1982;PAS-101(1):79-86.
[42] Cohen AI, Yoshimura M. A branch-and-bound algorithm for unit commitment. IEEE Transactions on Power Apparatus and Systems 1983;PAS-102(2):444-51.
[43] Madrigal M, Quintana VH. An interior-point/cutting-plane method to solve unit commitment problems. In: Proceedings of the 21st IEEE International Conference on Power Industry Computer Applications, 1999. PICA '99, p. 203-9, 1999. Santa Clara, CA, May 16-21 1999.
[44] Mantawy A, Soliman S, El-Hawary M. A new tabu search algorithm for the long-term hydro scheduling problem. In: Proceedings of the Large Engineering Systems Conference on Power Engineering, p. 29-34, 2002.

[45] Lin WM, Cheng FS, Tsay MT. An improved tabu search for economic dispatch with multiple minima. IEEE Transactions on Power Systems 2002;17(1):108-12.
[46] Mantawy A, Abdel-Magid YL, Selim SZ. A simulated annealing algorithm for unit commitment. IEEE Transactions on Power Systems 1998;13(1):197-204.
[47] Saneifard S, Prasad NR, Smolleck HA. A fuzzy logic approach to unit commitment. IEEE Transactions on Power Systems 1997;12(2):988-95.
[48] Sasaki H, Watanabe M, Kubokawa J, Yorino N, Yokoyama R. A solution method of unit commitment by artificial neural networks. IEEE Transactions on Power Systems 1992;7(3):974-81.
[49] Liang RH, Kang FC. Thermal generating unit commitment using an extended mean field annealing neural network. In: IEE Proceedings - Generation, Transmission and Distribution, p. 164-70, 2000.
[50] Juste K, Kita H, Tanaka E, Hasegawa J. An evolutionary programming solution to the unit commitment problem. IEEE Transactions on Power Systems 1999;14(4):1452-9.
[51] Venkatesh P, Gnanadass R, Padhy NP. Comparison and application of evolutionary programming techniques to combined economic emission dispatch with line flow constraints. IEEE Transactions on Power Systems 2003;18(2)688-97.
[52] Hindsberger M, Ravn HF. Multiresolution modeling of hydro-thermal systems. In: 22nd IEEE Power Engineering Society International Conference on Power Industry Computer Applications, 2001. PICA 2001. Innovative Computing for Power-Electric Energy Meets the Market, p. 5-10, 2001. Sydney, NSW, May 20-24 2001.
[53] Mantawy A, Abdel-Magid YL, Selim SZ. Integrating genetic algorithms, tabu search, and simulated annealing for the unit commitment problem. IEEE Transactions on Power Systems 1999;14(3): 829-36.
[54] Huang CL. Application of genetic-based neural networks to thermal unit commitment. IEEE Transactions on Power Systems 1997;12(2):654-60.
[55] Padhy NP. Unit commitment-a bibliographical survey. IEEE Transactions on Power Systems 2004;19(2):1196-205.
[56] Yamin H. Review on methods of generation scheduling in electric power systems. Electric Power Systems Research 2004;69(2):227-48.
[57] Hedman KW, O'Neill RP, Oren SS. Analyzing Valid Inequalities of the Generation Unit Commitment Problem. In: Power Systems Conference and Exposition, 2009. PSCE '09. IEEE/PES, p.1737-42, 2009. Seattle, WA, March 15-18 2009.
[58] Arroyo JM, Conejo AJ. Optimal response of a thermal unit to an electricity spot market. IEEE Transactions on Power Systems 2000;15(3):1098-104.
[59] Carrión M, Arroyo JM. A computationally efficient mixed-integer linear formulation for the thermal unit commitment problem. IEEE Transactions on Power Systems 2006; 21(3):1371-8.

[60] Liu C, Shahidehpour M, Li Z, Fotuhi-Firuzabad M. Component and mode models for the short-term scheduling of combined-cycle units. IEEE Transactions on Power Systems 2009;24(2):976-90.
[61] Aghaei J, Alizadeh MI. Multi-objective self-scheduling of CHP (combined heat and power)-based microgrids considering demand response programs and ESSs (energy storage systems). Energy 2013;55:1044-54.
[62] Mitra S, Grossmann IE, Pinto JM, Arora N. Optimal production planning under time-sensitive electricity prices for continuous power-intensive processes. Computers & Chemical Engineering 2012;38:171-84.
[63] Mitra S, Sun L, Grossmann IE. Optimal scheduling of industrial combined heat and power plants under time-sensitive electricity prices. Energy 2013;54:194-211.
[64] Electricity Reliability Council of Texas. Market Guides, available: http://www.ercot.com/mktrules/guides/. [Accessed: 12-Mar-2014].
[65] Adib P, Zarnikau J. Texas: the most robust competitive market in North America. Electricity Market Reform: an international perspective. Elsevier; 2006.
[66] Zarnikau JW. Demand participation in the restructured Electric Reliability Council of Texas market. Energy 2010;35(4):1536-43.
[67] Electricity Reliability Council of Texas. Qualified Scheduling Entities, available: http://www.ercot.com/services/rq/qse/index. [Accessed: 12-Mar-2014].
[68] Yee SK, Milanovic JV, Hughes FM. Overview and comparative analysis of gas turbine models for system stability studies. IEEE Transactions on Power Systems 2008;23(1):108-18.
[69] Rowen WI. Simplified mathematical representations of heavy-duty gas-turbines. Journal of Engineering for Power, Transactions of the ASME 1983;105:865-9.
[70] Rowen WI. Simplified mathematical representations of single shaft gas turbines in mechanical drive service. Turbomachinery International 1992;33:26-32.
[71] Demello FP, Ahner DJ, Anderson PM, Doudna JH, Kundur P, Richardson LM, Tandy G, Taylor CW, Vandemeulebroeke F. Dynamic models for combined cycle plants in power system studies. IEEE Transactions on Power Systems 1994;9(3):1698-708.
[72] Kakimoto N, Baba K. Performance of gas turbine-based plants during frequency drops. IEEE Transactions on Power Systems 2003;18(3):1110-5.
[73] Baba K, Kakimoto N. Dynamic behavior of a combined cycle power plant in the presence of a frequency drop. Electrical Engineering in Japan 2003;143(3):9-19.
[74] Kunitomi K, Kurita A, Okamoto H, Tada Y, Hara S, Pourbeik P, Price WW. Modeling frequency dependency of gas turbine output. In: Proceedings of 2001 IEEE Power Engineering Society Winter Meeting, p.678-83, 2001. Columbus, OH, January 28 - February 1 2001.
[75] Mantzaris J, Vournas J. Modeling and stability of a single-shaft combined cycle power plant. International Journal of Thermodynamics 2007;10(2):71-8.
[76] Maciejowski JM. Predictive Control with Constraints. Prentice Hall; 2000.

[77] Vroemen BG, Van Essen HA, Van Steenhoven AA, Kok JJ. Nonlinear model predictive control of a laboratory gas turbine installation. Journal of Engineering for Gas Turbines and Power, Transactions of the ASME 1999;121(4):629-34.
[78] Mu J, Rees D. Approximate model predictive control for gas turbine engines. In: Proceedings of the 2004 American Control Conference, p. 5704-9, 2004. Boston, MA, June 30 - July 2 2004.
[79] D'Amato FJ. Industrial application of a model predictive control solution for power plant startups. In: Proceedings of the 2006 IEEE International Conference on Control Applications, p. 243-8, 2006. Munich, Germany, October 4-6 2006.
[80] Utilitities and Energy Management. Powerring the University of Texas at Austin, available: http://www.utexas.edu/utilities/. [Accessed: 11-Mar-2014].
[81] Ontiveros JM. The University of Texas at Austin Combined Heat and Power Plant. Journal of Cogeneration & Distributed Generation 2007;22:49-53.
[82] Aghaei J, Niknam T, Azizipanah-Abarghooee R, Arroyo JM. Scenario-based dynamic economic emission dispatch considering load and wind power uncertainties. International Journal of Electrical Power & Energy Systems 2013;47:351-67.
[83] Amina M, Kodogiannis V, Petrounias I, Tomtsis D. A hybrid intelligent approach for the prediction of electricity consumption. International Journal of Electrical Power & Energy Systems 2012;43(1):99-108.
[84] Bunn DW. Forecasting loads and prices in competitive power markets. Proceedings of the IEEE 2000;88(2):163-9.
[85] Boggs PT, Tolle JW. Sequential quadratic programming. Acta numerica 1995;4(1)1-51.
[86] Byrd RH, Hribar ME, Nocedal J. An interior point algorithm for large-scale nonlinear programming. SIAM Journal on Optimization 1999;9(4):877-900.
[87] Kim JS, Edgar TF. Economic Dispatch of a Combined Heat and Power Plant. Essay of the 4th Auunal Symposium: Sustainability at the University of Texas at Austin; 2013, available: http://www.utexas.edu/sustainability/pssc/symposium/documents/2013_Kim_PowerPlant.pdf. [Accessed: 12-Mar-2014].
[88] Chacartegui R, Jimenez-Espadafor F, Sanchez D, Sanchez T. Analysis of combustion turbine inlet air cooling systems applied to an operating cogeneration power plant. Energy Conversion and Management 2008;49(8):2130-41.
[89] Kapoor K, Powell KM, Cole WJ, Kim JS, Edgar TF. Improved Large-Scale Process Cooling Operation through Energy Optimization. Processes 2013;1(3):312-29.
[90] Incropera FP, Dewitt DP, Bergman TL, Lavine AS. Fundamentals of Heat and Mass Transfer. John Wiley & Sons; 2007.
[91] Chaker M, Meher-Homji CB. Inlet fogging of gas turbine engines: Climatic analysis of gas turbine evaporative cooling potential of international locations. Journal of Engineering for Gas Turbines and Power - Transactions of the ASME 2006;128(4):815-25.

[92] Kim JS, Powell KM, Edgar TF. Nonlinear model predictive control for a heavy-duty gas turbine power plant. In: Proceedings of American Control Conference, p. 2952-7, 2013. Washington, DC, June 17-19 2013.
[93] Tavakoli MRB, Vahidi B, Gawlik W. An Educational Guide to Extract the Parameters of Heavy Duty Gas Turbines Model in Dynamic Studies Based on Operational Data. IEEE Transactions on Power Systems 2009;24(3):1366-74.
[94] Kim TS, Lee DK, Ro ST. Analysis of thermal stress evolution in the steam drum during start-up of a heat recovery steam generator. Applied Thermal Engineering 2000;20(11):977-92.
[95] Rachtan W, Malinowski L. An approximate expression for part-load performance of a microturbine combined heat and power system heat recovery unit. Energy 2013;51:146-53.
[96] Electricity Reliability Council of Texas. Emergency Response Service, available: http://www.ercot.com/services/programs/load/eils/. [Accessed: 12-Mar-2014].
[97] Simoglou CK, Biskas PN, Bakirtzis AG. Optimal self-scheduling of a thermal producer in short-term electricity markets by MILP. IEEE Transactions on Power Systems 2010;25(4):1965-77.
[98] Rajan D, Takriti S. Minimum up/down polytopes of the unit commitment problem with start-up costs. Technical report. IBM Research Devision; 2005, available: http://domino.research.ibm.com/library/cyberdig.nsf/1e4115aea78b6e7c85256b360066f0d4/cdcb02a7c809d89e8525702300502ac0?OpenDocument. [Accessed: 12-Mar-2014].
[99] Aghaei J, Ahmadi A, Shayanfar H, Rabiee A. Mixed integer programming of generalized hydro-thermal self-scheduling of generating units. Electrical Engineering 2012;95(2):109-25.
[100] Koetzier H, van der Veen W, McInally T, Arnhem KC. Setting of technical parameters for LRMC of CCGT. Technical report. KEMA; 2006, available: https://emaweb.ema.gov.sg/media/files/vesting_contracts/22120603413630KEMAfinalreport.pdf. [Accessed: 13-Mar-2014].
[101] Achterberg T. SCIP: solving constraint integer programs. Mathematical Programming Computation 2009;1(1)1-41.
[102] Kurz R. Gas turbine performance. In: Proceedings of the thirty-fourth turbomachinery symposium, p. 131-46, 2005. Houston, TX, September 12-15 2005.
[103] Suzaki S, Kawata K, Sekoguchi M, Goto M. Combined cycle plant model for power system dynamic simulation study. Transactions on Institute of Electrical Engineering of Japan 2000;120-B:1146-52.
[104] Sekhon R, Bassily H, Wagner J, Gaddis J. Stationary gas turbines - a real time dynamic model with experimental validation. In: 2006 American Control Conference, p. 1838-44, 2006. Minneapolis, MN, June 14-16 2006.
[105] Shridhar R, Cooper DJ. A tuning strategy for unconstrained SISO model predictive control. Industrial & Engineering Chemistry Research 1997;36(3):729-46.

[106] Powell KM. Dynamic optimization of energy systems with thermal energy storage. Ph.D. dissertation, Department of Chemical Engineering, University of Texas at Austin, Austin, TX; 2013.
[107] Zavala VM. Computational strategies for the optimal operation of large-scale chemical processes. Ph.D. dissertation, Department of Chemical Engineering, Carnegie Mellon University, Pittsburgh, PA; 2008.
[108] Biegler LT, Cervantes AM, Wachter A. Advances in simultaneous strategies for dynamic process optimization. Chemical Engineering Science 2002;57(4):575-93.
[109] APMonitor Optimization Suite. APMonitor Modeling Language, available: http://apmonitor.com/. [Accessed: 14-Mar-2014].
[110] Draper NR, Smith H. Applied regression analysis. In Wiley series in probability and mathematical statistics. John Wiley & Sons;1981.

Vita

Jong Suk Kim was born in Seoul, South Korea. He received the degree of Bachelor of Science in Chemical and Biomolecular Engineering from Georgia Institute of Technology, Georgia. After completion of his Bachelor's degree, he worked for a half year in Samsung Engineering as a researcher and a process engineer. In August, 2009, he started his graduate program in the Mcketta Department of Chemical Engineering at the University of Texas at Austin. In December, 2011, he received the degree of Master of Science in Chemical Engineering from the University of Texas at Austin, Texas.

Email: jkim0916@gmail.com

This dissertation was typed by the author.